Proceedings of the Thirteenth BGA Young Geotechnical Engineers' Symposium

Thirteenth BGA Young Geotechnical Engineers' Symposium

30th June 2014 - 2nd July 2014

University of Manchester

PROCEEDINGS

Edited by Dr C Lam and Dr M A Syed

Contents

Physical Modelling of Vibro Stone Column Foundations using Transparent Soil

P. Kelly

University of Portsmouth

ABSTRACT: The development of transparent synthetic soil has allowed opportunities to develop non-intrusive geotechnical modelling techniques. This work aims to examine group interaction characteristics of small vibro stone column groups using transparent soil in conjunction with Particle Image Velocimetry (PIV) to capture soil deformation patterns and development of pre-failure strains. The novel technique allowed the author to gain a new insight into column-column and column-structure interactions that govern the behaviour of stone columns. In contrast to the isolated columns which failed in an axisymmetric manner, local shear failure, bulging, bending, punching and block failure were all observed for column strip foundations, depending on the geometrical configurations employed. It was concluded that column length, foundation overhang and Area replacement ratio play particularly important roles in governing foundation behaviour and performance.

KEYWORDS: Lab tests, Transparent Soil, Ground Improvement, Soil/Structure Interaction, Group Mechanics, Bearing Capacity

1 INTRODUCTION

The vibrated stone column technique is a ground treatment process used to improve the load bearing capacity and settlement characteristics of soft and compressible soils. The traditional application of stone columns is to support widespread loading using a large infinite column group; however, in recent years the technique has been extended to stabilise isolated pad and strip footings using smaller group configurations. Current design practice is based on the unit cell concept whereby it is proposed that each stone column in the group acts independently (Priebe, 1995). Previous investigations (Hu, 1995; McKelvey, 2002 and Black, 2007), have shown that group columns exhibit complex behaviour and the overall stability is dependent on column-column, column-soil and column structure interactions.

Many fundamental concepts associated with vibro stone column behaviour have originated from understanding gained through reduced scale physical model experiments. Pioneering work by Hughes and Withers (1974) on isolated stone columns determined that (i) two failure modes were prevalent; bulge failure and end bearing, (ii) the mode of failure was controlled by column length to diameter (L/d) ratio and that (iii) L/d = 4 was optimum for bearing capacity. Recent investigations by Hu (1995) and McKelvey (2002) evaluated the behaviour of large and small group configurations respectively. In addition to postulating a revised L/d = 6 for bearing capacity, the authors stated that the proximity of columns contributed to non-uniform column distortions that compromised column integrity and overall foundation settlement performance. Post failure observations by Hu (1995) revealed that in addition to exhibiting axisymmetric bulging similar to that observed for an isolated column by Hughes and Withers (1974), columns within a group formation were susceptible to 'buckling and bending' that instigated shear failure.

Black (2007) investigated the aspect of settlement performance and cited an L/d ratio of 8 for serviceability criteria. This work also identified that a "block failure mechanism" was prevalent in small column groups whereby the columns and confined central clay region acted as a single entity.

The degree of group interaction is highly dependent on design criteria such as column spacing, column aspect ratio (L/d) and group configuration. Other influencing factors are believed to be the stress concentration ratio between the column and soil, the shear strength of supporting medium and the rigidity of the foundation. The uncertainty surrounding how these factors influence group performance further exacerbate limitations of the current design protocol and make confident predictions of group performance problematic.

With the exception of Hughes and Withers (1974) work, most of the physical modelling work to date was based on the post examination of exhumed columns after loading to failure. For this reason, it was decided to examine group interaction characteristics of small column groups using a novel non-intrusive physical modelling technique of transparent soil in conjunction with Particle Image Velocimetry (PIV). The technique enabled visualisation inside the soil, real time continuous displacement tracking and the quantification of pre-failure strains up to failure. The transparent soil mixture used in this research was that developed by Gill (1998) and further enhanced by Hird and Stanier (2011).

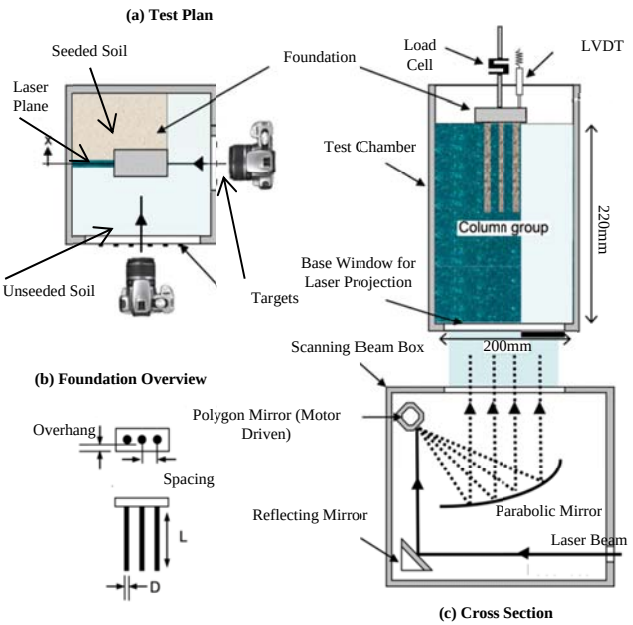

Figure 1. Experimental Configuration

2 T EST CONFIGURATION

Two large test chambers (200mm[L] x 200mm[W] x 560mm[H]) were constructed, in which repeatable soft 'clay' beds (c_u = 12kN/m^2) were prepared from slurry. These were fabricated from aluminium and incorporate Perspex windows to allow laser field illumination and photographic imagery. To enable non-axisymmetric conditions to be modelled the laser field was introduced from the base of the model using a laser scanning beam box (Figure 1). This box incorporates a motor driven polygon mirror and secondary parabolic mirror to disperse the main laser beam to produce a parallel continuous sheet of laser illumination. The stone columns were installed using a using a replacement technique with stress controlled compaction, ensuring repeatable dense and uniform columns, whereby the initial stress state in each column and the surrounding soil was assumed to be consistent throughout the test programme. A digital SLR camera was used to record images during loading of the foundation using the continuous shooting mode. Algorithms are used to minimise error caused by photogrammetric lens.

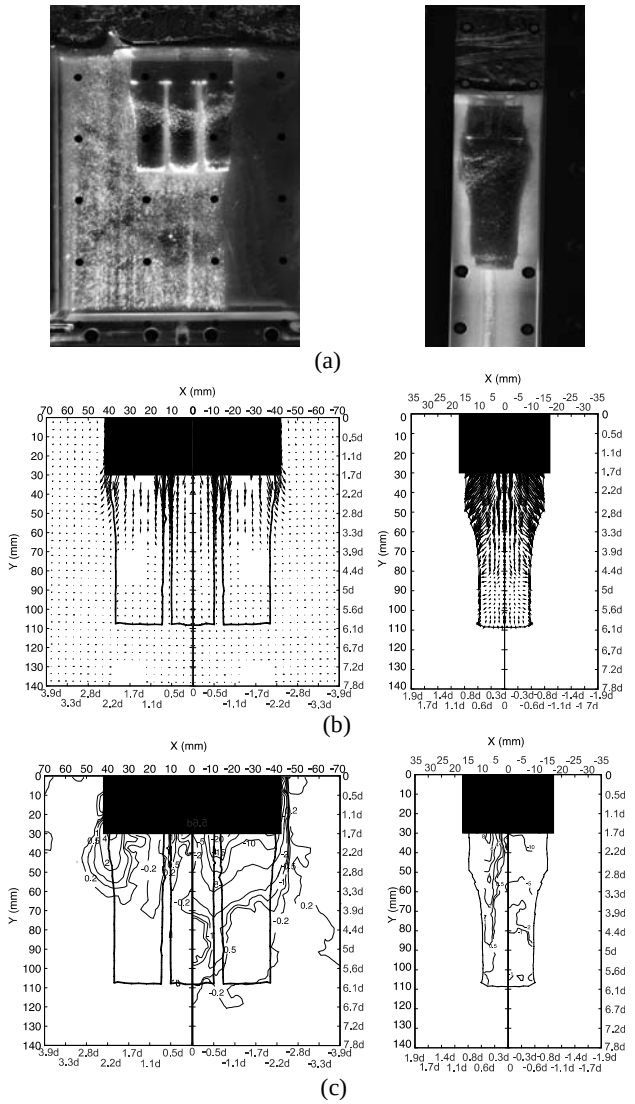

Figure 2. Test 2. (a) front and side view photographs (b) velocity vector fields and (c) horizontal and vertical contour displacement fields.

3 CONCLUSIONS

A total of 6 column strip foundation tests were carried out using 18mm diameter stone columns. The test programme concentrated on assessing the influence of the fundamental dimensionless parameters, recognised in previous research to have the most influential effect on stone column behaviour and bearing capacity, L/d and A_r.

Typical test images and PIV output are presented in Figure 2 (Test 2 - L/d = 6, A_r = 3 shown). Figure 2(a) shows test images from the dual camera system, while Figures 2(b) and 2(c) portray velocity vector fields and contours of soil displacement in the x and y directions respectively at 30mm footing displacement.

In contrast to the isolated columns which failed in an axisymmetric manner, local shear failure, bulging, bending, punching and block failure were all observed for column strip foundations, depending on the geometrical configurations employed. Column length played a particularly important role in optimising the bearing capacity of column strip foundations. Increasing column length from 4d to 6d and 8d at a spacing of 1.55d was shown to improve the load capacity of the composite foundation by 29% and 67%. It was concluded that the critical length in terms of optimising the bearing capacity of a vibro strip foundation is 8d.

Increasing foundation size rather than column length was found to be more effective in increasing the bearing capacity of vibro column strip foundations. Increasing footing size and correspondingly increasing A_r from 3 to 4 and 5 was seen to protect the upper column from bulging and increase its radial zone of influence of the column in the surrounding soil, resulting in increases in bearing capacity of 22% and 29% respectively. It was concluded that provision of a footing overhang of over 0.4d should prevent shear failure in vibro strip foundations.

4 ACKNOWLEDGMENTS

Financial support to this project by EPSRC (grant reference GR-0123783) is gratefully acknowledged. This project was conducted in collaboration with Keller Ground Engineering and was supervised by Dr Jonathan A Black. The work was completed at the University of Sheffield.

REFERENCES

Black, J.A. (2007). The settlement performance of a footing supported on soft clay reinforced with vibrated stone columns. *PhD Thesis.* The Queens University of Belfast.

Gill, D. (1999) Experiemental and theoretical investigations of pile and penetrometer installation in clay. *PhD Thesis*, Trinity College Dublin.

Hird, C., Ni Q. And Guymer, I. (2008). Physical modelling of displacements around continuous augers in clay, Proc. 2nd British Geotechnical Association International Conference on Foundations 1:565-574.

Hu, W. (1995). Physical modelling of group behaviour of stone column foundations. *PhD Thesis*, University of Glasgow.

Hughes, J.M.O. and Withers, N.J. (1974). Reinforcing of soft cohesive soils with stone columns. *Ground Engineering*, Vol. 2, p42-49.

McKelvey, D. (2002). The performance of vibrated stone column reinforced foundations in deep soft ground. *PhD Thesis.* The Queens University of Belfast.

Priebe, H.J. (1995) The design of vibro replacement. *Ground Engineering*, Vol.28, No. 10, pp 31-37.

Stanier, S. (2011).Physical modelling of deep foundations. *PhD Transfer Report.* University of Sheffield.

White, D.J., Take, W.A. and Bolton, M.D. (2003) "Soil deformation measurement using particle image velocimetry (PIV) and photogrammetry" *Geotechnique* 53, No.7, 619-631.

Investigating rock-steel interfaces for tidal stream generator gravity foundations

A. D. Ziogos
Division of Civil Engineering, University of Dundee, UK
Supervisor: M.J. Brown

ABSTRACT: As a part of a larger study which aims to develop enhanced gravity foundations for marine energy generators, field investigations and laboratory interface testing were carried out in order to explore the shear behaviour of rock-steel interfaces at relatively low normal stresses, similar to those encountered at foundation-seabed interfaces. Results revealed that the shear strength of the interface reduces with increasing compressive strength of the rock analogue but increases with increasing roughness of the steel.

KEYWORDS: rock-steel interface, direct shear, gravity foundations, marine generators

1 INTRODUCTION

Tidal energy generators form a relatively new technology in the nearshore/offshore renewables sector which offers a long term predictable energy resource. Tidal energy is in a rather early stage of development and that keeps the levelised cost of energy high, since a predominant technology is yet to be established. Many significant tidal resources lie around the UK, but a cost reduction needs to be achieved in order to make the deployment of commercial tidal arrays financially viable. Foundation and deployment of the generators account for up to 33% of the total cost and a reduction in cost is necessary to allow the expansion of tidal energy (Carbon Trust 2011).

Gravity based structures (GBS) –usually made from steel or concrete- seem to be a promising foundation solution, as they can be constructed onshore and deployed in a relatively narrow time window, keeping the vessel costs low. In addition, recovery is also relatively straight forward and environmental impact is minimised.

Tidal generators are mostly deployed in locations where strong tidal currents occur ($v > 2.5$m/s) which may wash out the seabed sediments and leave exposed bedrock as foundation surface (Small et al 2014). This poses the significant challenges of how steel and concrete foundation interfaces perform under predominantly horizontal loading on exposed rock seabeds. This requires an understanding of interface behaviour of varying rock types and surface character and roughness at relatively low effective stresses.

This paper discusses field work carried out at locations with significant tidal resources, as well as, direct shearbox tests, carried out in order to investigate the rock-steel (seabed-foundation) interface shear behaviour.

2 FIELDWORK

Onshore field investigation was carried out in the vicinity of the Pentland Firth, Scotland, UK which represents a very significant portion of total UK tidal stream energy potential (Carbon Trust 2011). The fieldwork was intended to recover rock samples for laboratory characterisation and investigate the challenges to tidal stream sea-bed interaction through relevant site visits. For example, the wave cut platform of Old Red Sandstone; 200m north east of John O' Groats was visited. The obvious dip of the rock has led to fronts of stratigraphy in the wave cut platform that give rise to a saw-blade type structure with a leading edge and an inclined shielded zone (figure 1). These formations may complicate the deployment and levelling of tidal generators and the utilisation of footings with adjustable height or seabed preparation may be required. The site visited resulted in the recovery of fresh and weathered samples of Old Red Sandstone and Caithness Flagstone which will be used for further testing.

Figure 1: Old Red Sandstone wave cut platform at John O' Groats, UK. Zigzag line displays saw blade structure.

3 LABORATORY INTERFACE TESTING – EXPERIMENTAL EQUIPMENT AND MATERIALS USED

Initial interface testing between cement blocks (rock analogue) and steel plates (foundation analogue) were carried out utilising a 60x60mm modified direct shearbox. Testing was carried out under constant normal stress conditions and four normal stress levels (σ_v = 10, 50, 100 and 200 kPa) were used in order to cover the range of the stresses normally induced by a tidal generators' GBS. The shearing rate was constant at 1.2mm/min and the total shear displacement was 10mm for each test.

The shearbox assembly was modified in order to increase the reliability of the results. The bottom half of the shearbox was replaced by a steel block with an interchangeable surface (so that various levels of steel roughness and pattern could be tested). This steel block was longer along the direction of shearing, so the rock analogue (placed on the top half) was always in contact with the steel surface during the whole test. The problem of snagging of the cement block at the edges of the bottom half of the shearbox is also tackled with this configuration. Surface characterisation of tested materials was carried out utilising a stylus contact profilometer.

Simulating rock, especially rock joints, using concrete is common in the literature (de Toledo & Freitas 1993), so high strength cement was used in order to manufacture rock analogues with both controllable roughness (R_a) pattern and unconfined compressive strength (UCS). Various techniques (e.g. polishing and machining) were used for the surface preparation of the steel samples resulting in a wide range of rock-steel relative interface roughness. Properties of the rock analogues and steel plates used are presented in table 1.

Table 1: Rock analogue and steel, roughness and strength properties

	Rock Analogue		
	Type1	*Type 2*	*Type 3*
R_a (μm)	2.4	2.4	2.4
UCS (MPa)	15.0	35.0	65.0
	Steel Plate		
	Type 1	*Type 2*	*Type 3*
R_a (μm)	0.4	8.5	34.0

4 RESULTS AND DISCUSSION

The effect of surface roughness on the interface behaviour along with the effect of rock's unconfined compressive strength was investigated.

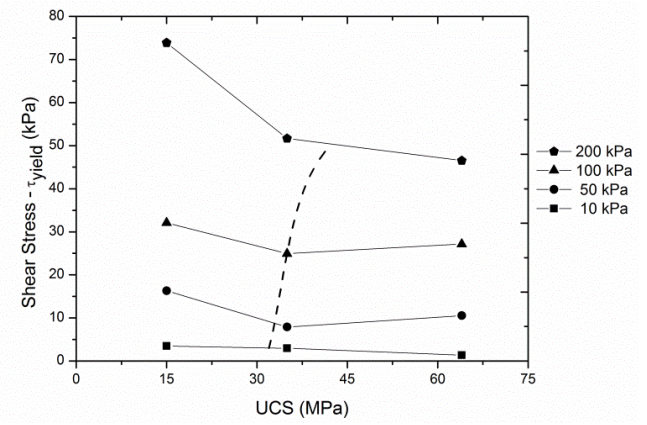

Figure 2: Relationship between shear strength and UCS for rock analogues against steel plate type 1 with R_a=0.4μm.

As seen in figure 2, the strength of the interface increases as rock's compressive strength decreases and this occurs for higher value of UCS as the normal stress level increases. The dashed line connects assumed points of compressive strength (at each stress level), at the point where compressive strength seems to affect shearing resistance. To the left of this assumed contour the shear stress is seen to increase significantly. This is relatively crude based upon the limited data shown but it highlights a critical UCS/σ_v ratio at which enhancement of shear strength occurs, possibly due to crushing on the cement's surface.

An increase in steel's surface roughness led to an increase in the shear strength and generated a rather ductile behaviour. Interface strength doubles when the steel's R_a increases from 0.4 to 8.5μm, but a very small difference is noticed between 8.5 and 34μm, as seen in figure 3. This suggests that interfacial behavior is governed by relative roughness of the materials, so a relative roughness ratio $R_{a,steel}/R_{a,cem}$ may be considered similar to the R/D_{50} ratio used for sand steel interface testing (Uesugi and Kishida 1986). For a specific rock analogue's roughness (R_a=2.4μm in this case), there is possibly a value of the steel's roughness, above which, further increase (in steel's roughness) doesn't significantly affect the shear strength. This is the value which establishes the maximum interlocking of the interface and further investigation is required to determine it for different rock types. The results in figure 3 have been normalised by UCS, as is often adopted for rock socket pile design (adhesion factor, α) but α is several orders of magnitude smaller in this case.

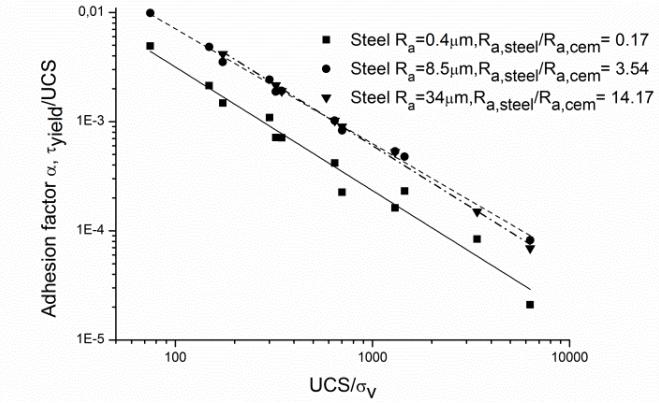

Figure 3: Adhesion factor α vs normalised UCS for three values of relative roughness of rock analogue-steel interfaces.

This difference is likely to be by the higher normal stresses encountered. Also, dilation in rock sockets is confined by the surrounding rock mass (constant normal stiffness conditions) and as a result the normal load increases when dilation occurs. In addition, the interface is bonded (typically cast insitu pile). The values of UCS have also been normalized by σ_v as this appears to have significant effect (figure 2), but this is not undertaken for socket piles as σ_h is difficult to determine.

5 CONCLUSIONS

Field investigations carried out and revealed issues that complicate the deployment of support structures and should be considered during the design process.

Interface tests on rock analogue-steel interfaces revealed that the shear strength reduces with increasing compressive strength of the rock analogue but increases with increasing roughness of the steel. Results indicate that interface behaviour is governed by two critical ratios, UCS/σ_v and $R_{a,steel}/R_{a,cem}$ (compressive strength and roughness effect, respectively) and further laboratory investigation is needed in order to establish a better understanding of this phenomenon.

Material characterization and interface testing with real rock samples, similar to those found at locations with significant resources is being undertaken at the time of writing in order to verify the initial findings. In the near future a larger (300mm x 300mm) shearbox is planned to be utilized in order to investigate a wider range of real rock steel combinations with natural surfaces under a wider range of shear stresses.

6 ACKNOWLEDGEMENTS

This project is sponsored by the Energy Technology Partnership (ETP) and Lloyd's Register EMEA and co-supervised by Ana Ivanovic, University of Aberdeen.

7 REFERENCES

Carbon Trust (2011): "Accelerating Marine Energy". [online] Available at: https://www.carbontrust.com.

de Toledo, P.E.C. & de Freitas, M.H. (1993): "Laboratory testing and parameters controlling the shear strength of filled rock joints". *Geotechnique* 42(1): 1-19.

Small, A.A., Cook, G.A., Brown, M.J. (2014) "The geotechnical challenges of tidal turbine projects". Proc. of the ASME 2014 33rd Int. Conf. on Ocean, Offshore and Arctic Engineering (OMAE2014) 8-13 June, 2014, San Francisco, USA.

Uesugi, M., & Kishida, H., (1986a) "Influential factors of friction between steel and dry sands". *Soils and foundations* 26(1): 33-46.

Uesugi, M., & Kishida, H., (1986b) "Frictional resistance at yield between dry sand and mild steel". *Soils and foundations* 26(4): 139-149.

Screw piles as offshore wind turbine foundations

T. A. Al-Baghdadi
Division of Civil Engineering, University of Dundee, UK.

ABSTRACT: Screw piles with large diameter helical plates may prove a useful alternative to current foundation solutions for deeper water offshore renewable foundations. Currently these foundations are relatively small diameter and have low lateral capacity (H) although have the benefits of efficient axial capacity and easy low noise installation. In order to upscale these foundations for offshore renewable foundations 3D FE analysis has been used to look at optimisation of helical plate positioning (S/D ratio) and near surface plate installation. The results of this modelling will be used to inform the optimisation of centrifuge model testing of inflight installed screw anchors. A new apparatus is currently being built to be used in the centrifuge tests, so that screw piles models will be installed and tested in flight. Initial results from the 3D FE work suggest that near surface helical flanges are beneficial for lateral capacity under compressive vertical loading (V) but their effect is reduced when in tension.

KEYWORDS: screw piles, sand, offshore wind power, centrifuge physical modelling, numerical modelling.

1. INTRODUCTION

The future wind farm developments in the UK that will take place under Round III will be in deeper water (up to 70 m) and will be further from shore (up to 80 km). The monopiles which are currently used as wind turbine foundations are manufactured from steel with large diameters (up to 6 m) and are deployed in water depths typically not exceeding 20 – 25 m (Scharff & Siems, 2013). As the water depth increases the economic suitability and ability of this foundation solution to perform reduces with alternative foundation solutions such as gravity based and jacket structures becoming more attractive in water depths above 35 m (BVG Associates, 2013).

The dominating loads in the offshore foundation are lateral and moment loads rather than vertical loads due to the water depth in addition to the wind loading on the turbine at high level.

If it is assumed that in deep water that jacket structures (or similar) will be used then suitable foundations need to be designed to support the V-H-M loading generated by the turbine and loading on the jacket. Historically these may have consisted predominantly of piles driven through the structure or pre-installed in a template. Unfortunately, pile driving requires specific installation plant and its use is being restricted due to the perceived noise impact on marine mammals (SMRU Ltd, 2007). This means a quick and noise free alternative with reduced plant requirements is needed.

The first recorded use of screw piles (or helical piles/anchors) was by Alexandre Mitchell in 1836, for ship mooring, and since then, they have been used widely at limited size for onshore applications (Perko, 2009). This type of foundation has many advantages which can lead to substantial reductions in foundation costs mainly through material costs and time. They also have the benefit of limited noise during installation and existing simple techniques for estimating capacity based upon the torque measured during installation. Where they do lack in performance is in the ability to carry lateral loads and the large axial loads associated with offshore application. Thus, there is a need to look at upscaling the onshore equipment to fit this new application and also novel solutions to the need for enhanced lateral capacity. This study aims to develop this new format of screw pile and test performance under varying load directions and develop solutions to enhance lateral capacity. It will look at the effects of size and S/D ratio on vertical capacity, explore optimum positioning of helical plates to enhance lateral capacity and investigate and develop improved capacity design techniques taking into account torque-capacity relationships.

2. NUMERICAL MODELLING

2.1 3D Finite Element Modelling (FEM)

The Finite Element software "PLAXIS 3D 2013" was used to model and analyse screw piles with shaft diameter 0.219 m and 2 m diameter helical plate in saturated dense sand. This numerical analysis was carried out to investigate the applicability of FEM analysis for screw piles under lateral and vertical loads to allow design and testing of optimised pile arrangements in centrifuge testing. Centrifuge testing will also be used to verify the results of FEM.

Hardening soil with small-strain stiffness model (HS small in Plaxis) which was previously calibrated by Al-Defae et al. (2013) was used as a constitutive model for the HST95 sand with a relative density of 80%. Sand with high relative density has been chosen to determine the maximum capacity of the screw pile so the equipment can be specified accordingly for the centrifuge testing. The pile and helical plate parameters are shown in table 1. The screw piles have been modelled using the symmetrical assumption about the y-axis, so that the plate has modelled as a horizontal plates and the slight change in plate inclination has been neglected.

The vertical and lateral failure load has been assumed to be given a displacement equal to 0.1 of the pile diameter (d). The helical plate spacing (S) to helical plate diameter (S/D) ratio has been varied from 1 to 4.9 to investigate the effect of S/D ratio on the screw pile capacity. The top helical plate was placed at 0.5m below the ground or seabed surface to increase lateral capacity.

Table 1. Pile and helical plate parameters for 3D FEM

Pile and helical plate parameters	value
Pile type	Plate
Material type	Linear elastic
Unit weight: kN/m^3	68
Young's modulus E_p: (kPa)	2.05×10^8
Poisson's ratio (ν)	0.3
Pile diameter (d): m	0.219
Pile length (L): m	20
Helical plate diameter (D): m	2.0
Thickness (t): m	0.01

2.2 Results and discussion

The results of the FEM show there is a significant increase in the screw pile vertical capacity under tension and compression loads when compared to a straight shafted pile of 0.219m diameter (Figure 1). In contrast, the lateral capacity under tension loads is very similar to that experienced for the straight shafted pile with enhancement (approximately 30%) only

occurring as the vertical load tends to zero. The benefit on lateral capacity of including the near surface helical plate becomes apparent under vertical compressive loading where the lateral capacity over a straight shafted pile effectively doubles. The use of S/D ratio equal to 3 appears to be the optimum giving the highest vertical capacity. Knappett et al. (2014) found that the optimal S/D ratio is about 3 for screw pile in dense sand and they highlighted that this ratio resulted in strong cylindrical shear instead of the weaker individual shear for the helical plates. Also, the field tests results for uplift screw piles in sand conducted by Lutenegger (2011) showed that the transition from cylindrical shear to individual shear for the helical plates happens at S/D ratio equal to 3. It is apparent from the results that the addition of helical plates has significant beneficial effects on vertical tension and compression behaviour and that near surface helical plates can be beneficial in resisting lateral loading in conjunction with vertical compression.

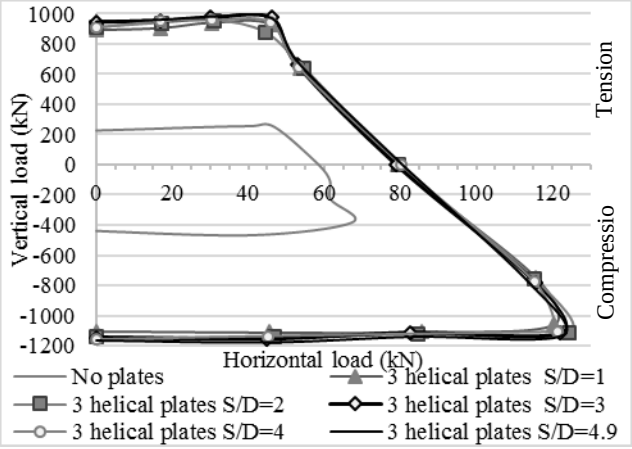

Figure 1. FEM results of V-H failure envelope for screw pile with different helical plate spacing to helical plate diameter ratio (S/D).

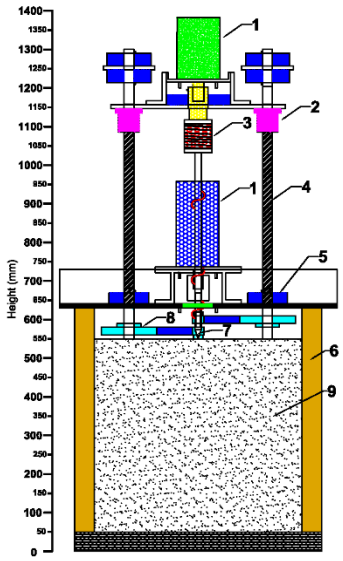

1 Servomotor 2 Rolled ball screws 3 torque &force transducer
4 Screw shaft 5 Flange bearing unit 6 Container
7 Screw pile 8 Gear transmission 9 Sand

Figure 2. Schematic of the proposed centrifuge installation system under construction.

3. CENTRIFUGE MODELLING

3.1 Test apparatuses

The centrifuge tests will be performed in the geotechnical centrifuge of the University of Dundee, which can carry a model of up to 1000kg (including the container). A container with internal dimension 500 mm width, 767 mm length, and 550 mm height will be used for this work. In order to install and test screw piles models in flight in the centrifuge at 50g. A new apparatus will be designed and manufactured to be used in the centrifuge tests, so that screw piles models will be installed and tested in flight. This apparatus will be consist mainly of two motors to provide rotation and vertical translation for the screw pile, a torque and axial force transducer and displacement measurement as shown in Figure 2.

3.2 Soil properties

The soil will be used in centrifuge tests is Congleton HST95 well-rounded silica sand with maximum and minimum density are 17.58 kN/m^3 and 14.59 kN/m^3 respectively, and the critical angle of friction 32° (Lauder et al., 2013). This sand will be used in dry state with wide range of relative densities in the centrifuge tests.

4. CONCLUSIONS

In this study, a novel approach has been suggested to use screw piles for offshore wind turbine foundations. Numerical modelling has been used to investigate the (S/D) ratio effect on the pile capacity, and it has been found that using S/D=3 is the optimum value to give maximum vertical resistance for the screw pile. Also, the lateral capacity of the screw pile has increased significantly by adding the helical plate near the surface. However, their effect is reduced when in tension. A new apparatus will be design and manufacture to be used in the centrifuge tests for screw pile installation and testing.

However, these results of the numerical modelling need to be verified and validated with the result centrifuge modelling tests.

5. ACKNOWLEDGEMENTS

This is a 3 year research project supported by the Iraqi Ministry of Higher Education and Scientific Research (MOHESR) with collaboration and assistance from the Ministry of Municipalities and Public Works in Iraq (MMPW).

6. REFERENCES

Al-Defae, A., Caucis, K., and Knappett, J. (2013). Aftershocks and the whole-life seismic performance of granular slopes. *Géotechnique*, 63 (14), 1230–1244.

BVG Associates. (2013). *Towards Round 3 : Building the Offshore Wind Supply Chain. A review for The Crown Estate on how to improve delivery of UK offshore wind*. Retrieved from http://www.energyparkfife.co.uk/content/publications/Supply_Chain_gap_analysis_-_BVG.pdf

Knappett, J.A., Brown, M.J., Brennan, A.J. and Hamilton, L. (2014). Optimising the compressive behaviour of screw piles in sand for marine renewable energy applications. Int. Conf. On Piling & Deep Foundations, Stockholm, Sweden, 21st-23rd May 2014.

Lauder, K., Brown, M.J., Bransby, M.F. and Boyes, S. (2013). The influence of incorporating a forecutter on the performance of offshore pipeline ploughs. *Applied Ocean Research Journal.* Vol. 39. pp 121–130.

Lutenegger, A.J. (2011). Behavior of multi-helix screw anchors in sand. In proceeding of the 14th Pan-American Conference on Soil Mechanics and Geotechnical Engineering, Toronto, Ont.

Perko, H. A. (2009). *Helical piles : A practical guide to design and installation.* Hoboken, N.J: John Wiley & Sons Inc

Scharff, R., and Siems, M. (2013). Monopile foundations for offshore wind turbines - solutions for greater water depths. *Steel Construction*, *6*(1), 47–53. doi:10.1002/stco.201300010

SMRU Ltd. (2007). Assessment of the potential for acoustic deterrents to mitigate the impact on marine mammals of underwater noise arising from the construction of offshore windfarms. Commissioned and Published by COWRIE Ltd (Project reference DETER-01-07).

Spudcan-Footprint Interaction Issues During Offshore Jack-up Rig Installation

S. A. Whyte
Fugro GeoConsulting Limited

ABSTRACT: Repeated installation and removal of jack-up rigs create footprints on the seafloor. Spudcan-footprint interaction issues can occur during the reinstallation of jack-up rigs at sites where numerous spudcan footprints already exist, due to the planned spudcan positions overlapping the footprints. Three-dimensional large-strain finite element analysis (FEA) is presented to assess the effect that spudcan footprints have on the installation behaviour of a jack-up rig for a typical site in the North Sea. Single leg FEA predicted that spudcan sliding and induced bending moments within the legs are expected at a spudcan-footprint centre-to-centre offset of 0.65 times the spudcan diameter. Single leg analysis is found to be suitable for estimating the expected spudcan sliding by considering the two extremes of leg-hull fixities; however, it has been shown that FEA of the full jack-up rig incorporating all three legs and the hull is required to more accurately predict the magnitude of expected spudcan sliding and induced bending moments within the legs. Based on an assessment of several potential remediation strategies, soil excavation is considered to be the most feasible remediation strategy at several sites within the North Sea in respect of spudcan-footprint interaction issues.

KEYWORDS: spudcan-footprint interaction, offshore, finite element analysis, jack-up rig

1 BACKGROUND

In the offshore oil and gas industry, mobile jack-up rigs are regularly positioned at fixed jacket platforms for drilling operations. Jack-up rig installation can cause several geotechnical issues.

A jack-up rig consists of a floating hull, generally triangular, with large diameter steel lattice legs at each corner. The rig is towed to the platform location and, once in position, the legs are lowered until they are in contact with the seafloor. By continuing to lower the legs, the hull raises out of the water providing a stable platform from which drilling can be performed.

Figure 1. Example of jack-up rig alongside a fixed platform

Jack-ups rigs usually have spudcans (footings) with diameters (D) of between 15 m and 24 m. The spudcans penetrate to the required depth by applying a maximum preload which is higher than the operating load to ensure an adequate bearing capacity safety factor for the footings. Penetrations can be up to 1.5 D within very soft clay; however, typically within the North Sea, where stiffer clays are more common, penetrations are significantly lower.

2 SPUDCAN-FOOTPRINT INTERACTION ISSUES

Repeated installation and removal of jack-up rigs create spudcan footprints on the seafloor. Spudcan-footprint interaction issues can occur during the reinstallation of jack-up rigs at sites where numerous spudcan footprints exist, due to the planned spudcan positions overlapping the footprints (Stewart and Finnie 2001; Jardine et al. 2001; Cassidy et al. 2009).

The Society of Naval Architects and Marine Engineers (SNAME) provides recommended practice for a wide range of operational issues of mobile jack-up rigs. SNAME (2008) states that spudcan-footprint issues are likely to occur at spudcan-footprint centre-to-centre offsets up to and including 1.0 D.

Spudcan-footprint interaction issues during jack-up installation have become a common issue for jack-up rig operators, particularly in the North Sea where a significant number of jack-up installations are performed alongside fixed jacket platforms.

Fugro is aware of several instances in the North Sea in which spudcan-footprint interaction issues have caused significant delays in drilling operations. Figure 2 presents example bathymetry data from a site in the North Sea in which several jack-up rig installations resulted in a significant number of footprints on the seabed.

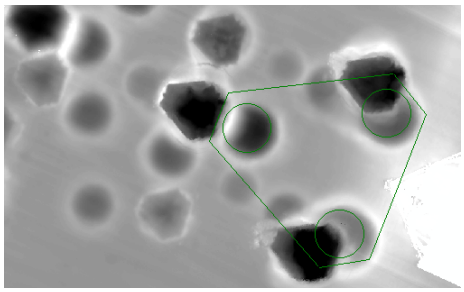

Figure 2. Example spudcan footprint bathymetry data

3 FINITE ELEMENT ANALYSES

SNAME (2008) provides little guidance on the analysis of spudcan-footprint interaction issues; however, it recommends that where sufficient geotechnical data exist, finite element analysis (FEA) is preferred to review the risks associated with spudcan-footprint interaction.

FEA spudcan-footprint interaction was carried out at a site in the North Sea (Figure 3) with multiple footprints. In this study a single leg was modelled with a spudcan-footprint centre-to-centre offset of 0.65 D to the deepest footprint. Within the FEA, clay layers were modelled as undrained, using a linear elastic-perfectly plastic Von Mises model; the sand layers were modelled with a Mohr-Coulomb model. Within the FEA the spudcan was penetrated under an axial load corresponding to

the preload level for the jack-up rig. Owing to the large-strain nature of the problem, adaptive re-meshing was incorporated, allowing the finite element mesh to be initially optimised and then to be re-meshed whenever element distortions exceeded a predetermined level. Previous spudcan footprint interaction FEA studies have utilised the less efficient 'mosaic approach' to accommodate excessive mesh distortion (for example Jardine et al. 2001).

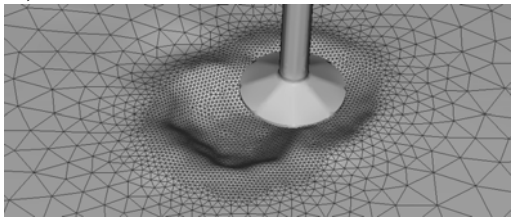

Figure 3. Spudcan-footprint FEA model with imported bathymetry

The FEA model was validated by comparing the predicted penetration to that of limit state solutions and data obtained from recorded spudcan penetrations (Figure 4).

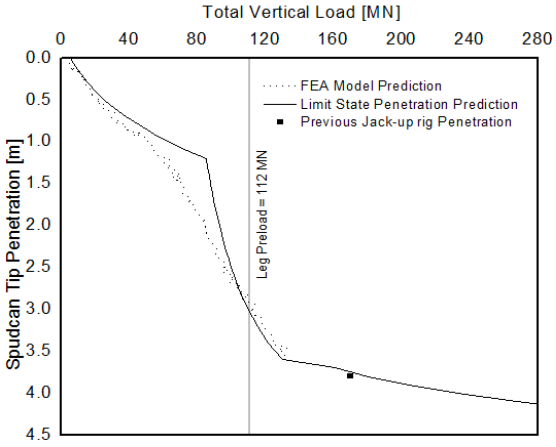

Figure 4 FEA Validation example

Previous spudcan-footprint FEA interaction studies incorporate a single idealised footprint (for example Jardine et al. 2001). However, in some instances planned spudcan deployment positions will result in interaction with two footprints which have complex geometry. Therefore, when carrying out FEA for a spudcan-footprint interaction study it is important to correctly model the seafloor geometry. The seafloor profile was created in the FEA model by importing bathymetry data directly into the model (Figure 3).

The fixity assumed at the leg-hull connection is critical for single leg analysis. A fixed connection results in the prediction of the maximum induced bending moment within the jack-up leg. A lateral roller connection (i.e. fixed in rotation and free for lateral movement) results in the maximum lateral movement of the spudcan (Figure 5). Therefore, these two fixity cases provide an upper and lower bound solution. The FEA predicted that, during preloading, the spudcan will slide in the order of 3 m towards the existing spudcan footprint with an associated maximum bending moment of 235 MNm within the leg.

Single leg analysis is sufficient to predict the mechanism at one leg of the jack-up rig. However, in some instances due to the footprint locations relative to the planned position of the spudcans, it is advantageous to predict the global performance of the jack-up rig. Additionally, during jack-up rig installation the magnitude of any lateral spudcan movements may be controlled by the sequencing of the leg lowering and the subsequent fixity created at each leg. For example, if one leg leads installation, it is possible to create a greater fixity during lowering of the other legs. It is shown that by performing FEA of the full jack-up rig incorporating all three legs and the hull it is possible to predict a more accurate prediction of the global performance of the system during installation.

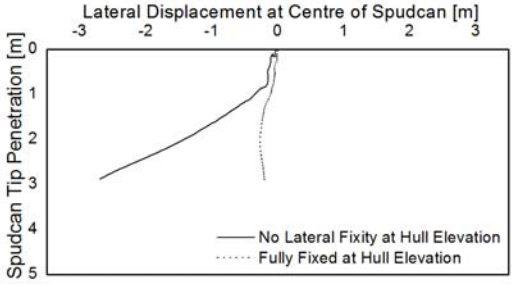

Figure 5. Leg-hull fixity effect

Sensitivity analysis needs to be performed as part of any FEA. Parameter sensitivity analysis is particularly crucial for spudcan-footprint interaction assessments because of the high degree of uncertainty in the soil parameters within the footprints (unless cone penetration testing data from the footprints are available). Previous jack-up rig installations cause a change in the soil profile due to deformation of the soil layers and a change in soil parameters due to remoulding and reconsolidation effects (Cassidy et al. 2009).

4 POTENTIAL REMEDIATION

Several retrospective remediation strategies exist to mitigate spudcan-footprint interaction issues in the North Sea: footprint infilling, stomping and excavation. A review of spudcan-footprint remediation strategies at several North Sea sites shows soil excavation to be the most beneficial.

5 CONCLUSION

FEA is a useful tool to assist in determining the potential risks in jack-up rig installations due to spudcan-footprint interaction. Single leg analysis was found to be suitable for estimating the expected spudcan sliding by considering two extreme leg-hull fixities; however, FEA of the full jack-up rig incorporating all three legs and the hull is required to more accurately predict the magnitude of expected spudcan sliding and induced bending moments within the legs. Single leg FEA from a North Sea site which experienced spudcan-footprint interaction issues shows that spudcan sliding and excessive induced bending moments within the leg are likely at a spudcan-footprint centre-to-centre offset of 0.65 D.

6 ACKNOWLEDGEMENTS

The author extends thanks and appreciation to Nigel Kee, Mike Rattley and Laura Connochie for their support.

7 REFERENCES

Cassidy, M.J., Quah, C.K. and Foo, K.S. 2009. Experimental investigation of the re-installation of spudcan footings close to existing footprints. Journal of Geotechnical and Geo-environmental Engineering (ASCE), 135, pp. 474-486.

Jardine, R.J., Kovacevic, N., Hoyle, M.J.R., Sidhu, H.K. and Letty, A. 2001. A study of eccentric jack-up penetration into in filled footprint craters. *Proc. 8th International Conference, The Jack-up Platform*, City University, London.

Society of Naval Architects and Marine Engineers (SNAME), 2008. *Recommended Practice for Site Specific Assessment of Mobile Jack-up Units*. Technical and Research Bulletin 5-5A, First Edition, Revision 3.

Stewart, D.P. and Finnie, I.M.S. 2001. Spudcan-footprint interaction during jack-up work overs. *International Society of Offshore and Polar Engineers (ISOPE)*, Cupertino, California. (1). pp. 61-65.

Developing instrumented model piles for geotechnical laboratory testing

J T Landers
Ove Arup & Partners Ltd. (Formerly undergraduate student at the University of Limerick, Ireland)
Supervisor: D T Phillips
University of Limerick, Ireland

ABSTRACT: In this paper, a method for installing electrical resistance strain (ERS) gauges on the inside surface of small diameter pipes is presented. A mounting device to install the gauges is discussed. An aluminium model pile of 40mm O.D., 35mm I.D. and 700mm long is instrumented with sixteen ERS gauges, arranged in pairs along the axis of the pile. The results of a rigorous calibration testing exercise are presented and are in good agreement with the theory. A lateral load test was carried out on the instrumented model pile in sand and the bending moment profile during each of the five loading cycles is presented.

KEYWORDS: Instrumentation, model pile testing, electrical resistance strain gauge, calibration, lateral loading,

1 INTRODUCTION

Pile foundations make it possible to build in areas where the soil conditions are unfavourable for shallow foundations. For tall buildings and transmission towers, wind action is the key design force a foundation must resist. In the case of earth retaining structures, piles are used to support open excavations; here also, there is no significant axial force and the only role of the piles is to resist lateral forces.

The majority of experimental testing involving laterally loaded piles are full-scale. This involves a considerable amount of resources, coordination and time. The pile also has to be heavily instrumented to correctly measure the bending moment throughout the depth of the pile. Model piles are a more compact method for testing laterally loaded piles which have seen increased use in recent years. This research aims to identify a simple, reliable approach to instrument model piles with electrical resistance strain (ERS) gauges to allow accurate and repeatable tests to be conducted.

2 LITERATURE REVIEW

A method developed by Caliendo et al. (1999) uses a tool to install ERS gauges on the inside surface of a hollow aluminium model pile. This device consisted of two wings which can expand and contract by means of a rotating screw. The gauges sit on a 'seat' on the edge of the wings which has a curvature to match the inside diameter of the pipe.

O' Looney (2009) instrumented a model pile with ERS gauges to measure the negative skin friction of a pile in sand. His method involved splitting a PVC pipe in two halves, fixing the gauges to the inside surface of the pile, and re-joining the two halves of the pile back together. While this was a very effective method of installing ERS gauges on the inside surface of the pile, it gives no certainty over the distribution of stress across the two joined pieces.

Micro-Measurements (2010) describe a process for installing ERS gauges inside small diameter holes using an inflatable tube inside the pipe. The gauges are temporarily mounted onto the deflated tube, The tube is inserted into the hollow pipe and inflated to a pressure of about 70kPa. After a period of time, the carrier tube can be removed or trimmed to leave the gauges inside the pipe.

3 METHODOLOGY

A mechanical device was built to install ERS gauges on the inside of a model pile. Mechanical construction toy pieces were assembled to create a curved carrier block system which is allowed to pivot on a two strut truss connected to a screw mechanism which allows expansion and contraction of the wings. An image of the device can be seen in Figure 1.

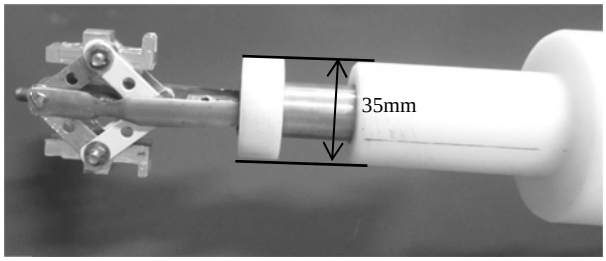

Figure 1. Completed bi-winged ERS gauge installation device with nylon wedges for stability.

ERS gauges type CEA-13-250UW-350 were used to instrument the model pile. The gauges were installed in diametrically opposite pairs. The location of each gauge pair down the length of the pile is shown in Figure 2. The following procedure outlines the sequences of installation using the device;

1. The aluminium pipe was cut to a length of 800mm. 100mm of this was used to cut a notch in the end of the pipe. The notch served to allow a staging area for the device.
2. The inside of the pipe was etched using grit 400 abrasive paper attached to the end of a rotating drill end. The etched pipe was then degreased using acetone. Any acetone residue in the pipe was neutralized using ethanol. The pipe was then allowed a period to dry.
3. A small square of PVC tape was applied on both arms of the installation device. A small square of clear double sided adhesive tape was applied to the outside of the PVC tape to hold the ERS gauge to the PVC tape. The gauge was then bonded, top side down, to the adhesive tape. This step can be seen in Figure 3.
4. A small amount of AE-10 epoxy was prepared and applied to the exposed back of the ERS gauges.
5. The mounting device was inserted into the pipe to the desired distance. The arms were expanded, pressing the ERS gauges to the wall of the pipe. After 24 hours the wings were contracted and the device was removed. The ERS gauges remained bonded to the inside wall of the pipe.

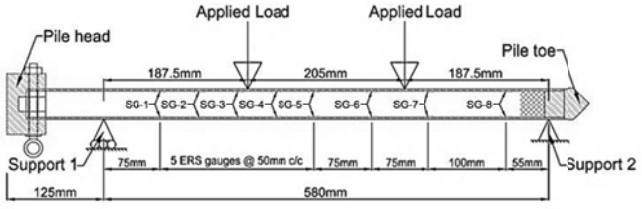

Figure 2. Schematic drawing of the ERS gauges and the loading arrangement of the four-point bending test.

Eight ERS gauge pairs were installed in the model pile. The pile was capped with a block of aluminium machined to allow the wires to safely protrude while also providing an air-tight seal. ERS gauge pair SG-2 was damaged during the installation process and was rendered inoperable. A video of the installation procedure can be viewed at the following link; https://www.youtube.com/watch?v=mr-orc43q-i.

Figure 3. Two ERS gauges sitting on the installation device prior to epoxy resin application.

4 CALIBRATION

The accuracy of the ERS gauges was determined from 13 three-point bending tests and 11 four-point bending tests. Figure 4 shows the results of one four-point bending test. Each ERS gauge pair was averaged and processed to give the bending moment on the external surface of the pile. This was compared against the theoretical bending moment for the same position in the pile. A calibration factor was calculated for each ERS gauge pair based on the three and four point bending tests. The calibration factors were used to reduce potential errors induced during gauge installation.

The resolution of readings to the nearest microstrain, the sensitivity of the gauges to strain change, and repeatability of the measurements were also tested. No significant noise or drift in the strain readings was observed.

Figure 4 shows the results of one four-point bending test on the instrumented pile. The test setup can be seen in Figure 2. The pile head is a free head and attracts no bending moment.

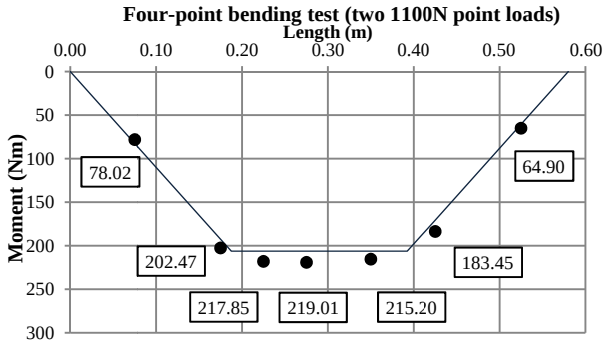

Figure 4. Four-point bending test results showing theoretical and measured bending moments.

5 GEOTECHNICAL LABORATORY TESTING

A lateral load test was carried out on the instrumented pile. The pile was driven into a container of poorly graded medium sand compacted to a relative density of 8.9%. A point load horizontal force was applied to the free pile head 100mm above the top of the sand surface. The pile was loaded with horizontal forces of 196.2N, 392.4N, 588.6N, 784.8N and 981N. The bending moment profiles measured by each of the ERS gauge pairs for the five lateral load tests are shown in Figure 5. Each ERS gauge pair bending moment has been adjusted with the calibration factors. The bending moment in the model pile at the top of the sand was calculated from the applied horizontal force.

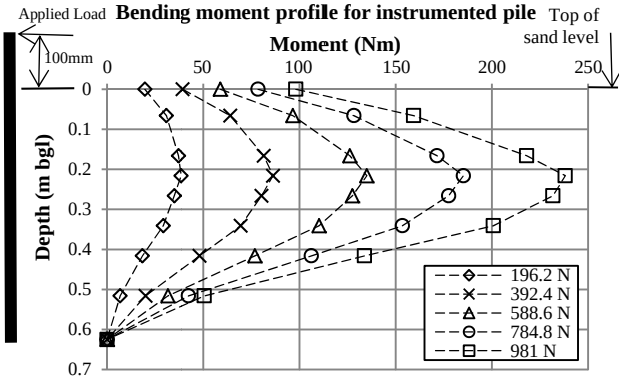

Figure 5.Calibrated bending moment profiles for various horizontal loads with model pile indicatively shown to left of figure.

6 TEST RESULTS, ANALYSIS AND DISCUSSION

Calibration factors ranging between 0.9349 and 1.0561 with R^2-values between 0.992 and 0.997 were calculated for the seven operational ERS gauge pairs installed in this pile.

The calibrated instrumented model pile was used to measure bending moments during a lateral load test in sand with a low relative density.

The method used for installing ERS gauges by using a mechanical installation device allowed accurate and repeatable installation of paired gauges inside a pipe.

7 CONCLUSION

The ERS gauge installation device was a success and will be useful for laboratory based instrumented tests over a range of applications. The calibrated instrumented model pile allowed for measurements of the bending moments during a lateral load test and shows laboratory testing promise for the future.

8 ACKNOWLEDGEMENTS

The author would like to thank Ove Arup & Partners Ltd. for their support to participate in the YGES 2014.

9 REFERENCES

Caliendo, J.A., Anderson, L.R., Rawlings, M.A., 1999. Cyclic lateral loading of a model pile group in clay soil. Report to the Mountain Plains consortium, Utah Transport Center, Report MPC 99-99A.

Landers, J.T., 2013, Strain gauge installation on the inside of a pipe, video, YouTube, 8 January, viewed 20 June 2014, <https://www.youtube.com/watch?v=mr-orc43q-i>.

Micro-Measurements, V. P. G. 2010. How to Install a Strain Gage in a Small, Deep Hole. Application Note VMM-6.

O' Looney, D. A. 2009. Measurement of Negative Skin Friction in Sand Using Instrumented Model Piles. Construction Management Bachelor of Science, University of Limerick. BSc.

Development of coupled centrifuge-numerical modelling: investigation of global tunnel-building interaction

A. Franza, A. M. Marshall, A. O. Abdelatif & C. M. Cox
Faculty of Engineering, University of Nottingham, UK

ABSTRACT: There is an increasing demand for underground space in urban areas for infrastructure development. This has resulted in tunnel construction taking place in close proximity to buried infrastructure and building foundations. Various studies have considered the effect of tunnel construction on buildings; however the global tunnel-ground building interaction problem is still not well understood. This is due partially to the fact that the available modelling tools do not accurately replicate the global behaviour of soil-structure domains. This research aims to enhance physical modelling capabilities by coupling centrifuge and numerical techniques. The research focuses on tunnelling beneath buildings which are founded on piled foundations. In this paper, the proposed method and the developed equipment are presented. The expected outcomes of this research will provide a better understanding of complex tunnel-ground-building interactions which will help to improve the design approach of tunnels beneath buildings.

KEYWORDS: centrifuge, numerical, modelling, coupled, tunnel, soil, structure, interaction, pile

1 INTRODUCTION

In urban areas, the excavation of tunnels for the development of infrastructure and services is becoming increasingly important. Due to the limited availability of underground space, tunnels are generally excavated close to existing surface and buried structures. This scenario is particularly important when constructing tunnels beneath buildings founded on piled foundations. In order to prevent possible damage to structures, engineers need to accurately assess the soil-structure interaction induced by the tunnelling. Although tunnel-soil-structure interaction has recently received considerable attention, a comprehensive understanding of the problem has not yet been achieved. This is due in part to the complexity and non-linear response of the global system (Standing and Potts 2008). To investigate the effect of global interactions, this research aims to develop a new method for modelling the problem of tunnelling beneath framed structures on piled foundations.

In previous studies, the tunnel-piled foundation interaction problem has been analysed using field trials, physical modelling, and numerical simulations (Mroueh and Shahrour 2002, Jacobsz et al. 2004, Kaalberg et al. 2005). However both current physical and numerical modelling methods cannot give an accurate representation of the global tunnel-ground-building interactions. A geotechnical centrifuge allows testing of small scale models within a controlled laboratory environment by increasing the self-weight of the model and thereby reproducing full-scale prototype stresses. Thus soil behaviour and soil-structure interactions are properly modelled within the centrifuge model. Nevertheless, centrifuge methods tend to assume constant loads from the structure to reduce the complexity of the experimental set up. In this way, the superstructure contribution to the foundation response is not modelled and the effect of the modified behaviour of the foundation on the behaviour of the soil is not accounted for. The use of numerical methods is common in structural and geotechnical engineering. Nevertheless, they generally provide poor predictions of tunnelling-induced ground movements unless unrealistic material parameters or sophisticated constitutive models are used (Franzius et al. 2005).

2 METHODOLOGY

The proposed global tunnel-structure analysis method is illustrated in Figure 1. The method couples experimental and numerical modelling tools to benefit from their respective strengths: the numerical model allows accurate simulation of the structure, the tunnel-ground-foundation system is modelled with the centrifuge to accurately reproduce soil and soil-structure interaction behaviour and the coupling is achieved by means of a real-time data acquisition and load-control interface.

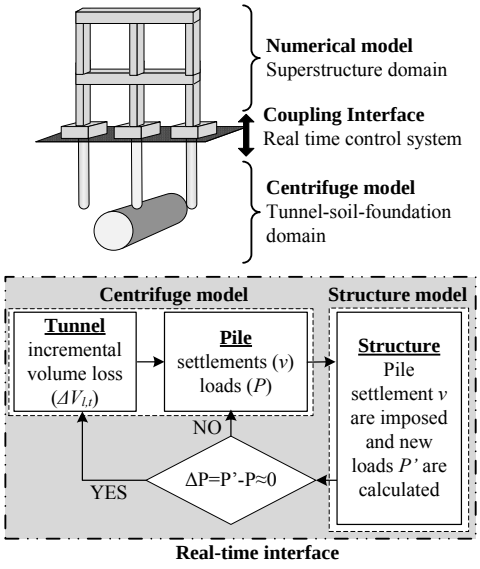

Figure 1. Proposed coupled numerical-centrifuge method

This method can be summarized in the following steps. 1) In the centrifuge, the model piles are driven within sandy ground and loaded using independent actuators to replicate serviceability building loads P_0. After the pile installation, 2) an incremental tunnel volume loss, $\Delta V_{l,t}$, is induced in the model tunnel by using an external volume control system. This volume loss causes ground movements and consequently settlement of the pile group, v. 3) The pile displacements, v, are measured and fed into a real time control system where the numerical simulation is carried out. 4) The incremental pile displacements, v, are passed to the structural numerical model to calculate the

new pile loads, *P'*, accounting for the structure. 5) The modified loads, *P'*, are then fed back into the centrifuge model to adjust the pile loads to the demand values. The cycle, 3) to 5), continues until the coupled system reaches convergence. It is possible afterwards to apply further incremental tunnel volume loss. In order to obtain an accurate coupling of the centrifuge and numerical domain, it is necessary to minimize the incremental volume loss and the load convergence time (i.e. number of required cycles).

The vertical loads and settlements are the main parameters affecting tunnelling beneath piled foundations. Therefore, to minimize the experimental set up complexity, the proposed tests will only consider the vertical pile loads in the centrifuge. The numerical model is designed with this assumption.

3 EXPERIMENTAL EQUIPMENT, REAL-TIME DATA INTERFACE, AND NUMERICAL MODEL

3.1 *Centrifuge equipment*

The experimental facilities will be tested using the University of Nottingham (UoN) geotechnical centrifuge. The following components are part of the equipment (Figure 2).

- Centrifuge package previously developed for tunnelling in greenfield condition (Zhou et al. 2014), including a strong box, a 90 mm diameter model tunnel, a tunnel volume control system, and tunnel pressure measurement.
- Model pile foundation, consisting of a transverse row of full section model piles. The piles are jacked into the ground in-flight prior to tunnel volume loss to properly model the installation of displacement piles. The model piles consist of an 8 mm diameter aluminium alloy round bar over a length of 175mm. The tip is a 4 mm cylinder, with enlarged conical tip, fixed within the round bar. The model piles are instrumented for measurement of axial loads and head settlements. Seven full bridge strain gauges, protected with a 2mm epoxy coating, are placed along the pile shaft at 20mm spacing. An additional half-bridge strain gauge is located at the pile tip, allowing reliable measurement of the base load.
- Loading system. Each pile is independently loaded through a lever system by 5 kN capacity ballscrew actuators with 100 mm stroke. A load cell is installed in-line with the pile head to have a reliable measurement of the head load, which is a critical measurement for the coupling system. In this way the measurement is not influenced by the loading system.
- Foundation settlement measurement system. Each pile settlement is measured with a Linear Variable Displacement Transducer (LVDT) mounted on the instrumentation beam

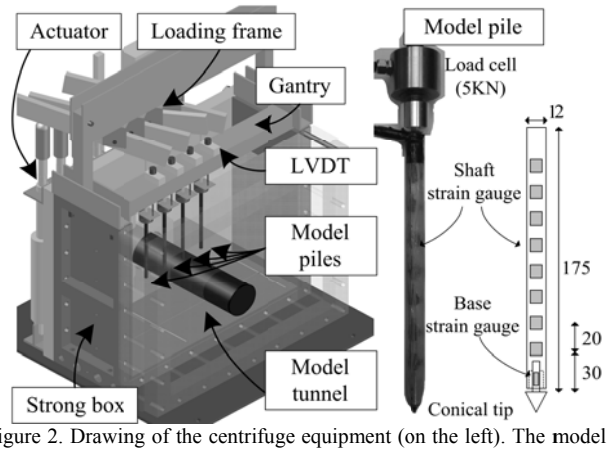

Figure 2. Drawing of the centrifuge equipment (on the left). The model pile (on the right).

3.2 *Real-time interface and control system*

The interface system between the centrifuge and numerical models is designed to allow real-time communication of data between the centrifuge and the numerical models.

The real-time interface is developed in the LabVIEW environment and run on a National Instruments real time embedded controller and motion controller mounted on the centrifuge. The system is designed to 1) retrieve pile settlements and load data from pile LVDTs and load cells, to 2) communicate with the numerical process, to 3) control tunnel volume loss, and to 4) control pile loads.

3.3 *Numerical model*

The numerical model is developed to 1) accept an input of foundation displacements, 2) efficiently perform the structural analysis in less than five milliseconds and 3) output the new pile loads based on the derived solution.

The accurate simulation of prototype framed structures can be performed using the finite element method. At this stage of the research, the global interaction is assessed for the case of linear elastic frames. The effect of various geometries and non-linear plastic behaviour will be considered in future work.

4 CONCLUSION

The paper presents a novel method to study soil-structure interaction through a real-time coupling of numerical and centrifuge modelling. The research aims to investigate the effects of tunnelling beneath buildings founded on piled foundations. The accurate simulation of the global interaction will allow for a more accurate assessment of the behaviour of piled foundations which accounts for the effect of the superstructure.

This research provides a direct link between ground and structural engineering, enhancing centrifuge modelling potential in studying global interaction problems. In general, the outcomes are expected to provide useful data for tunnel design engineers in case of construction of tunnels in urban areas. The method may also be used to study specific and current construction related problems, such as the effect of Crossrail tunnels on buildings in London.

5 ACKNOWLEDGEMENTS

The authors would like to thank the Engineering and Physical Sciences Research Council (EPSRC) for financial support.

6 REFERENCES

Franzius, J. N., Potts, D. M. and Burland, J. B. 2005. The influence of soil anisotropy and K0 on ground surface movements resulting from tunnel excavation. *Géotechnique*, 55 (3), 189-199.

Kaalberg, F. J., Teunissen, E. A. H., Van Tol, A. F. and Bosch, J. W. 2005. Dutch research on the impact of shield tunnelling on pile foundations. *Proceedings of the 16th International Conference on Soil Mechanics and Geotechnical Engineering,* 16 (3), 1615–1620.

Jacobsz, S. W., Standing, J. R., Mair, R. J., Hagiwara, T. and Sugiyama, T. 2004. Centrifuge modelling of tunnelling near driven piles. *Soils and Foundations*, 44(1), 49-56.

Mroueh, H. and Shahrour, I. 2002. Three-dimensional finite element analysis of the interaction between tunneling and pile foundations. *International Journal for Numerical and Analytical Methods in Geomechanics*, 26 (3), 217-230.

Standing, J. R. and Potts, D. M. 2008. Contributions to Géotechnique 1948-2008: Tunnelling. *Géotechnique,* 58(5), 391-398.

Zhou, B., Marshall, A. M. and Yu, H. S. 2014. The effect of relative density on settlements above tunnels in sands. *Proceedings of the 3rd GeoShanghai International Conference on Geotechnical Engineering,* 96-105.

Acoustic emission monitoring of active waveguides to quantify slope stability

Alister Smith & Neil Dixon
School of Civil and Building Engineering, Loughborough University, Leicestershire, UK

ABSTRACT: The active waveguide is installed in a borehole that penetrates stable stratum below any shear surface or potential shear surface that may form beneath a slope. It comprises a metal waveguide rod or tube that provides a low resistance path for acoustic emission to travel from the source at the shear surface to the sensor at the ground surface. The annulus surrounding the waveguide is backfilled with granular soil. When the host slope deforms, the column of granular soil also deforms and this induces inter-particle friction and releases relatively high levels of acoustic emission that can propagate along the waveguide. Field trials and laboratory experiments reported by the authors have demonstrated that acoustic emission rates generated by active waveguides are proportional to the velocity of slope movement. This summary describes the operation of the active waveguide and Slope ALARMS acoustic emission sensor for use in slope stability monitoring. An on-going research project aiming to develop an algorithm that can quantify slope displacement rates through monitoring active waveguide generated acoustic emission is introduced.

KEYWORDS: Acoustic emission (AE) - Slope stability - Landslide - Instrumentation - Monitoring

1 INTRODUCTION

Landslides cause many thousands of fatalities each year all over the globe (e.g. Petley (2012) reported records of over 32,000 landslide induced fatalities that occurred during the period 2004 to 2010) and damage built environment infrastructure costing billions of pounds to repair, resulting in thousands of people being made homeless and the breakdown of basic services such as water supply and transport. The cost of remediation subsequent to landslide failure is very high compared to the cost of corrective measures and repairs prior to collapse; this highlights the importance of slope stability monitoring. Current monitoring systems are either too expensive for wide-scale use or have technical limitations. There is a clear need for affordable instrumentation that can provide continuous, remote, real-time information with high temporal resolution on slope movements for use in the protection of people and infrastructure by practitioners.

An approach, Assessment of Landslides using Acoustic Real-time Monitoring Systems (ALARMS) based on detecting and quantifying acoustic emission (AE) generated by an active waveguide installed through a deforming soil slope has been developed and trialled using unitary battery operated sensors. Results from long-running field trials of the Slope ALARMS system (e.g. Dixon et al. 2014a) demonstrate the potential for the system to provide real-time information on slope displacement rates at low-cost.

This paper will describe the AE measurement system and will present typical field data to exhibit the performance of the system. The current research project that is focussed on the development of a method to derive slope displacement rates from active waveguide generated AE will be introduced.

2 THE AE MONITORING SYSTEM

The active waveguide (Figure 1) is installed in a borehole that penetrates stable stratum below any shear surface or potential shear surface that may form beneath a slope. It comprises a metal waveguide rod or tube that provides a low resistance path for AE to travel from the source at the shear surface to the sensor at the ground surface. The annulus surrounding the waveguide is backfilled with granular soil. When the host slope deforms, the column of granular soil also deforms and this induces inter-particle friction and releases relatively high levels of AE that can propagate along the waveguide.

A transducer coupled to the waveguide at the ground surface converts the AE stress waves to electrical signals which are sequentially processed by the AE sensor. The AE sensor amplifies the signal and removes frequencies outside of the 20 to 30 kHz range. This is an important step in removing low frequency (<20 kHz) background noise such as wind, traffic and construction activity. The sensor then logs the number of times the waveform crosses a pre-programmed voltage threshold level within pre-set time intervals; ring-down counts (RDC) per unit time.

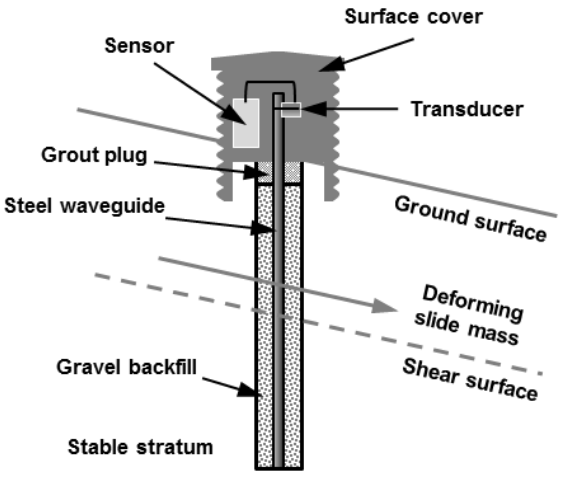

Figure 1. Schematic of an active waveguide installed through a slope deforming on a shear plane, with AE monitoring sensor attached to the top of the waveguide and protected by a cover (after Dixon et al. 2012)

3 TYPICAL SYSTEM RESPONSE TO LANDSLIDE MOVEMENT

A series of reactivated landslides at Hollin Hill, North Yorkshire, UK have been instrumented with active waveguides and Slope ALARMS sensors in order to compare performance with other deformation monitoring techniques and instruments (see Dixon et al. 2014a for further details). The landslides at

Hollin Hill can be characterised as shallow rotational failures at the top of the slope that feed into larger-scale slowly moving lobes of slumped material. Slope movement at Hollin Hill typically occurs in the winter months (i.e. January and February) when the slope is at its wettest and pore-water pressures in the vicinity of the shear surface are at their greatest magnitude. Figure 2 shows typical data produced in response to a period of reactivated slope movement at Hollin Hill; the plot shows the AE rate (RDC/hour)-, rainfall (mm/hour)-, inclinometer measured displacement (mm)- and AE derived cumulative displacement-time series for the event. It is important to note that the inclinometer measurements (produced from manual surveys of the casing) are separated by an interval of 7 days and therefore has low temporal resolution. During the reactivation event both the velocity of the sliding mass and the AE rates generated by the active waveguide increase exponentially until they reach a peak, at which point they subsequently decay exponentially as the slope and active waveguide backfill become stable (analogous to the conceptual velocity-time relationship for reactivation events described by Leroueil (2001)). This generates the 'S'-shaped displacement-time curve which was derived from the AE rate data (through determination of the rate of change with respect to time and equating the area under the bell-shaped curve to the magnitude of displacement measured by the inclinometer) and provides increased temporal resolution for the deformation event. Note that the response of the system to first-time slope failures (i.e. the development of a full shear surface during progressive failure and eventual collapse as a result of brittle strength loss) is expected to result in a continuous increase in AE rates as the velocity of slope movement increases throughout the failure event (i.e. progress over several orders of magnitude).

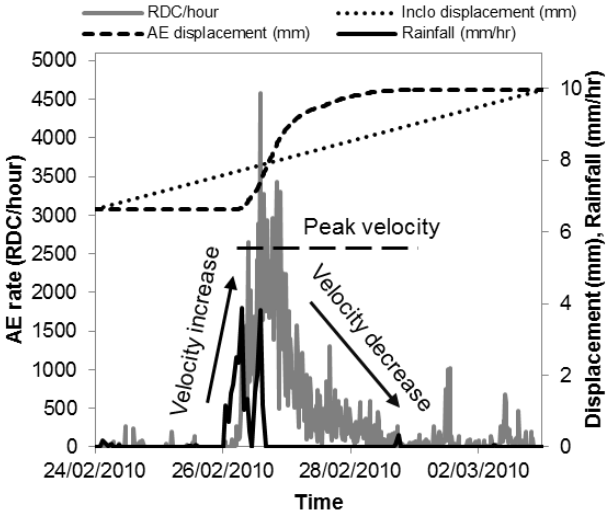

Figure 2. Typical AE response to a reactivated slope movement event at Hollin Hill (after Dixon et al. 2014a)

4 QUANTIFICATION OF LANDSLIDE VELOCITY

The magnitude of AE rates generated from the active waveguide-sensor system in response to applied rates of slope movement are different for each installation due to differences in several variables, such as the following: the sensor sensitivity controlled by signal amplification and voltage threshold; the depth to the shear surface that influences the magnitude of AE signal attenuation as it is transmitted from the shear zone to ground surface by the waveguide; and active waveguide properties such as the tube geometry and backfill properties. The magnitude of AE rate responses produced by each measurement system will depend on these factors, in addition to the rate of slope displacement. A significant proportion of the current research is focused on the development of a universal algorithm that can be used to quantify landslide velocity from active waveguide generated acoustic emission, where the influence of each of the variables stated above is understood and quantified. The function that defines the AE rate-velocity relationship is shown in Equation 1 and the function that defines the coefficient of proportionality (C_p) is shown in Equation 2.

$$\text{Velocity} = C_p \times AE_{\text{rate}} \quad (1)$$

$$C_P = f(d, s, p \ldots) \quad (2)$$

Where d is the depth to the shear surface, s is the sensor sensitivity, p are the properties of the active waveguide and '…' signifies that other variables also have influence upon the system, although with seemingly less significance. The influence of such variables upon the systems AE response are currently being investigated and quantified through a series of physical model experiments. Such experiments include: constant strain rate loading and dynamic strain-controlled loading tests to simulate landslide movements on full scale active waveguide models; attenuation testing on buried waveguide pipes; and large-scale first-time landslide failure simulations on active waveguide models.

5 SUMMARY

The paper detailed the use of active waveguides as sub-surface instrumentation to monitor AE generated in response to slope movements, and to assess the stability of soil slopes. The operation of the active waveguide and unitary battery operated Slope ALARMS sensor has been described. Results from a field trial at Hollin Hill, North Yorkshire, UK have demonstrated that AE rates generated by active waveguides are proportional to the velocity of slope movement. The approach taken and research plan to quantify slope velocity from active waveguide generated acoustic emission has been introduced. Field trials at Hollin Hill and other sites within the UK (e.g. Dixon et al. 2014b), Austria, Italy and Canada (e.g. Smith et al. 2014) are on-going in order to assess the performance of the system in the field environment.

6 ACKNOWLEDGEMENTS

The Authors would like to acknowledge the contribution of Phillip Meldrum and Edward Haslam of the British Geological Survey for their involvement in the development of the Slope ALARMS sensor.

7 REFERENCES

Dixon, N, M P Spriggs, P Meldrum, and E Haslam. 2012. Field Trial of an Acoustic Emission Early Warning System for Slope Instability. In *Landslides and Engineered Slopes: Protecting Society Through Improved Understanding*, 1399–1404.

Dixon, N, M P Spriggs, A Smith, P Meldrum, and E Haslam. 2014a. Quantification of Reactivated Landslide Behaviour using Acoustic Emission Monitoring. *Landslides*, 1- 12. DOI: 10.1007/s10346-014-0491-z

Dixon, N, R Moore, M P Spriggs, A Smith, P Meldrum, and R Siddle. 2014b. Performance of an Acoustic Emission Monitoring System to Detect Subsurface Ground Movement at Flat Cliffs, North Yorkshire, UK. In *IAEG XII Congress - Torino*.

Leroueil, S. 2001. Natural Slopes and Cuts: Movement and Failure Mechanisms. *Geotechnique* 51 (3): 197–243.

Petley, D. (2012). Global patterns of loss of life from landslides. *Geology*, *40*(10), 927-930.

Smith, A, N Dixon, N Berg, A Take, and D Proudfoot. 2014. Listening for Landslides: Method, Measurements and the Peace River Case Study. *Geohazards 6, Kingston, Ontario.*

Rapid Assessment of the Risk of Damage to Structures due to Ground Movements Arising from Construction

R. E. Blackmore
Coffey Geotechnics

ABSTRACT: This paper describes the automation of empirical calculation methods used to derive the magnitude of surface movements near retaining walls and cuttings to aid in the preliminary design and Phase 1 damage assessment for a new transport corridor in the UK. The three phase process proposed by Mair et al. (1996) for potential damage assessment of buildings due to ground movement is widely accepted and has been successfully used on the Jubilee Line Extension and Channel Tunnel Rail Link. Calculation to predict ground movement around retaining walls and cuttings can be time-consuming, particularly for designs in a constant state of flux. The use of computer programs to automate calculations can significantly reduce the time needed for preliminary assessment of a proposed alignment and be a useful value engineering tool.

KEYWORDS: Retaining wall, cutting, ground movement, damage assessment, transport corridor design.

1 INTRODUCTION

Rapid assessment of structures and services considered to be at-risk due to ground movement arising from construction activity is essential for economic design of transport corridors. Such quantification of risk facilitates optioneering and refinement of route alignments.

The analysis of ground movement due to construction of retaining walls and cuttings for a transportation project has been undertaken using adapted empirical models to provide robust estimates of displacement. Spread sheets were devised to speed up the calculation process and to generate contour data which could be directly fed into a three- dimensional model of the corridor alignment.

The model data were used to identify structures and services which may be damaged due to displacement of the ground in accordance with Phase 1 of the three stage damage assessment process devised by Mair et al. (1996) as follows:

Phase 1 - movement predictions for a "green-field" site.
Phase 2 - assessment of building strain resulting from Phase 1 movements.
Phase 3 - development of detailed building analysis.

2 GROUND MODEL DEVELOPMENT

The first stage in this ground movement assessment was the creation of a robust ground model. During the preliminary stages of this project the ground profile and associated soil parameters were derived from published sources rather than comprehensive ground investigation.

The geological and environmental information gathered was consolidated into a Geographic Information System (GIS) in AutoCAD to create a single ground model on to which design route alignments could be superimposed. This allowed engineers to identify quickly the geological conditions at retaining wall and cutting locations for subsequent corridor designs.

3 GROUND MOVEMENT DUE TO RETAINING WALL INSTALLATION

The assessment of ground movement due to retaining wall construction was straightforward as there was already a body of data available in CIRIA C580 (2003). Empirical methods proposed in CIRIA C580 were used to calculate ground movements. During the assessment, the corridor design was in a state of flux due to continual refinement of the alignment. Therefore, the type of retaining wall to be installed at each location was not finalised.

To compensate for this uncertainty, a "design line" was adopted, based on the data presented in Figure 2.11(b) of CIRIA C580 shown in Figure 1. This approximation of 0.15% of retained height as maximum settlement was considered conservative as the majority of the scheme retaining walls were expected to be large, and high stiffness systems were proposed in most cases. The ratio of distance from the retaining wall to zero movement and maximum excavation depth was taken to be 4 to account for the extent of movement where low stiffness walls may be installed.

For the purpose of preliminary design, the settlement profile behind the retaining wall was assumed to be linear, resulting in a slope angle of 1V:666H behind the wall crest. This slope angle is shallower than the 1V:500H limit specified as critical for the damage assessment, therefore consideration of ground slope following settlement around retaining walls was disregarded.

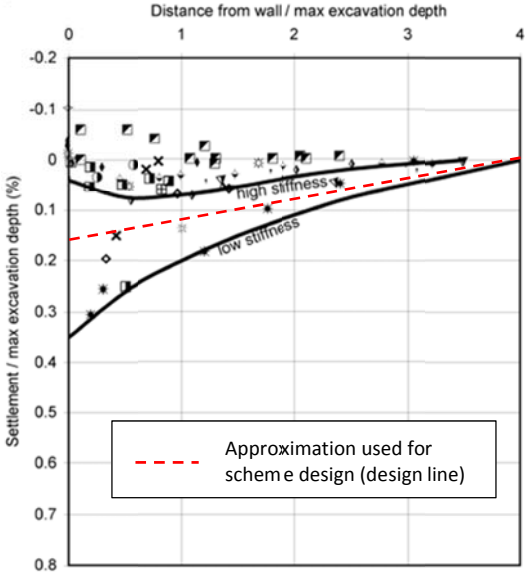

Figure 1. Ground surface movements associated with walls embedded in stiff clay. Adapted from Figure 2.11(b) of CIRIA C580

4 GROUND MOVEMENT AROUND CUTTINGS

There is comparatively little published information on measurements of movements around cuttings. It was therefore necessary to devise a methodology for this project. Two particular ground movement studies were reviewed. Hird and Pierpoint (1997) carried out finite element modelling of movements around a 10 m deep cutting in Oxford Clay. Measurements were taken for less than three months after excavation, and it is likely that long-term movements would have been greater.

Kovacevic et al. (2007) carried out a finite element study of a 25m deep, over-steep cutting in London Clay, proposed as temporary works. The results presented could be regarded as both an over-estimate of movements as the slopes considered are over-steep and an underestimate of movement because displacement was assessed in the short-term, not the long-term. Although there is no guarantee that the two effects will cancel out, the maximum movement of 0.5% of cutting depth was considered a reasonable estimate of ground movement for the purposes of this assessment.

4.1 *Assessment of Settlement*

The findings of the study by Kovacevic et al. (2007) were used as a basis for the ground movement assessment. A series of "rules" to estimate ground movements were derived from inspection of the displacement vectors.

1) Ground movements were shown to have approximately halved at a distance equal to the cutting depth; therefore the distance to zero movement was taken as twice the cutting depth.
2) At the cutting crest, horizontal and vertical movements are approximately equal, with around 100mm displacement for 20m of excavation. This approximates to a ground movement equal to 0.5% of the cut depth (k_2 on Figure 2).
3) Vertical displacement is shown to decrease to zero at around one third of the slope height.

4.2 *Assessment of Heave*

Heave under the centre of a cutting was estimated using one-dimensional consolidation theory, similar to estimation of settlements under embankments. The only difference is that the coefficient of swelling for most materials is lower than the coefficient of consolidation: i.e. the material is stiffer in swelling. Heave was assumed to be constant over the base of the cutting and estimated thus:

$$k_1 = n D Z m_{vs} \quad (1)$$

Where:

k_1= heave (mm)
n= unit weight of excavated material (kN/m^3)
D= depth of cutting (m)
Z= thickness of compressible material below cutting (m)
m_{vs}= coefficient of swelling (m^2/MN)

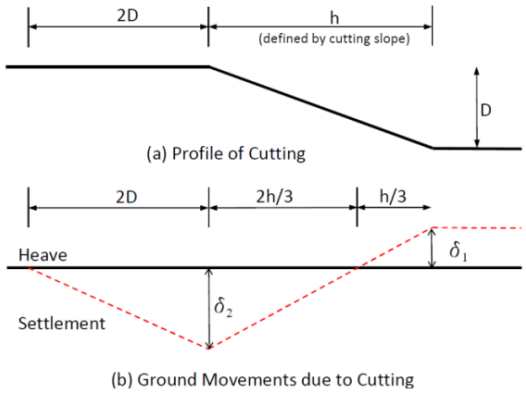

Figure 2. (a) Typical cutting profile used for modelling purposes and (b) typical ground movements for a given cutting.

Given the ground conditions along the corridor, it expected that the majority of soil heave will occur during construction and the effects masked by excavation.

4.3 *Ground Movement Model*

The ground movement assessments described in 4.1 and 4.2 were combined into a single movement model as illustrated in Figure 2. To keep the model simple, it was assumed that ground movement profile between the points of zero movement and those where maximum heave (k_1) and settlement (k_2) occur is linear.

5 DATA PROCESSING AND RISK ASSESSMENT

Spread sheets were specially developed to automate the calculation process. Geological data and cutting geometry were input to the calculation sheets directly from the GIS for analysis. Three-dimensional, geo-referenced ground movement contours were calculated at 50m chainage intervals along each retaining wall and cutting.

The contour data were output in a file format compatible with the GIS enabling the data to be fed into the 3D model, from which plans and cross were created. Ordnance survey map data and services plans were also input to the GIS and used to identify assets within the zone of influence (ZOI).

For this project, the ZOI was defined as the 1mm ground surface settlement contour, in accordance with the requirements of Phase 1 of the damage assessment process by Mair et al. (1996). Assets outside of the 10mm settlement contour or where the ground slope due to settlement was less than 1V:500H were screened out, and no further assessment was undertaken.

Assets falling within the 10mm contour, along with heritage buildings lying wholly or partly within the 1mm contour, were considered in much greater detail in accordance with Phase 2 of Mair's assessment process. The Phase 2 analysis process is outwith the scope of this paper.

6 CONCLUSION

Empirical calculations of ground movement can be used to generate movement contours in sufficient detail to satisfy the requirements of a Phase 1 damage assessment. The use of these relatively simple models empowers the geotechnical engineer to tailor analyses to a specific project with simple assumptions regarding geometry and ground conditions. This is particularly powerful for transport corridor development where standard designs are generally adopted for earthworks.

The design charts in CIRIA C580 enabled an assessment of ground movement to be carried out for retaining walls, whilst the assessment of cuttings required a new methodology to be developed for this project.

The automation of movement calculations in spread sheets significantly sped up the analysis process and allowed multiple alignments to be considered in a very short time. Coupling the calculation sheets and the 3D GIS model facilitated rapid visualisation of ground movements and assessment of structures and services put at risk.

Rapid analysis using standard calculation techniques enabled direct comparisons could be made between the number of buildings and services put at risk by numerous corridor designs. This value engineering tool was not considered at project inception, but became a useful tool during the iterative design process.

7 REFERENCES

Gaba, A. R., Simpson, B. Powrie, W., and Beadman, D. R., 2003, *Embedded retaining walls – guidance for economic design (CIRIA C580)*, CIRIA, London

Hird, C. C. and N. D. Pierpoint. 1997. Stiffness determination and deformation analysis for a trial excavation in oxford clay. *Geotechnique 47(3): 665–91.*

Kovacevic, K., Potts, D.M. & Vaughan, P.R. 2007. Predicting the stand up time of temporary London clay slopes at Terminal 5 Heathrow Airport. *Géotechnique 57, No. 1, 2007. pp63-74*

Mair, R. J., Taylor, R. N. and Burland, J. B. 1996. Prediction of ground movements and assessment of risk of building damage due to bored tunnelling. *Proceedings. of the International. Symposium. On Geotechnical. Aspects of Underground Construction in Soft Ground, 713 – 718, Balkema, Rotterdam.*

Rock mass characterisation and numerical analysis for the stability assessment of an underground feeder chamber in Glensanda Super Quarry, NW Scotland

A. Stavrou, M. Hatley and A. Koe
URS Infrastructure & Environment UK Limited, Chesterfield S41 7SL, UK

ABSTRACT: A detailed rock mass characterisation and numerical modelling analysis of jointed igneous rocks has been undertaken as part of the 'Project Highlander' at Glensanda super quarry in the North West Scotland region. The project includes the raise bore of a 210m deep, 3.8m diameter shaft known as the 'Glory Hole' and the development of several other interior openings including access tunnels, feeder chambers and ore passes. This paper presents the findings of a stability assessment that was implemented for the feeder chamber located directly beneath the new glory hole shaft. Underground mapping revealed information regarding the rock mass quality, the extent of blast disturbance and the condition, strength and geometric characteristics of the major joint set patterns. Preliminary rock reinforcement design and geomechanical parameters are obtained using the Q-system, empirical expressions, theoretical relationships and experience from hard rock engineering. Numerical modelling using the Distinct Element Code (UDEC) is performed to investigate the rock mass behaviour and the response of the rock reinforcement. Upon completion of the excavation, the observed rock responses and support performance are discussed and compared with the results of the numerical analysis.

KEYWORDS: underground excavation, stability, rock, discontinuity, reinforcement, numerical modelling, UDEC

1 INTRODUCTION

Glensanda Super Quarry is one of the world's largest quarrying operations and involves the production of crushed granite aggregates. The Quarry is located in North West Scotland and characterised by the innovative 'Glory Hole' method, which reduces the environmental impact of quarrying and provides an efficient and economic extraction of the granite reserves. Crushed rock produced at the quarry's level is discharged via the 'Glory Hole', a 300m deep and 3.8m diameter vertical shaft, into a horizontal 1.8km tunnel belt conveyor, which in turn carries the granite to a massive stockpile ready for ship loading.

'Project Highlander' includes among others the raise bore of a new 210m vertical glory hole and the underground excavation of 350m access roadways, a glory hole (feeder) chamber (14.5m x 12.5m x 10m high), a double ore pass system (10m deep x 2m diameter) and a conveyor belt chamber (21m x 12m x 10m high) which will feed material onto the existing operational tunnel conveyor (Figure 1). The project will enable the further extraction of granite deposits, extending in this way the life of the quarry for another 15 to 20 years.

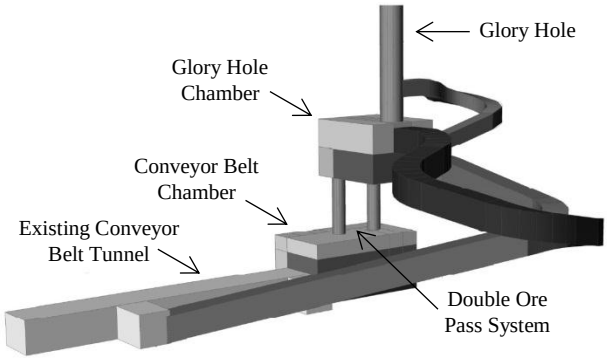

Figure 1. 3D view of Glensanda quarry's underground excavations.

The aim of this paper is to present a detailed rock mass characterisation and numerical modelling analysis undertaken for the stability assessment of the feeder chamber located directly beneath the new glory hole shaft. Due to the discontinuous and blocky nature of the rock mass, numerical modelling was performed using the two-dimensional Distinct Element Code UDEC, Version 5 (Itasca, 2011) in order to investigate the rock mass and rock reinforcement response, to assess possible deformations triggered by the excavations and to examine potential structurally controlled instabilities.

2 UDEC MODEL DESCRIPTION

The model has a rectangular geometry, with outer dimensions 160m wide and 400m deep. The overburden cover to the glory hole chamber roof has been fixed at 210m and the model was positioned to coincide with the wider span of the chamber, including the glory hole shaft (Figure 2). Although, none of chamber's dimensions is much greater than the other two and the cross-section under consideration does not fulfil UDEC's basic formulation, a 2D plane-strain analysis is still considered able to give sufficiently reliable results.

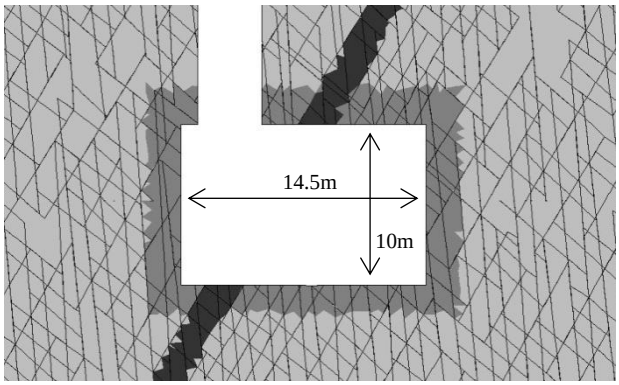

Figure 2. Model geometry (detail of excavation and joint sets).

Joint geometry was based on information collected during the underground mapping. Although, joints were found to have large variations in dip and strike, four dominant joint sets were identified (a pair of sub-vertical and near perpendicular to each other and two joint sets of moderate dip), with average spacing of around 200-500mm and with joint surfaces generally traced over the full height of mapped faces. The mapping revealed the critical role of discontinuities and the effect of discrete, interacting rock blocks on the rock mass behaviour and the formation of rock wedges.

The vertical boundaries and the lower horizontal boundary were fixed in the x and y directions respectively, whereas the top boundary was simulated as a free surface.

In the absence of rock stress measurement data, initial *in-situ* stress conditions are simulated by gravity loading and by assuming conservatively that the initial horizontal principal stress state is isotropic and equal to the vertical stress component (i.e. hydrostatic stress conditions). A zone of finer and denser mesh was defined around the excavation to increase numerical accuracy and quality of solution.

3 GEOMECHANICAL PROPERTIES

The intact rock blocks were assigned to behave as an elastoplastic material following the Mohr-Coulomb yield criterion, while joint behaviour was assumed to satisfy the joint area contact-Coulomb slip model with residual strength.

3.1 Intact rock

The principal lithological unites of the site include two granitic igneous rock types (Pink Granite and White Granite) which are intersected by numerous basaltic dykes. The thickness and trace length of these dykes can be of several meters and are often associated with a higher degree of fracturing, elevated permeability and weathering. A basalt dyke, 1.5m thick was mapped to cross the full length of the chamber's roof and for this reason it was included in the UDEC model (the dark grey zone intersecting the chamber in Figure 2).

In the absence of laboratory tests, the intact rock strength (Mohr-Coulomb) and stiffness properties were back-calculated by using the Generalized Hoek-Brown failure criterion (Hoek et al. 2002) through the program RocLab and by considering the scale effects of the *in-situ* block sizes. These properties were calculated by weighting the RocLab's recommended values in regards with the predicted Q-rock classes and the estimated GSI-values. The current analysis also assumes the presence of a 2-3m wide disturbed zone around the excavation due to blast damage and stress relaxation (the grey zone adjacent the excavation in Figure 2).

3.2 Rock joints

The joints walls were generally found to be irregular, of moderate roughness and tight. Clay and talc infill was present on many of the major sub-vertical joints especially in the contact with the basalt dykes.

The joint shear strength parameters were estimated by calculating equivalent Mohr-Coulomb strength parameters from a non-linear relationship that was developed by Barton (1973).

As part of the joint characterisation and the estimation of joint properties, the underground survey included the application of the Schmidt rebound hammer (for joint wall compressive strength and residual friction angle estimation) and the utilisation of interpreting joint roughness profiles along the discontinuity surfaces (for shear strength and dilation estimation). Scale corrections considering the average *in-situ* block sizes were taken into account by using the expressions proposed by Barton and Bandis (1982).

Normal and shear stiffness values were back-calculated from expressions provided by Itasca (2011) and by assuming that the fractures can be represented as three orthogonal joint sets.

4 ROCK MASS CLASSIFICATION – GROUND SUPPORT

Rock mass classification was undertaken using the rock tunnelling quality index 'Q' scheme (Barton et al. 1974). The estimation of Q value revealed a range of between 1-10 indicating 'Fair to Good' rock in the majority of the chamber. Rock support was estimated by using the empirical support chart of the Q-system and by considering the geometry of the chamber and the degree of safety required.

For the stabilisation of potential local wedge failures, spot bolting was applied and this was followed by a 1.5m pattern of 2.6m long 25mm diameter rock bolts, with 150mm square face plates, anchored using cement resin capsules. The grouted rock bolt characteristic parameters (i.e. no partial safety factors applied) were adopted from recommended values given for a 25mm diameter bar, whereas the grout shear stiffness and cohesive strength were estimated empirically from equations and guidelines provided in the UDEC manual (Itasca, 2011).

5 ANALYSIS SEQUENCE

A supported full face excavation was modelled although the chamber excavation required multiple drill and blast drifts, following a top heading and bench approach. The convergence - confinement method of analysis was applied and some relaxation of the rock mass prior the rock bolt installation is considered to simulate actual excavation construction and the 3D effect of an advancing tunnel face.

6 RESULTS AND DISCUSSION

The current analysis shows that force-equilibrium has been reached and that stable conditions have been achieved. However, localised block failures and/or high displacements are predicted, an issue also observed during the construction phase. Although the rock mass adjacent to the excavation has experienced plastic deformations, the amount of deformation is small and does not seem capable of causing major instability issues. As a result of the excavation, stress rearrangements within acceptable limits occur in the area adjacent the chamber and the estimated range of displacements is within reasonable limits (1mm - 6mm). The average predicted axial forces in the rock bolts are below their capacity with higher forces occurring in the bolt segments that intersect the basalt dyke (Figure 3).

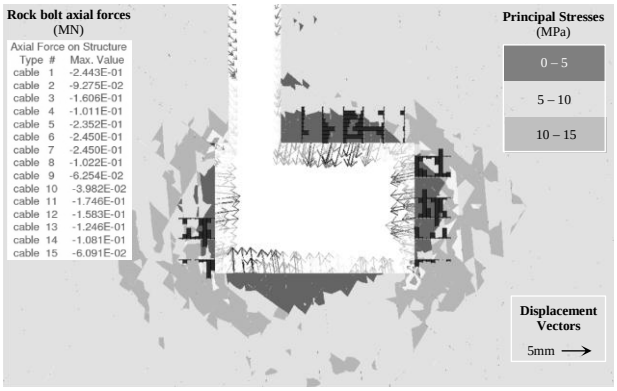

Figure 3. UDEC numerical modelling results.

7 CONCLUSION

In this work it was proved how the precise rock mass characterisation in conjunction with the empirical estimation of geomechanical parameters and numerical analysis, enables a realistic simulation of underground excavations in hard rock. Compared to the numerical modelling results, the rock mass behaviour during excavation of the chamber showed a considerable similarity. It is concluded, that the accuracy of the results depends on the choice of appropriate method of analysis and the engineering geological judgement of the analyst.

8 REFERENCES

Barton, N. 1973. Review of a new shear strength criterion for rock joints. *Engineering Geology, Elsevier*, Amsterdam, 7, 287-332.

Barton, N.R., Lien, R. and Lunde, J. 1974. Engineering classification of rock masses for the design of tunnel support. *Rock Mechanics* 6 (4), 189-239.

Barton, N. and Bandis, S. 1982. Effects of block size on the shear behaviour of jointed rock. *Keynote Lecture, 23rd US Symposium on Rock Mechanics*, Berkeley, California.

Hoek, E., Carranza-Torres, C.T., and Corkum, B. 2002. Hoek-Brown failure criterion – 2002 edition. *Proc. North American Rock Mechanics Society meeting*, Toronto.

Itasca Consulting Group 2011. *UDEC (Universal Distinct Element Code), Version 5.0. User's Guide*. Minneapolis, Minnesota.

Pulse Discharge Technology in Geotechnical Engineering

A. Dmitriev* , B. Clarke*
*University of Leeds, Woodhouse Lane, Leeds, LS2 9JT

ABSTRACT: This research analyses Pulse Discharge Technology application to pile construction, its advantages and weaknesses. The electro-hydraulic effect, which takes place during pulse discharge treatment, will be considered as a source of mechanical work. The principles of the electric discharge will be described and the types of energy created explained. There are a number of applications of pulse discharge technology in geotechnics but this study will focus on piles, the most developed of the applications. The study will cover safety problems relevant to PDT and the impact of PDT on adjacent structures. The aim is to produce a set of design curves that will be applicable to enlarged piles and enhanced shaft capacity in layered soils. The zone of influence in different soil conditions will be investigated.

KEYWORDS: pulse discharge technology, electro-hydraulic effect, plasma, gas-vapour cavity, densification, CFA, FEM

1 INTRODUCTION

Pulse Discharge Technology (PDT) is a technique that can be used to increase the radius of a pile over a defined length using a series of high voltage electric discharges in a wet concrete or bentonite slurry in a preformed borehole. The electric discharge effectively expands the cavity creating an increased bearing area and densifies soil around the pile. PDT in geotechnical construction is well known only in Russia and South Korea. Its effectiveness has been confirmed by numerous successful projects.

2 THEORETICAL APPROACH

The electro-hydraulic effect, which is the generation of shock waves and highly reactive species in a liquid as the result of application of very brief but powerful electrical pulses, has been known for more than 60 years and successfully applied in mechanical engineering, metal forming, mining, rock defragmentation, chemical industry, agro-industrial sector, etc. Application of the electro-hydraulic effect in construction became possible with development of appropriate Pulse Discharge Technology by researchers and construction companies. PDT can be described as a series of explosive pulses in a concrete liquid mortar using electrical discharge. Electrical energy is converted into mechanical energy through the formation of high-pressure gas vapour. As a result, the preformed hole is forced to expand and the soils around the borehole compact if granular or consolidate if cohesive.

Experiments with spark discharges in liquid have been studied since the 18th century. In 1766, an English pharmacist Timothy Lane (1767) wrote to Benjamin Franklin, describing a device (Figure 1) he called the electrometer.

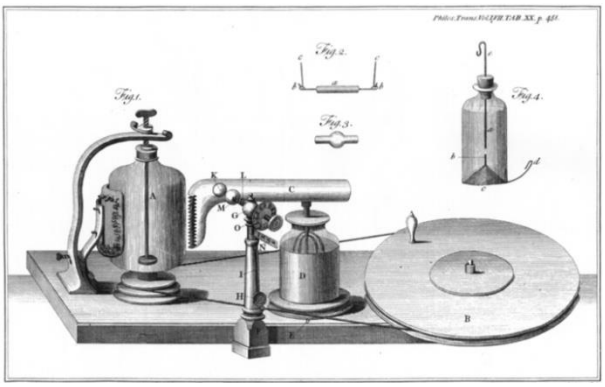

Figure 1 Machine of Mr. Read with electrometer of Mr. Lane (1767)

He had undertaken experiments in air, tobacco-pipe clay, Portland stone and phial full of water to show the impact of electric discharges. He was able to observe patterns between the amounts of accumulated electricity and the movement between the brass spheres of the electrometer and the destruction of the brass polish initiated by spark. The effects of the mechanical impact were observed on tobacco-pipe clay, which inflated if wet or burst to pieces if dry showing ductile and brittle behaviour. Priestley repeated the experiments in 1769 (Priestley, 1769).

Later in the 20th century, Frungel (1948) showed that an electric discharge in liquid would produce mechanical work. This phenomenon was called the electro-hydraulic effect. Yutkin (1986) suggested many applications of the electro-hydraulic effect. The most common areas of electro-hydraulic application have been in the processing of solids, hydraulic punching, beading, fettling a casting, fracturing of rock, etc.

The electro-hydraulic effect is a rapid means of converting electrical energy into mechanical energy through an electric discharge in a liquid medium. The energy (W) of the electric discharge is determined from the formula (1):

$$W = {}^{V^2C}/_{2} \quad (1)$$

where V - voltage, C-discharge capacitance.

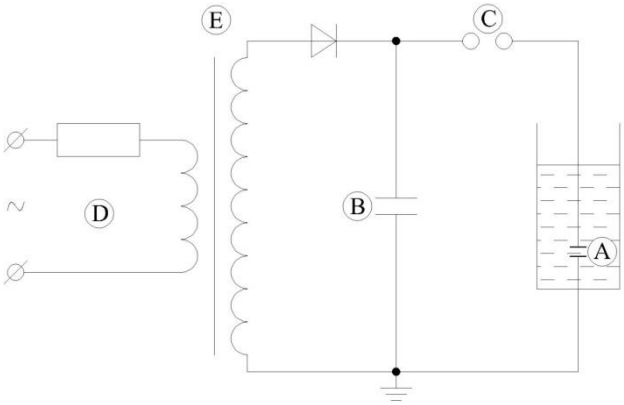

Figure 2. Schematic diagram of the electric circuit used to create the electro hydraulic effect:

The electro-hydraulic effect is a result of an electric arc forming between two electrodes (A) in a liquid. The electric arc vaporizes the liquid creating a shockwave.

Most liquids are not normally conductive, that is the resistance is too great to allow the current to flow. However, if the voltage is increased there comes a point when the difference in voltage exceeds the electrical resistance causing an electric arc to form.

The electrical energy is built up in a capacitor (B) using direct current. The energy release is controlled by a spark gap (C). A power source (D) generates an alternate current in the primary circuit. This creates a magnetic flux in the transformer (E) core, which, in turn, generates an alternate current in the secondary circuit at a higher voltage. A rectifier is used to convert the alternate current to a direct current, which supplies the voltage to the capacitor.

This circuit ensures a high pulse of energy to the liquid. The discharge produces a plasma channel in the liquid, which raises the temperature and pressure. A shockwave is created. The plasma channel forms within a gas cavity, which is a result of evaporation and electrolysis of the liquid. The gas cavity expands due to the pressure. This lasts microseconds. A high pressure wave of about $10^9 – 10^{10}$ Pa acts for a short time t (t ~ 10-6 sec.) (Samarin, 2005). Such a shockwave is one of the main sources of mechanical impact on the boundary of the borehole wall in a pile. A gas-vapour cavity is formed and expanded by merging of bubbles of dissolved gases caused by the electric breakdown of the liquid between the electrodes. This cavity is a further source of mechanical stress on the borehole wall.

The energy potential of the gas-vapour cavity and the shockwave depends on the voltage (V) and capacitance (C) of the capacitor. The energy (W) stored in the capacitor is 0.5 CV2. Varying these parameters at a constant energy (W) results in a redistribution of energy between the gas-vapour cavity and the shockwave. In cohesive soils, a higher capacitance extends the time of treatment thus giving more time for the gas cavity to expand. In granular soils, the shockwave is more important. Increasing the voltage increases the shockwave.

3 APPLICATION OF PULSE DISCHARGE TECHNOLOGY FOR BORED PILE CONSTRUCTION

There are different installation schemes for boring piles with PDT treatment. Bentonite or grout can be used; the reinforcement cage can be installed before or after PDT treatment. The pile installation starts with drilling the borehole, using bentonite suspension to stabilize the excavation and as a liquid medium for the electric discharge treatment. After boring a hole to the required depth, the discharge electrodes are plunged into the bentonite mud and a series of electric pulses are initiated at a predetermined level of a soil layer, which requires densification. After finishing treatment the bentonite is replaced by grout or concrete and reinforcement inserted.

It is possible to implement electric discharges in grout or concrete mortar (Bakholdin & Dzhantimirov, 1998). The borehole is created using a standard CFA process leaving a borehole filled with mortar. A series of pulses expand it at the required depth. Due to enlargement of the borehole volume by electric discharges it is necessary to refill the borehole after treatment.

To reduce the possibility of disturbance of borehole walls a reinforcing cage can be inserted before PDT treatment (Figure 3). Although there is wide experience to treat piles with and without a reinforcing cage, the impact of the reinforcing cage on the PDT process has not been analysed.

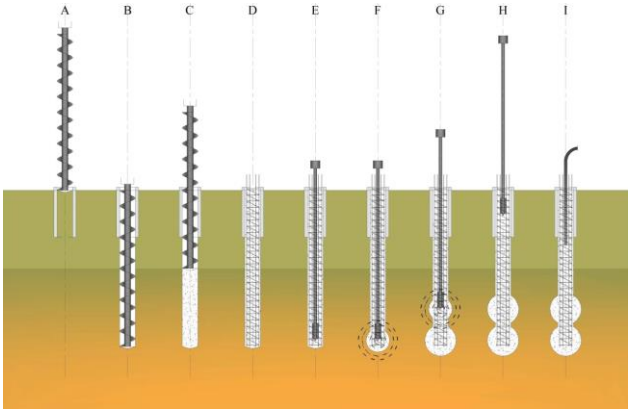

Figure 3 Installation of pile with PDT treatment with inserted reinforcing cage

4 CONCLUSION

Development of science determined research and use of new technologies in Civil Engineering. Electro-hydraulic effect based on findings from 18th century allowed elaborating different application in mechanical engineering, metal forming, mining, rock defragmentation, chemical industry, agro-industrial sector, etc. In geotechnical engineering PDT became the method of enlargement of foundation structures and it can eliminate several disadvantages of bored and cast-in-place replacement piles.

The main aims of this research are to study the effect of PDT on the capacity of a pile, to appreciate the process of expansion during PDT treatment and to determine the optimum conditions for PDT application.

5 REFERENCES

Bakholdin, B., & Dzhantimirov, K. (1998). New electric-discharge technologies in geotechnical construction,. *Soil Mechanics and Foundation Engineering, Volume 35, Issue 4-5*, 154-159.

Frungel, F. (1948). Mechanical Efficiency of Liquid Sparks. *Optik, Vol III*, 124-127.

Lane, T. (1767). Description of an Electrometer Invented by Mr. Lane; with an Account of Some Experiments Made by Him with It: In a Letter to Benjamin Franklin. *Philosophical Transactions 57*, 451-460.

Priestley, J. (1769). Experiments on the lateral Force of Electrical Explosions. *Philosophical Transactions 59*, 57-62.

Samarin, D. (2005). *Improving of method of pile installation in slightly saturated soils using pulse discharges [in Russian], dissertation of a Doctor tech.* Tomsk.

Tomlinson, M., & Woodward, J. (2008). *Pile design and construction practice, 5th edition.* Taylor & Francis.

Yutkin, L. (1986). *Electrohydraulic Effect and Its Industrial Application [in Russian]*. Leningrad: Mashinostroenie.

Leigh to Ellenbrook Guided Busway

J. K. Smith
Atkins Ltd.

ABSTRACT: This is a project summary for the Leigh to Ellenbrook Guided Busway; a design and build project undertaken by Balfour Beatty (BB) for Transport for Greater Manchester (TfGM), with Atkins Ltd. (Atkins) acting as BB's Designer. Atkins designed several earthworks and structures along the busway route and are currently providing site supervision and support services to BB. Atkins initially assessed historical earthworks along the busway to determine suitability, which then enabled the design of new earthworks where required. A rock slope present in a particularly constrained site area was also assessed for stability using modelling software. Retaining wall structures were then designed where earthwork slopes could not be safely accommodated within the proposed busway alignment; these were assessed for sliding, overturning, bearing, settlement and overall stability. The project has so far progressed well into the construction stage.

KEYWORDS: Guided Busway, Slope Stability, Retaining Walls, Rock Slopes, Earthworks, Eurocode 7, SLOPE/W, Pdisp, DIPS.

1 INTRODUCTION

Atkins Ltd. (Atkins) has been working with Transport for Greater Manchester (TfGM) and Balfour Beatty (BB) to design and construct a guided busway, which follows an old railway line between Leigh and Ellenbrook. This guided busway is currently one of the most geotechnically interesting projects in the North West for Atkins. The main challenges associated with the scheme were assessing the stability of the existing earthworks, the proximity to residential areas and buildings, and the interactions between existing infrastructure and new construction. The overall scheme cost is approximately £26m.

Atkins was responsible for a number of design deliverables, and this project summary highlights some of the key geotechnical designs. Initially an assessment of historical earthworks along the route was undertaken, subsequently followed by the design of new earthworks. Atkins identified a rock cutting along the route which was assessed for its slope stability. Retaining walls were designed where earthwork slopes could not be safely accommodated within the proposed busway alignment.

2 EARTHWORKS

The busway has many historical earthworks along the proposed alignment, which were not designed to current standards. Assessments of both historical and new earthworks were performed as part of the design, with new earthworks assessed in line with Eurocode 7 (EC7) guidance, and historical earthworks assessed based on their past performance. Earthwork slope gradients of 1 in 2.5 were adopted in the designs; therefore the purpose of the analyses was to check that this gradient provided stable slopes to EC7.

2.1 *Existing Earthworks*

Atkins considered the impact of the proposed works on the stability of the historical earthworks and where a potential risk to the earthwork stability was identified, a sensitivity analysis was undertaken.

The sensitivity analysis utilised SLOPE/W software (GeoStudio 2004) to establish a reference overall factor of safety (FOS) for the cutting or embankment slope using unfactored characteristic parameters. The SLOPE/W model was then modified to include proposed changes to the earthwork and the loading to be imposed by the busway. The modified FOS was then compared to the reference FOS to establish the risks to stability.

If the modified FOS did not reduce by a value greater than 5% compared to the reference FOS, the risk of earthwork instability was considered to be low and no remedial works were recommended. Where this was not the case, modifications were then suggested for the earthworks in question.

Following the assessment it was found that many of the historical earthworks could be maintained without modification, and this provided great cost savings to TfGM due to the reduced amount of material required for replacement.

2.2 *New Earthworks*

Where historical earthworks could not be used, and where there were significant changes in ground profile due to the chosen alignment, new earthworks were designed.

New cuttings and embankments were assessed using SLOPE/W to determine the safe slope angle based on EC7 design standards. This took into account the possible loadings that could be imposed by pedestrians, vehicles, and existing infrastructure, in addition to the known loading of the busway.

New embankments were constructed from site won material, except locally where particular performance criteria were required, such as at the interface with existing bridge structures. The majority of site won material consisted of Made Ground (embankment fill), and to a lesser extent Glacial Till, and was generally suitable for re-use.

The re-use of material provided additional cost savings to TfGM, however it was not possible to construct all new earthworks from this material due to width restrictions and settlement requirements.

2.3 *Settlement*

Settlement analyses were carried to support the design of new earthworks, and these analyses were critical to meet the very tight settlement tolerances of 2mm in 10 years specified by TfGM for three locations along the busway (East and West of Hough Lane and East of Sale Lane). The earthworks were analysed using Oasys Pdisp software which uses the Boussinesq method of analysis, modelling the soil as elastic.

The results showed that earthworks abutting the busway and existing infrastructure would require modifying to meet the strict settlement requirements. Earthworks not directly interacting with a structure did not have as tight restrictions on settlement: settlements could not exceed 10mm in total over a length of 15 metres. Only one section of the busway did not meet this requirement and dynamic compaction was suggested as a method of reducing this settlement.

Where the earthworks interact with structures granular fill material was specified to reduce settlement to acceptable levels. In immediate proximity to the structures new embankments are made entirely of granular fill to strictly control settlement at this interface. The profile of the granular material is benched with cohesive fill beyond this zone so that the thickness of granular

material tapers to ensure a smooth settlement profile on the approach to the structure.

3 ROCK SLOPE ASSESSMENT

A rock cutting exists to the west and east of Hough Lane, in Tydlesley, where the busway will intersect with the existing road network. The cutting needed to be assessed due to the narrow site area and proposed partial infilling and excavation into existing rock faces to accommodate the busway. This section of the busway is tightly constrained due to the presence of residential properties to the South and a UU attenuation tank to the North.

An assessment was undertaken to assess the stability of the rock so that mitigation measures could be identified. Due to external constraints it was not permitted to use rock blasting to plane the rock slope, and therefore the lines of any fractures or discontinuities would be utilised by site machinery to alter the existing rock face.

Figure 1 shows a photograph taken during the site visit annotated with some identified features.

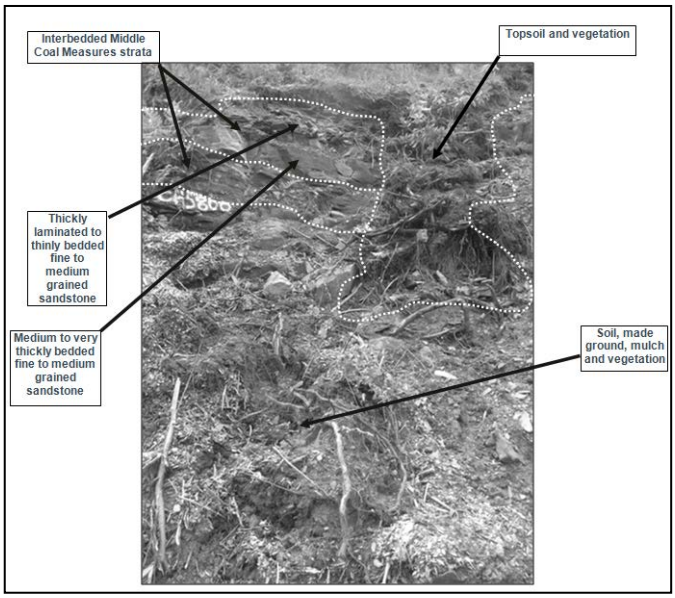

Figure 1. Site photograph of rock slope near Hough Lane

The rock cutting was geologically mapped and discontinuity data was obtained by recording dip and strike information. The data was then plotted in a computer model that utilises stereographic projections to model discontinuities, and predict possible failure mechanisms. This allowed a kinematic analysis to be performed using DIPS software by Rocscience. This assessment utilised a friction angle of 35° for the joints within the sandstone. The analysis assessed the stability of the rock face with regards potential failure through planar sliding, wedge failure, and toppling.

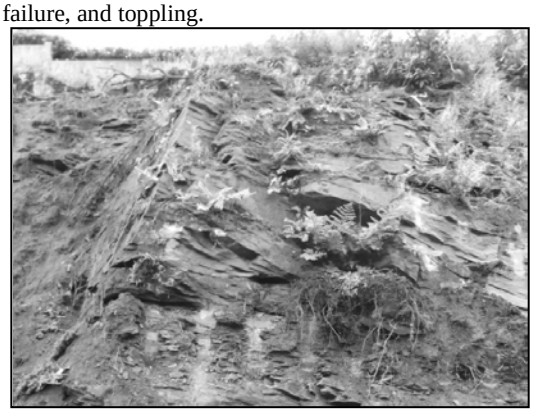

Figure 2: Saw-tooth Rock formation at Hough Lane

Analyses were carried out for an overall slope angle for a cut face parallel to the proposed busway and also for faces cut along the line of the two main joints to demonstrate that rock will break preferentially along these joints. Removing material along the two joints produced a 'saw-tooth' like effect (as seen in Figure 2) and the resulting rock slope is stable.

The assessment concluded that minimal alteration to the existing rock slope was required to satisfy stability. Some areas could require a rock mesh solution, as it is possible that minor instability or small falls of rock debris could occur during the lifetime of the cut face.

4 RETAINING WALLS

Four retaining walls were designed for the scheme, the wall details are provided in Table 1 below:

Table 1. Summary of Retaining walls

Retaining Wall	*Length*	*Max Height*
RWA	25m	1.6m
RWB	12m	1.2m
RW0	44m	0.8m
RW4	216m	3.2m

A reinforced earth wall was also designed by Reinforced Earth Company Ltd. (RECo), to support the busway infrastructure adjacent to the United Utilities attenuation tank at Hough Lane.

For the retaining wall designs, calculations were undertaken in accordance with EC7. Loading from the soil was evaluated using Coulomb's theory for active earth pressure (Coulomb 1776) and the bearing resistance was calculated using Terzaghi's equation (Terzaghi, et al. 1996). Settlement was then calculated using the m_v method taken from Barnes (2010). The maximum settlement for walls RWA, RWB and RW0 was less than 10mm, and for RW4 was less than 20mm. The overall stability was then assessed with SLOPE/W software for drained and undrained conditions.

The retaining walls were all adequate, and settlement was acceptable as the walls are all set back from infrastructure.

5 CONCLUSION

The design phase of the project was successful, and the designs produced by Atkins for the earthworks, rock slope and retaining walls are currently under construction. Atkins are now providing site supervision and support services to BB during the construction stages.

6 ACKNOWLEDGEMENTS

Rachel Stringer; Cedric Allenou; Thomas Clifford – Atkins Ltd.

7 REFERENCES

Barnes, G. (2010). *Soil Mechanics: Principles and practice*. Third Edition.

Coulomb C.A. 1776. *Essai sur une application des regles des maximis et minimis a quelques problemes de statique relatifs a l'architecture. Memoires de l'Academie Royale pres Divers Savants.* Vol. 7.

Eurocode 7 1997. *Geotechnical Design (EN1997).*

GeoStudio 2004. *SLOPE/W software*.

Oasys. *Pdisp*. Version 19.2.

Rocscience. *DIPS*. Version 6.0.

Terzaghi, K., Perk, R.B. and Mesri, G. 1996. *Soil mechanics in engineering practice*. 3rd Edition.

Geoenvironmental Input into AMP6 - "Project X" Case Study

O. Akinola
Graduate Geoenvironmental Engineer, Geotechnical Engineering, United Utilities Group PLC, Warrington, UK

ABSTRACT: United Utilities has identified "Project X" (name withheld) as a necessary output for delivering its Asset Management Plan 6 (AMP6) programme. This paper presents an overview of "Project X"; with particular focus on the various geoenvironmental constraints and strategies for resolution encountered on the project.

KEYWORDS: AMP6, contamination, rising main, outfall, Wastewater Treatment Works, Pumping Station

1 INTRODUCTION

Since privatisation of the Water Industry, there are five-year regulated investment cycles referred to as AMPs; we are currently in the last year of AMP5. In order to deliver its AMP6 Targets, United Utilities is carrying out a number of 'Transition Investment' (TI) projects; early concept work supporting AMP6 commenced late in AMP5; this paper considers one such project.

"Project X" is located in a tidal-influenced, coastal area of North West England. The objective is to dispose of wastewater and to enhance the environment - this is achieved through identification of the main project driver: meeting the European Union Bathing Water Directive. The project will deliver a reduced number of spills to nearby bathing waters, in line with the Environment Agency's National Environment Programme requirement. An additional driver is to improve operability and maintenance of the existing outfall that is subject to transitory sand movement near the coast, resulting in burial of the pipe below the seabed and inundation of the diffuser ports.

The proposed design for "Project X" involves increasing the pass forward flow and providing additional storage and treatment at the Wastewater Pumping Station (PS) and Wastewater Treatment Works (WwTW) respectively. The PS and WwTW are connected by a rising main which will require twinning to accommodate the increased forward flow. A new outfall pipe is required for marine discharge.

2 BACKGROUND INFORMATION

The current WwTW (approx. 6km south of the PS) is located adjacent to a Site of Biological Interest (SBI). The current outfall pipe (3.1km long) transports treated effluent from the WwTW mainly through a leisure complex, out to sea to the West. The surrounding area previously consisted of a petroleum refinery to the North, and a chemical works to the West and South that manufactured aviation fuel, nitric acid, fertiliser and the like, as part of WWII efforts; these operations continued up until the late 1970s.

The PS is located in a dense residential area; with some historic industrial activity recorded in the surrounding area. The rising main pipe connecting the PS to the WwTW carries sewage from the surrounding towns (population of approx. 35,000), runs through the residential area and then, for most of its length, mainly drained agricultural fields to the South.

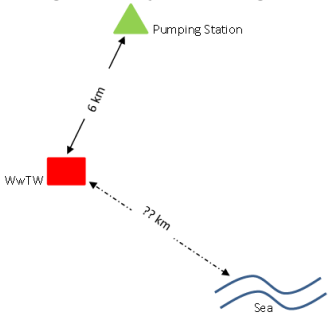

Fig 1: Schematic Diagram of Proposed Design

2.1 *Geology and Hydrogeology*

Varied geology is expected across the entire site area including Raised Tidal Flat, Lacustrine and Storm Beach deposits, Glacial Till and occasional accumulations of Peat; overlying the Millstone Grit, Cumbrian Coast and Sherwood Sandstone Groups.

The entire site area overlies a Secondary A bedrock Aquifer (Millstone Grit); with the outfall route also overlying a Secondary B bedrock Aquifer (Millstone Grit) and a Principal bedrock Aquifer (undifferentiated Triassic Rocks).

3 PROPOSED DESIGN

In order to meet the AMP6 requirements to reduce the number of storm water spills during the Bathing Season to nearby bathing waters, the following improvements are proposed as part of "Project X":

3.1 *Pumping Station*

Additional storm water storage tanks are required; involving various construction techniques. Storm transfer pumps and tank cleaning are also proposed.

3.2 *WwTW*

There is a need for increased capacity as the WwTW will be required to receive more pass forward flow from the PS. Plans include improving process technology and provision of 6mm inlet screens. The proposed design includes a new UV channel (for final treatment), tidal tanks and associated pumps, pipe work and control kiosks.

For the above changes, additional space is required potentially involving purchase of adjacent land.

3.3 *Rising Main*

An additional pipe (approx. 6km) is required to augment the existing rising main; resulting in a twin pipe solution which would accommodate the required increase in pass forward flow.

3.4 *Outfall*

Various locations for the outfall pipe are being considered by the Design Team including maintaining or extending the existing outfall, and relocation within the estuary.

The outfall pipe must be appropriately located to allow for adequate dilution and dispersion by the receiving water. Furthermore, the diffusers need to be the right size and shape to ensure that 'negative buoyancy' is achieved; ensuring placement and stability of the pipe on the sea bed.

At present, options are still under consideration in order to decide on a location with optimum dilution, sand movement and minimal disruption of marine ecosystems.

4 CONSTRAINTS

Various physical constraints have been identified by the project team including: hazard pipeline and high voltage electricity cables (constraining construction around the WwTW and pipeline routes); tidal groundwater regime; sea and river flood risk; soft/compressible ground; tidally-affected access; ecologically sensitive habitats; Unexploded Ordnance (UXO) risk (area is recorded to have been targeted during WWII) and mobile sediment in the estuary.

Other project constraints include crossing agricultural fields and dykes (along the pipe routes), contamination (discussed in section 2.3), different land ownerships (e.g. land purchase), and relatively high costs of construction, waste management and operation.

5 HISTORICAL CONTAMINATION

From a series of historic site investigations (SIs), the site, particularly near the WwTW, has been identified as potentially significantly contaminated from historic activities.

In summary, previous SIs confirm the ground beneath the site as having elevated soil and/or groundwater concentrations of Petroleum (TPH) and Polyaromatic Hydrocarbons (PAH), including coal tars, Benzene, Toluene, Ethylbenzene and Xylene (BTEX); acetone and inorganic substances (incl. copper, lead, mercury, nickel, sulphate and zinc).

The 2007 SI arranged by the Environment Agency (EA) confirmed the site did not fit the criteria of a "Part 2A" site based on the risks to controlled waters; thus no remediation was required at that time.

Asbestos is also expected, particularly adjacent to the WwTW, buried within demolition waste and Made Ground.

The hazard map (Fig 2) shows various constraints to the project including historic and current landfills, hazard pipeline, environmental designations and historic structures (associated with the petroleum refinery and chemical works). This has significantly helped to influence 'optioneering' for the project e.g. selection of pipeline route alignment.

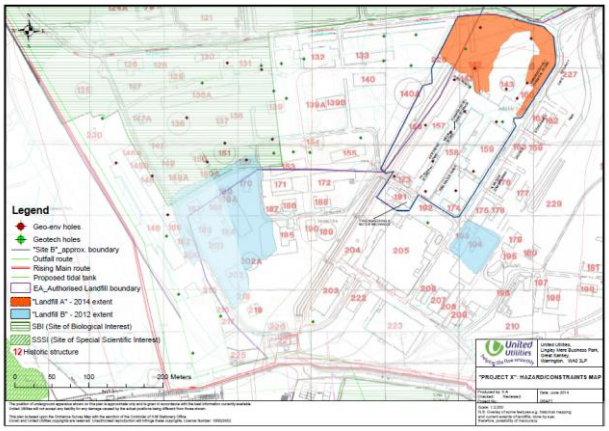

Fig 2: Hazard/Constraints Map for area surrounding WwTW

6 PLANNED GROUND INVESTIGATION WORKS

6.1 *Land Section*

Due to the sensitivity of the area and possible impacts of "Project X" during Ground Investigation (GI) and construction, a great deal of time has been invested in planning and designing the GI. For example, assessment of the UXO risk was carried out for the WwTW, PS and along part of the outfall route. Based on the possibility of UXO encounter near the WwTW, classified as "Medium" to "High", certain mitigation measures have been planned for GI and subsequent construction works; including a magnetometer survey and presence of UXO scanning during drilling.

Early engagement of various stakeholders such as the local authority, nearby house-owners, Hazard Pipeline owners and EA, is important in order to inform them of the proposed works in an open and empathetic manner. A Stakeholder Management Plan has been developed to record and monitor engagement.

6.2 *Marine Section*

According to the UXO risk assessment, possibility of UXO encounter in the marine section of the outfall was classified as "Medium"; hence, similar mitigation measures to the land section are planned.

As the outfall pipe will be discharging into the marine environment, a Marine Management Organisation (MMO) application is being prepared to assess and prove that the project's impacts on the marine environment (specifically sediment transport and aquatic life) will be minimal. Sampling and testing (in accordance with Centre for Environment, Fisheries and Aquaculture Science (CEFAS) standards) is to be incorporated into the planned GI. The results from these tests will be required to feed into the MMO application and eventually the Environmental Impact Assessment (EIA) for the project as a whole.

Table 1 shows a subset of the rationale behind the marine GI works.

Table 1: Example Rationale for Marine Outfall GI (Onshore)

Hole No.	Hole Type	Depth (m)	Likely Installation requirements	Contamination Rationale
TP501	Trial Pit	3	N/A	Sample MG or observed contamination if present
BH501	Rotary Borehole	15	Dual gas and groundwater monitoring standpipe to provisionally 8m	Sample MG and sample for sewage/ heating oil, if observed

7 CONCLUSION

The design for "Project X" is developing and being modified to reflect the additional information as it is gathered. Understanding of the ground model (i.e. geotechnical and geoenvironmental aspects) is seen as a major factor in project success. It is the best means to understand and articulate and manage the prevailing ground risks in undertaking the project.

8 ACKNOWLEDGEMENTS

I would like to thank Helen B., Chris P., David J., Sabin H. and James N. from United Utilities, for their review and constructive criticism whilst writing this paper.

9 REFERENCES

BGS, Sheet 59 (1:50,000 scale), 1995 and BGS Online Geology of Britain Viewer (Accessed Nov. 2013)

"Project X": Hazard/Constraints Map, June 2014 (ArcGIS)

"Project X": Stakeholder Management Communications Plan, June 2014

"Project X": WwTW Outfall Options Report, June 2014

"Project X": Geotechnical & Geoenvironmental Desk Study, Dec. 2013

Digital Seismic Piezocone Penetration Tests: A Case Study

N. A. Christopher & B. Sampurno
Fugro GeoConsulting Limited

ABSTRACT: Fugro's seismic piezocone testing capabilities have recently improved with the launch of its digital seismic system. Where onshore testing is relatively simple, offshore testing presents many challenges; in particular, equipment unreliability can have negative effects on cost and data quality. This seismic piezocone has been used on several offshore geotechnical investigations since 2013. A large pool of data has been collected and reviewed to validate the results. The results were compared to those obtained through downhole P and S logging, advanced laboratory testing (i.e. bender element and resonant column) and common derivations from cone penetration testing. Fugro's seismic digital system showed that measured V_s data from offshore seismic peizocone are comparable to other methods, and provides immediate dynamic soil parameters that can be fed into design during site investigations.

KEYWORDS: offshore site investigation, seismic piezocone penetration test, case study, WISON, SEACALF, Fugro

1 INTRODUCTION

1.1 *Site Summary*

The data presented come from recent offshore work that Fugro has performed for various clients since 2013. The case study presented is based on soils deposited during the Quaternary and Cretaceous periods.

1.2 *Piezocone penetration test (CPTU)*

Continuous measurements of cone resistance (q_c), sleeve friction (f_s) and induced pore pressure (u) are made as the cone is pushed into the ground at a nominal rate of 20 mm/s (ISO 22476-1:2012). The cone is either pushed continuously from the surface or at intervals when deployed downhole. Using the measurements acquired, it is possible to accurately define the investigated stratigraphy and derive parameters to characterise the soils and assist in foundation design.

1.3 *Seismic piezocone penetration test (SCPTU)*

A SCPTU consists of a standard CPTU cone with additional instrumentation above the cone to measure seismic waves. Measurements are made using either geophones (as is the case with Fugro SCPTUs) or accelerometers. It is possible to detect both shear wave velocities (V_s) and pressure wave velocities (V_p) using an SCPTU, although this case study only considers V_s due to the type of the seismic source used. A seismic source is used to create an energy impulse (shot) that sends a shear wave through the soil. The shear wave is recorded in three axes by three geophones in the x, y and z directions, referred to as a geophone array. The seismic cone is pushed into the soil and stopped at regular intervals to carry out testing. Testing consists of a number of shots, which are then stacked to reduce noise and increase the true signal. The moment the source is triggered, the Fugro data acquisition unit starts recording seismic response of the soil to the shear wave produced.

From analysis of the signal traces recorded, the arrival time of the shear wave can be estimated. The difference in the shear wave arrival times between tests at different depths can be used to calculate interval velocities. When a cone with a single geophone array is advanced through the soil, the calculated interval velocities are regarded as pseudo interval velocities. This is because separate shots have been used to infer the difference in the arrival times and subsequently calculate the interval velocity. If two geophone arrays are used, spaced at a known distance from each other within the tool, then the actual difference in the arrival time from a single shot can be measured: this is the true interval velocity (Rice 1984). One main advantage when using a dual geophone array is that the results are much less affected by any error in the trigger timing and the start of data recording.

Maximum shear modulus (G_{max}), which is of particular importance in earthquake design studies, and analysis of dynamically loaded foundations can then be calculated using an assumed or measured soil density:

$$G_{max} = \rho . V_s^2 \quad (1)$$

Where ρ is the soil density.

2 FUGRO OFFSHORE SCPTU

This case study used seismic data from two methods of investigation using the digital seismic system. The first data set is from continuous push seabed tests (SEACALF®) using a single geophone array seismic piezocone. Pseudo interval velocities are measured using the SEACALF® system. The second data set is downhole wireline tests (WISON®) using a dual geophone array seismic piezocone. True interval velocities are measured when using the downhole WISON® system.

The source for the seismic tests was a hydraulic underwater shear wave hammer (HUSH) fixed to the base of a modified seabed frames.

A digital seismic trigger module was used to synchronise the activation of the source and the recording of the seismic data. The system was set up to record 100 ms pre-trigger data and up to 1000 ms of test data, all controlled through integrated data acquisition software.

The data collected from both seabed and downhole seismic tests are presented in Figure 1.

3 OTHER SOURCE OF SEISMIC DATA

To produce a complete seismic profile, a pressure and shear wave digital suspension logger tool (P and S logger) was deployed. The logger consists of two geophone arrays located 1 m apart and measures V_p and V_s. The full wave for each source pulse is measured. The data are plotted in Figure 1 (V_p are not presented).

Two anisotropically consolidated undrained triaxial compression (CAUc) tests with bender elements (BE) and a resonant column test were performed on soils, sampled downhole using a Fugro's wireline push sampler, obtaining 72 mm diameter samples.

The CAUc-BE tests were performed by triggering a shear wave through the samples at the end of the saturation, isotropic and anisotropic stages so as to determine the G_{max} of the soil. Shear wave velocities were measured in three orientations: vertically transmitted (s_v), horizontally transmitted with horizontal polarisation (s_{hh}), and horizontally transmitted with vertical polarisation (s_{hv}). For comparison, the V_s in the s_v direction are plotted in Figure 1.

One anisotropically undrained consolidated resonant column (RC) test was performed to determine G_{max} and the rate of shear modulus degradation, and damping ratio with increasing shear strain by torsional vibration. The V_s as shown in Figure 1 was calculated from G_{max} and the measured density of the sample.

Many correlations between V_s and CPTU data have been published. The correlations can be subdivided into three main types: cohesive soils only, cohesionless soils only, and general soils (McGann et al. 2014). An initial assessment was carried out to ascertain the most suitable empirical correlations to derived Vs data for the soils encountered. Based on this assessment, Andrus et al. (2007) and Robertson (2009) provided a closest match with the measured V_s values. The inferred Vs data using the correlation proposed by Andrus et al. (2007) and Robertson (2009) are presented in Figure 1.

4 DISCUSSION OF DATA

Figure 1 shows undrained shear strength, water content, unit weight, liquid limit and plastic limit, V_s data with a simplified soil profile at this case study location.

Laboratory testing results from BE and RC show good correlation with both SCPTU and downhole logging, plotting just below the general trend. This gives a good indication of soil sample quality and shows that the soils have been consolidated properly to the best estimate of in situ stress conditions.

The SEACALF® SCPTU data extend to a depth of approximately 24 m below seafloor (BSF) where the system achieved its maximum penetration. The V_s data do not completely overlap the downhole logging data at the same depth. It can be seen that the derived data from WISON® SCPTU increase relative to the derived data from the SEACALF® SCPTU from approximately 23 m BSF. This indicates there is a degree of lateral variability in the strata.

In general the measured V_s data from SCPTU shows good agreement with the downhole logging data, particularly from approximately 27 m to 29 m BSF. As expected where V_s was measured in excess of 450 m/s it was not possible to penetrate the cone sufficiently in to the soil to carry out SCPTU.

5 CONCLUSION

A review of the recent data acquired using the new Fugro seismic digital seismic system showed that measured V_s data from offshore SCPTU are comparable to data from other tools (e.g. laboratory testing and downhole logging).

The seismic data can be rapidly processed offshore during the site investigation and the V_s data can be presented to the end user within 24 hours of completion of testing. This data combined with soils and CPTU information provide immediate dynamic soil parameters that can be fed into the design or analysis, during the site investigation, providing quick and cost effective alternatives to downhole logging and increased confidence in laboratory test results.

6 RECOMMENDATION

By performing a more in-depth analysis of the results, it should be possible to further process pseudo interval velocities from WISON® SCPTU results, something that is not always possible during the fieldwork due to time constraints.

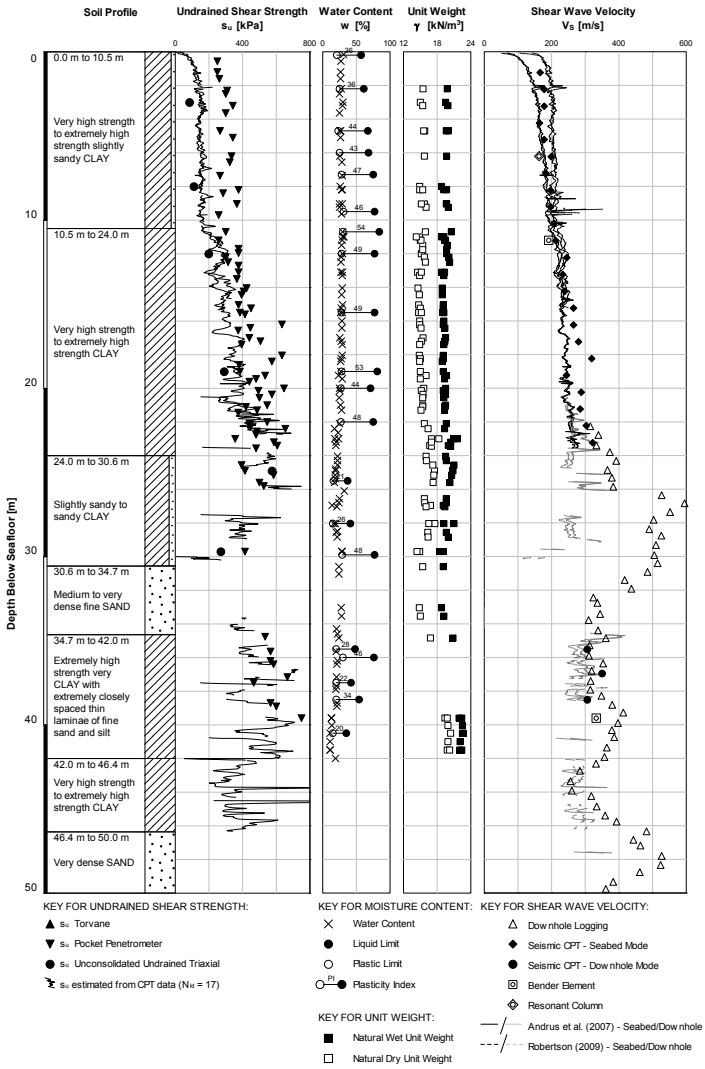

Figure 1. Case Study Location: laboratory, in situ and seismic data profile. V_s data points represent the interval velocity over 1 m for SCPTU and downhole logging. For BE and RC testing the interval is approximately 140 mm

7 ACKNOWLEDGMENTS

The authors would like to thank Tim Carrington and Laura Connochie for their help and support.

8 REFERENCES

Andrus, R.D., Mohanan, N.P., Piratheepan, P., Ellis, B.S., and Holzer, T.L. 2007. Predicting shear-wave velocity from cone penetration resistance. Proc. 4th International Conference on Earthquake Geotechnical Engineering, Thessaloniki, Greece, June 25-28, Paper No. 1454.

McGann, C.R., Bradley, B.A., Cubrinovski, M., Taylor, M. and Wotherspoon, L.W. 2014. Comparison of existing CPT-V_S correlations with Canterbury-specific seismic CPT data. Auckland, New Zealand: 2014 New Zealand Society for Earthquake Engineering Conference (NZSEE), 21-23 Mar 2014. 8pp.

Rice, A. 1984. The seismic cone penetrometer, thesis submitted in partial fulfilment for Master of Applied Science, Department of Civil Engineering, University of British Columbia.

Robertson, P.K. 2009. Interpretation of cone penetration tests – a unified approach. Canadian Geotechnical Journal, Vol 46(11): 1337–1355.

International Organization for Standardization (ISO), 2012. ISO 22476-1:2012 Geotechnical investigation and testing – Field testing – Part 1: Electrical cone and piezocone penetration test. Geneva: ISO.

Mechanisms controlling the liquefaction resistance of desaturated sand

Zeybek, A. & Madabhushi, S.P.G.
University of Cambridge, UK

ABSTRACT: Liquefaction resistance of saturated sand can be markedly increased when the sand is slightly desaturated. The entrapped air in the pore fluid can prevent the excess pore pressure generation during earthquake loading. In this study, air injection technique was used to prepare partially saturated sand. 1g shaking table tests on fully and partially saturated sand with and without shallow foundations were undertaken. Comparison of results has shown that, contrary to the previous studies, the settlement of shallow foundations placed in the desaturated zone is much larger than that in fully saturated sand. However, consistent with previous research, free ground surface settlement of partially saturated sand was found to be less than that in fully saturated sand. The results obtained indicate that the mechanism controlling the liquefaction resistance of partially saturated sand is different for models with and without the shallow foundations. Shear deformation mechanism controls the liquefaction resistance of partially saturated sand with foundations, whilst the increased compressibility of the soil matrix dominates the behaviour of partially saturated sand without any foundations.

KEYWORDS: Soil liquefaction, ground improvement, desaturation of sand, shaking table, compressibility, shear deformation

1 INTRODUCTION

It has been established by many experimental studies that the degree of saturation *Sr* has a strong effect on the liquefaction resistance. Based on the cyclic triaxial tests and measurement of the Skempton's B value, it was shown that the liquefaction potential of sandy soils can be markedly decreased by even a several reduction in *Sr* (e.g. Chaney 1978). The underlying reason behind this was attributed to the presence of gas bubbles in saturated sand. It has been suggested that even small quantity of air pockets in saturated sand increases the compressibility of the soil matrix. The air bubbles in the pore fluid play a role of absorbing the excess pore water pressure generated by cyclic loading by reducing their volume.

In recent years, several researchers have been investigating the inclusion of air in soil as a method for decreasing liquefaction potential of saturated sand. Okamura and Teraoka (2006) have explored the method that relies on pumping pressurized air into sand. Yegian et al. (2007) have proposed a method to introduce small-sized bubbles into sand skeleton by using two laboratory techniques: water electrolysis and drainage-recharge. Similarly, Eseller-Bayat et al. (2013) have investigated the use of eco-friendly chemical compound that involves the generation of oxygen bubbles in sand model through its reaction with water. Important issues regarding these methods such as mechanism of air bubble formation, dissolution of air bubbles below ground water table, have been also investigated by several researchers (e.g. Kutter 2013).

The results of these studies show that liquefaction resistance of fully saturated sand was consistently increased once it was desaturated such that the degree of saturation *Sr* is only a few percent below 100. The generation of excess pore water pressure was gradual and less for the desaturated models than fully saturated models. Moreover, horizontal displacement, settlement and rotation of structures resting on fully saturated were effectively reduced by desaturation.

In this study, several desaturation techniques (e.g. air injection, use of sodium perborate monohydrate) were applied to mitigate the liquefaction of sand and a series of 1g shaking table tests on fully and partially saturated sand were performed. In this paper, the settlement behaviour of fully and partially saturated ground with and without shallow foundations resting on it is presented, giving particular attention to the results of desaturation via air injection technique.

2 MODEL PREPARATION AND TEST PROCEDURE

2.1 Model Preparation

An experimental programme consisting of a series of shaking table tests on fully and partially saturated sand was carried out to study the desaturation as a liquefaction countermeasure. All models were constructed in a rigid container with inner sizes of 700 mm in length, 300mm in width and 500 mm in height. The container was divided at the middle by a flexible, cut-off wall in order to examine simultaneously fully and partially saturated sand. The saturation pipework and air injection system were placed at the bottom of the model box. A 35 mm layer of gravel with 5 mm diameter was first laid in the base of the box and a dry layer of Hostun sand (with specific gravity of 2.65, maximum and minimum void ratios of 1.01 and 0.555, mean particle size of 0.424 and particle size of 0.286) was manually poured to the desired depth of 235 mm at the target relative density by using air pluviation technique. To investigate the settlement behaviour of shallow foundation, a model foundation that is 300 mm long, 50 mm wide and 30 mm high was used. The mass of model shallow foundation is 3.2 kg, thus applying a bearing pressure of 2.093 kPa. Models were saturated slowly by infiltrating with water through saturation pipework. This procedure was operated slowly to avoid piping of sand. After saturating the sand, the instruments were placed at the required positions. The layout of models is presented in Fig. 1.

2.2 Model Desaturation

In air injection technique, the sand was desaturated by injecting the air through an air injection pipe with very tiny holes. During the desaturation process, the air was pumped gradually without hydrofracturing or fissuring the sand. Moreover, the degree of saturation of sand was checked measuring the water level rise in the model which attributes the generation of gas bubbles and replacement of water in the sand. Models were then shaken by a sinusoidal wave with a 3.5 Hz frequency and maximum input acceleration of 0.22g. In each test, first shaking was applied to fully and partially saturated sand model without shallow foundation to investigate the settlement response of free ground surface at several positions. Further shakings were employed on the models with foundation to explore the settlement behaviour of foundation in fully and partially saturated sand. The test conditions are summarised in Table 1.

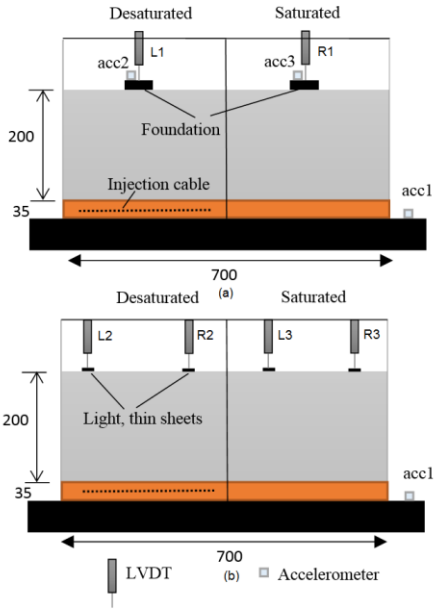

Figure 1. Test set up for models a) with and b) without foundation

Table 1. Test conditions of model

Test ID	AZ1	AZ2
Relative density Dr (%)	40	50
Degree of saturation, Sr (%)	90	90
Number of earthquakes	4	4

3 TEST RESULTS AND DISCUSSION

This section gives a comparison of the settlement behaviour of saturated and partially saturated models with and without shallow foundations, and it discusses two different dominant factors of liquefaction: pore fluid compressibility and shear deformation of liquefied sand.

Figure 2 shows that the settlement of free ground surface in desaturated zone is approximately one half of those of fully saturated models AZ1 and AZ2. This implies that the ground surface settlement is reduced by a factor of at least 2 by the desaturation through air injection technique. These results are relatively consistent with those in the literature (e.g. Okamura and Teraoka 2006).

On the other hand, in the tests on models with foundation resting on liquefiable sand, the settlement of foundation placed on partially saturated sand is found to be much larger than that in fully saturated sand for all cases.

The comparison of the settlement response of partially saturated sand with and without foundation indicates that the mechanism which controls the liquefaction resistance of partially saturated sand is qualitatively different for the models with and without foundation. The hypothesis proposed by previous researchers that *-the entrapped air in the pore of soil increases the compressibility of pore fluid, and therefore prevents the generation of excess pore water pressure by reducing its volume-* is only verified by the results involving the sand models without foundations. However, when a foundation was present on the soil surface the opposite seems to be the case, as confirmed by the settlement data in Fig.2. As evident from the experimental results, the compressibility of pore fluid dominates the ground surface settlement of partially saturated sand. However, in case of tests with foundations, shear deformation of sand is the dominant factor and it controls the settlement behaviour of foundations resting on partially saturated sand. The air introduced into the fully saturated medium significantly reduces the shear strength of soil. The reason behind this might be attributed to the fact that shear strength of soil is reduced more in the case of partially saturated soil compared to a fully saturated soil.

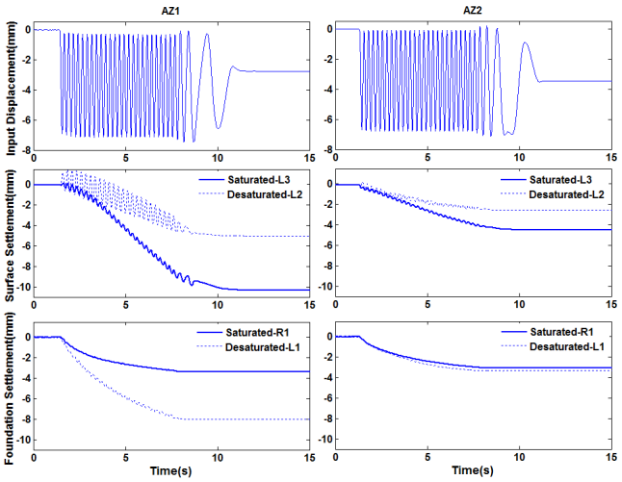

Figure 2. Settlement of fully and partially saturated sand with and without foundations

4 CONCLUSION

In this study, a series of shaking table tests were conducted on the partially saturated sand models with and without foundations.

It was found that the settlement of free field was lower in partially saturated sand than that in fully saturated sand, whereas the settlement of foundation was much less in fully saturated sand than that in partially saturated sand.

The results obtained reveal that the mechanism that controls the liquefaction resistance of partially saturated sand with and without foundation is different. The tests without foundations show good agreement with those in the literature and confirm that the compressibility of pore fluid is the dominant factor in the liquefaction resistance of sand. However, the results obtained for the settlement of foundations on partially saturated sand suggest that the liquefaction resistance of partially saturated sand with foundation is controlled by shear deformation of sand and that the settlement of foundations on partially saturated soil may be more than that for fully saturated case. If confirmed, these results will have serious implications for the use of air injection as a liquefaction countermeasure.

This test series were carried out in 1g shaking table, and further tests in centrifuge are underway to further understand the liquefaction behaviour of partially saturated sands.

5 REFERENCES

Chaney, R., 1978. Saturation effects on the cyclic strength of sands. Earthquake Engineering and Soil Dynamics, 1: 342–358.

Eseller-Bayat E., Yegian M. K., Alshawabkeh A., Gokyer S., "Liquefaction Response of Partially Saturated Sands: Experimental Results", Journal of Geotechnical and Geoenvironmental Engineering, ASCE, Vol. 6, No. 139, 06/2013

Kutter, B. (2013). "Effects of capillary number, Bond number, and gas solubility on water saturation of sand specimens." Canadian Geotechnical Journal, 50(2), 133-144.

Okamura, M. & Teraoka, T. (2006). Shaking table tests to investigate soil desaturation as a liquefaction countermeasure. *Proceedings of seismic performance and simulation of pile foundations in liquefied and laterally spreading ground* (GSP 145), pp. 282– 293. University of California, Davis, CA, USA.

Yegian, M. K., Eseller-Bayat, E., Alshawabkeh, A. & Ali, S. (2007). Induced-partial saturation for liquefaction mitigation: experimental investigation. J. Geotech. Geoenviron. Eng, ASCE 133, No. 4, 372–380.

Rubber based foundation for liquefaction resistant residential structures

G. Nikitas & S. Bhattacharya
Department of Civil and Environmental Engineering, University of Surrey, Guildford, United Kingdom

ABSTRACT: Soil liquefaction, in most of the latest large earthquakes, has left behind large ground deformations that set structures unusable. Existing mitigation methods, such as deep pile foundations, gravel drain columns and dynamic compaction can reduce the effects of liquefaction on structures, but their costs seem prohibitive for most common residential buildings. This research provides experimental results from a series of shaking-table tests carried out at 1g of a new low cost mitigation technique against liquefaction. According to this technique, shredded waste tires packed in permeable sandbags are used for ground improvement underneath the structure. This technique has only recently been developed in Japan in order to find immediate application on typical domestic houses following the 2011 Tohoku earthquake. A number of parametric scenarios concerning the thickness of the ensuing elastic base were considered. The experiments indicate that the tyre shreds' addition can act both as a seismic isolation (i.e. filtering effect) as well as an efficient drainage method. This mitigation approach also proposes an innovative and sustainable way to reuse waste tires, which otherwise set a serious environmental problem due to their large volumes produced and their recycling complications.

KEY WORDS: Liquefaction mitigation, shaking table test, shredded tire foundation, soil improvement

1 INTRODUCTION

Under moderate to large vibrations, loose to medium density saturated soil deposits are prone to liquefaction; see for example the Great East Earthquake on 2011, which caused many liquefaction phenomena around Tokyo Bay area and as a result, many structures were damaged (Bhattacharya, 2011). Many methods for liquefaction mitigation have been developed throughout the years, but they tend to be used only in big projects, because their cost is prohibitive for domestic houses. The current research considers such an economic mitigation technique against liquefaction.

In the proposed method, shredded scrap tires are used to minimize the earthquake and liquefaction impacts on a domestic building, such as a common 1 story house. The scrap tires are shredded into small pieces (around 2.5 mm wide) and then, after being put inside sandbags, are placed underneath the foundations of the structure. The layout of the proposed mitigation technique can be seen in Figure 1

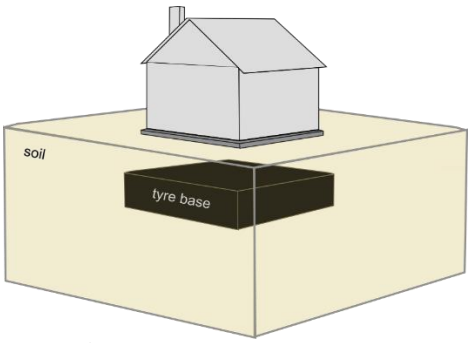

Figure 1. Layout of the proposed ground improvement technique.

The perceived benefits of the proposed technique are:

a) Due to the increased permeability of this resulting sub-base (because of the larger than sand void ratio), it is expected to effectively act against the pore water pressure built up that is a pre-requisite for liquefaction.
b) With the added damping and elasticity of the new foundation type is supposed to reduce the transmission of the shear waves, so actually to reduce the acceleration transmitted to the structure.
c) It provides an innovative way to reuse waste tires.

For verifying the above hypotheses, a series of 1g shaking-table experiments were conducted in order to provide experimental data that could validate and scrutinize the performance characteristics of the developed technique.

2 EXPERIMENTAL PROCEDURE

The 1g shaking-table tests were conducted in the Earthquake and Large Structures Laboratory (EQUALS) at the University of Bristol (U.K.).

For the test arrangement, a rigid plastic container, which was separated in 2 partitions, was rigidly mounted centrally on the top of the shaking-table. One partition had the foundation model, with the cushion of tire chips underneath and the other had the model without the cushion. Each model was scaled to weight a total of approximately 2kg. Figure 2 illustrates in detail the side view of the model apparatus that was tested.

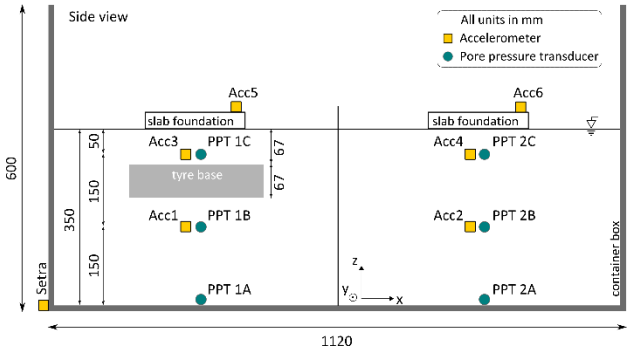

Figure 2. Side view of the test arrangement.

To form the tyre base used in the test, the tyre chips were packed inside perforated small bags, which were arranged evenly underneath the slab foundation. To ensure the liquefaction occurrence, the soil consisted of loosely poured, fully saturated Redhill Sand 110. The properties of both the tyre chips and the sand used (Kelly, 2007) in this test are summarized in Table 1.

Table 1. Physical properties of tyre chips and Redhill Sand 110

Material	D_{50} *(mm)*	e_{min}	e_{max}	γ_{dmin} *(kN/m³)*	γ_{dmax} *(kN/m³)*
Tire Chips	2.45	1.600	2.320	4.92	7.73
Redhill 110	0.12	0.547	1.037	12.76	16.80

The apparatus is shaken first with low amplitude white-noise (0 to 80Hz), in order to retrieve all relevant modal characteristics of the scaled models and then the 40% and 100% scaled (in terms of Peak Ground Acceleration) of Christchurch earthquake of 22 February 2011are used as an input motion.

3 TEST RESULTS

3.1 *Response of the models under white noise test*

Before getting into the earthquake response outcomes, it is interesting to see how the apparatus natural frequencies in the two cases with and without tire chips under the foundation would change. Intuitively the less rigid elastic foundation is expected to respond at a lower fundamental frequency, because the building supported on tire base will have lower stiffness and hence lower natural frequency. Additionally this softening effect is probably expected to be more pronounced along the z axis where the spring action of the tire chips is more evident.

According to the white noise test results, it is found that on the x and y axes, the dynamic characteristics seem almost identical regardless of the foundation type, but in the case of z axis they are different. Evidently the stiffness drop appears as expected. Thus interestingly on x and y axes the two models behave the same for any input acceleration and the tire inclusion affects only the vertical movement.

3.2 *Response of the models under Christchurch earthquake*

First of all, it is interesting to observe the pressure effect that the earthquake has on both the models. In Figure 3 the closer to surface PPTs from the two models (i.e. PPT 1C and 2C) are plotted together with the synchronous input accelerations on the x and y axes during the 40% scaled Christchurch earthquake. It can be seen that when an elastic inclusion is in place the pore pressure does not rise to high values. This is the best means of proving the effectiveness of such a foundation solution, which can effectively eliminate the liquefaction phenomenon, which is synonymous to pore water pressure rise. Possible explanations for the attained result could be the higher permeability of the rubber cushions that do not strongly resist the water movement. To be more precise Figure 3 is only a local snapshot of the overall ground condition that centers on a specific position, the one above the tire base. One may argue that it could probably be some other change that brings up the radical differences of Figure 3. Such should well extend beyond the ground improvement region

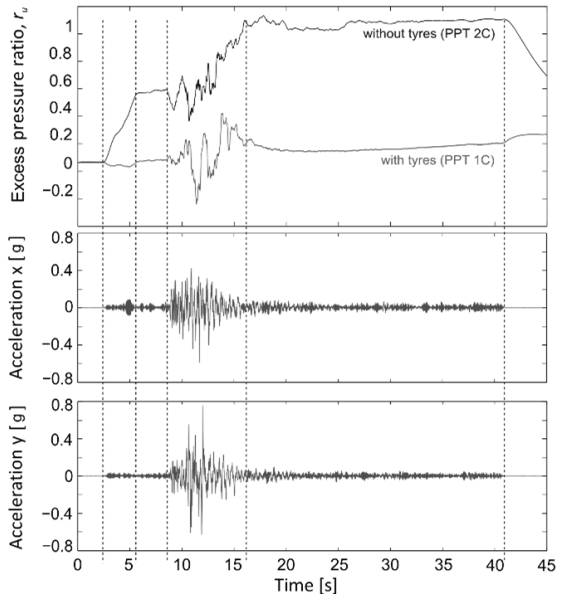

Figure 3 Pore pressure rise during the 40% scaled Christchurch shaking and its acceleration time histories

Figure 4 attempts to address any such implications by comparing the next set of PPTs, situated 150mm above the bottom level, it can be concluded that the pressures in the rest of the soil body progresses in a very similar manner.

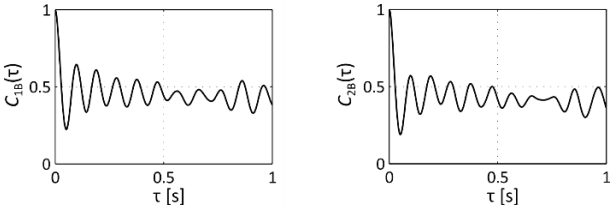

Figure 4 Correlation between PPT 1B and 2B during Christchurch shaking.

Figure 5 shows the autocorrelation of the surface accelerometers, in the z and x direction against lag time. In z direction, it can be witnessed that the two decay functions almost overlap meaning that the forced response is similar for both cases. Taking into account this, together with what was found earlier in white noise test, any changes should be probably unexpected. Yet the figure actually shows appreciable differences in the dynamic behavior in x direction. According to that, when tires are in place the x surface motion is much more damped and the harmonic forced character of the earthquake is much more difficult to make out. The same is also valid for the y axis.

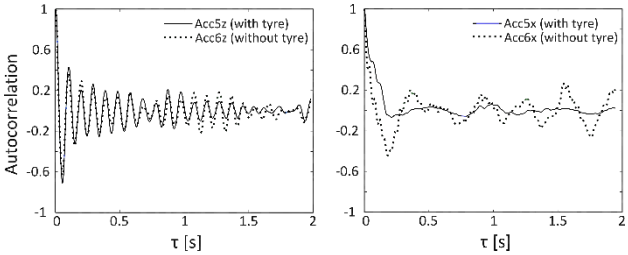

Figure 5 Correlation between surface accelerometers in the two cases z axis (left) and x axis (right)

4 CONCLUSION

The current research work attempts to address and understand the seismic mitigation measure of using an elastic sub-base consisting of scrap tire chips just below the slab foundation. Such a countermeasure resisting was previously found very effective for other types of structure (Yoshida, 2008).

Here it was clearly shown that the tire addition alters the liquefaction process reducing the close to surface pore pressure rise and prohibits permanent tilts. It was also found that dynamic characteristics change during the shaking largely in the horizontal plane isolating the structure from excessive ground motion. More importantly it was shown that the tire action cannot be realized as a single 1D action modeled e.g. by spring addition but it rather has a more elaborate 3-dimensional character.

5 REFERENCES

Bhattacharya S, Hyodo M, Goda K, Tazoh T, Taylor CA. *Liquefaction of soil in the Tokyo Bay area from the 2011 Tohoku (Japan) earthquake.* Soil Dynamics and Earthquake Engineering 31, 2011, p. 1618-1628

Kelly, R.B., Byrne, B.W., Houlsby, G.T. and Martin, C.M. *Tensile loading of Model Caisson Foundations for Structures on Sand*, Proceedings ISOPE. Conference, Toulon, 2007

Yoshida, M, Miyajima, M, & Kitaura, M. *Experimental Study on Mitigation of liquefaction-induced flotation of sewrage manhole by using permeable recycled materials packed in sandbags* The 14th World Conference on Earthquake Engineering (Beijing, China), 2008

Analysis of pile foundation in liquefied sand using p-y curve from element test

M. Rouholamin & S. Bhattacharya
Department of Civil and Environmental Engineering, University of Surrey, UK

ABSTRACT: In practice, piles are most often modelled as "Beams on Non-Linear Winkler Foundation" (also known as "p-y spring" approach) where the soil is idealised as p-y springs. These p-y springs are obtained through semi-empirical approach using element test results of the soil. For liquefied soil, a reduction factor (often termed as p-multiplier approach) is applied on a standard p-y curve for the non-liquefied condition to obtain the p-y curve liquefied soil condition. This paper presents a methodology to obtain p-y curves for liquefied soil based on element testing of liquefied soil considering physically plausible mechanisms. Validation of the proposed p-y curves is carried out through the back analysis of physical model tests.

KEYWORDS: p-y curve, Soil element test, Liquefaction, Pile foundation

1 INTRODUCTION

1.1 *Analysis of piles using Winkler method*

In Winkler method (Beam on Non-linear Winkler Foundation) of analysis of piles, the pile-soil interactions are represented by a set of nonlinear soil springs: p-y springs (commonly known as curves incorporate the lateral pile-soil interaction), t-z springs (models the shaft resistance i.e. pile-soil friction) and q-z spring (models the end-bearing interaction). Figure 1 shows a simple model of a pile which can be analysed using any standard structural software Second level heading. This paper deals with p-y springs/curves for seismically liquefied soil and explores method for its construction. p-y springs are generally constructed using a set of scaling rules as prescribed by codes of practice and necessary input parameters are obtained from stress-strain of the soil.

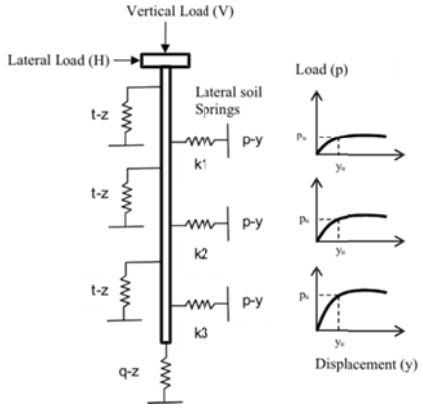

Figure 1: (a) Method of analysis a pile, (b) p-y curves

1.2 *Obtaining p-y curve*

In practice, p-y curves are obtained from codes of practice, see for example API (2000) and the input required is the stress strain of the soil. An interesting feature may be observed: the shape of the p-y curve for sand and clay is similar to their stress-strain behaviour. There is no standard p-y curve for liquefied soil and often a reduction factor is used to obtain empirical p-y curve for liquefied soil from its non-liquefied counterpart. In this method, both the stiffness and strength of a non-liquefied soil is multiplied by a factor known as "*p-multiplier*".

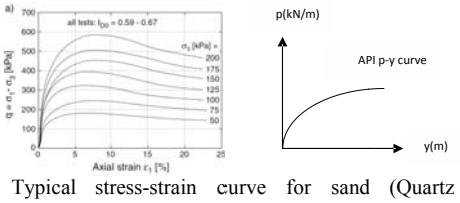

Figure 2: Typical stress-strain curve for sand (Quartz sand, (Wichtmann, 2005) and API p-y curve

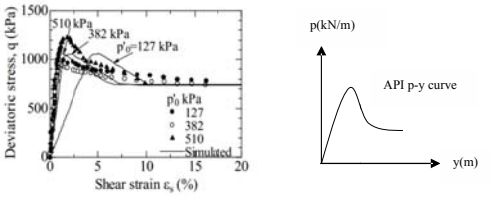

Figure 3: Typical stress-strain curve for clay (Ariake clay, (Chai et al., 2007) and API p-y curve

2 PROPOSED P-Y CURVE FOR LIQUEFIED SAND

The Lateral Pile-Soil Interaction (LPSI) is very much dependent on the p-y springs and as a result it is necessary to understand the stress-strain of liquefied soil. In order to obtain stress-strain of liquefied soil, a series of multi-stage cyclic triaxial tests have been carried out on Red Hill 110 sand using Cyclic Triaxial Apparatus (Figure 4a). The properties of the sand are given in Table 1. The tests were carried out at the Geomechanics laboratory of the University of Surrey. The sample is 100mm in diameter and 200mm in height and was first liquefied by applying stress controlled cyclic load. Following liquefaction, the soil sample was sheared using strain controlled monotonic load at a rate of 1mm/min. Figure 4b shows the stress path used in the tests. As may be noted that the final stage was to apply monotonic load to the liquefied soil to achieve the stress-strain curve.

Table 1.Red Hill-110 sand properties

Properties	Value
Specific gravity, G_s	2.65
D_{50}	144μm
Maximum void ratio, e_{max}	1.035
Minimum void ratio, e_{min}	0.608
Friction angle, ϕ	36^0

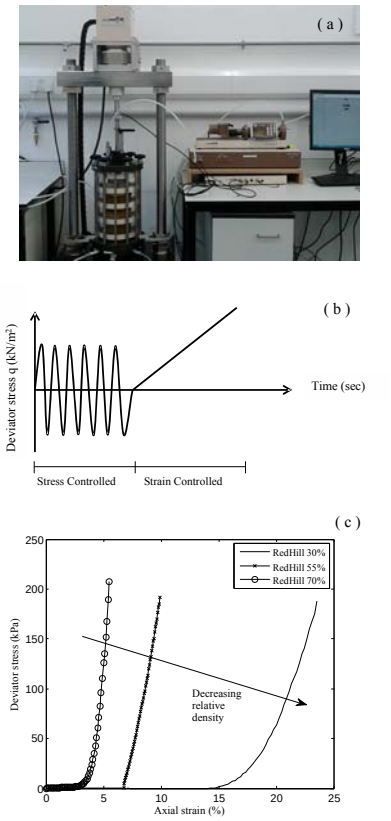

Figure 4: (a) Cyclic triaxial apparatus, (b) Multi-stage loading path, (c) Stress-strain curve of liquefied sand (Redhill-110 sand)

The most important distinguishing features are:

- There is no initial stiffness for the liquefied soil which implies that the effective stress is near zero.
- After a limiting strain which is termed as "*take-off strain*" the resistance increases. This is also expected, from micro mechanical point of view, as the particles are in suspension when liquefied and it would require deformation to re-engage them to provide resistance. This threshold strain depends on relative density of the soil.

The stress-strain curve comes from this experiment is used to derived p-y curve, where three parameters are required: M_s, N_s and D (pile diameter). M_s and N_s are scaling parameters and further details of obtaining them can be found in Dash (2010) and Bouzid et al (2013). It must be mentioned that M_S and N_S is based on Mobilizable Strength Design (MSD) concept developed Bolton (2012).

3 SHAKING TABLE TEST

A series of large scale shaking table tests were carried out at BLADE (Bristol Laboratory for Advanced Dynamics Engineering) at the University of Bristol. A rigid soil container with deformable boundaries was used to carry out experiments and necessary details of the tests can be found in Lombardi and Bhattacharya (2014). The experimental setup where 4 different structures (2 single pile denoted by SP1 and SP2 and 2 piles groups denoted by GP1 and GP2) were tested. However, in this paper only one of the structures whereby a single pile carrying a pile head mass is considered. Beam on Non-Linear Winkler Foundation analysis is carried of the structure out using SAP2000 where the proposed mechanism based p-y curve is used. Table 2 lists the structure properties.

Table 2. Properties of SP1 and input motion

Structure properties	Value
Structure ID	SP1
Outer diameter (mm)	25.4
Wall thickness (mm)	0.711
Length (m)	2
EI (Nm^2)	294
Pile cap dimension (mm)	100 × 100 × 50
Pile cap weight (kg)	1.9
Superstructure weight (kg)	5
Input motion	Christchurch earthquake Scaled by 0.5, A_{max} = 0.64g

4 DISCUSSION AND CONCLUSIONS

Figure 5 suggests that mechanism based p-y curves provide a better prediction of the bending moment profile in the pile. As discussed earlier, the mechanism based p-y curve used in the analysis is derived from the stress-strain curve of liquefied soil obtained from multi-stage Triaxial test. Beam on Non-Linear Winkler Foundation is commonly used to analyse pile foundations where the lateral pile-soil interaction is modelled as p-y springs. The current method to obtain p-y curve for piles in liquefiable soils is based on p-multiplier method whereby standard p-y curves are multiplied by a reduction factor to represent liquefiable soil. However, this form does not show the necessary features of liquefied soil. In this paper a p-y curve is proposed based on the properties of liquefied soil and the same has been used to simulate the shaking table tests. The results showed that the proposed p-y curves provide a better prediction of the bending moment in the pile.

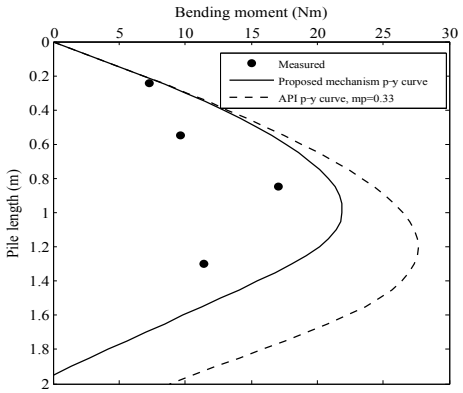

Figure 5: Results from shaking table tests for SP1

5 REFRENCES

American Petroleum Institute (2000). "*Recommended practice for planning, designing and constructing fixed offshore platforms-Load and resistance factor design."* API-RP-2A, 21st Edition.

Bolton, M.D. 2012 *Performance-based design in geotechnical engineering.* 52nd Rankine Lecture, ICE, Paper to apper to Geotechnique.

Bouzid, DJ., Bhattacharya, S., &Dash, SR. 2013. Winkler Springs (p-y curves) for pile design from stress-strain of soils: FE assessment of scaling coefficients using the Mobilized Strength Design concept. *Geomechanics and Engineering*5(5): 379-399.

Chai, JC., Carter, JP., &Hayashi, S. 2007. Modelling strain-softening behaviour of clayey soils. *Lowland technology international SI* 9(2): 29-37.

Dash, S.R. 2010.*Lateral Pile-Soil Interaction in liquefiable Soils*. PhD thesis, University of Oxford.

Lombardi, D., &Bhattacharya, S. 2014. Modal analysis of pile-supported structures during seismic liquefaction. *Earthquake Engineering & Structural Dynamic*43:119–138.

Wichtman, T. 2005. *Explicit accumulation model for non-cohesive soils under cyclic loading*, Dissertation, University of Bochum.

Finite Element Modelling of Laterally Loaded Monopile Foundations in Undrained Clay for Offshore Wind Turbines

Y. He
Department of Engineering Science, University of Oxford

ABSTRACT: This paper discusses the interaction of a monopile-soil system under monotonic horizontal loading in undrained clay soil. The simulation of the lateral loading test was carried out using the commercial FEM software-Abaqus. A kinematic multiple yield surfaces (KMYS) soil model has been implemented via the subroutine UMAT. Using this approach, the effect of the nonlinearity of soil, such as the small strain stiffness and the variable stiffness dependent on load history, on the lateral behaviour of pile can be determined. In addition, the variation of soil properties with pile depth has been accounted for. The results of load-displacement curves are presented and compared with other soil models.

KEYWORDS: FEM, lateral loading, monopile, multiple yield surfaces, clay

1 INTRODUCTION

Monopiles have been widely employed in the offshore renewable energy industry over the past ten years, because of the benefits of cost and time, in both fabrication and installation. This type of foundation can be constructed in water depths of 10-40 m. A monopile is subjected to a vertical load from the upper structure, and horizontal loads due to wind, waves and currents. Diameters of installed monopiles range from 5-7 m, however a diameter of 10 m may be required for future generation wind farms. Of course new fabrication and installation equipment will need to be developed.

The *p-y* method, initially developed from field test results of slender piles in the oil and gas sector, is recommended by API for the design of laterally loaded piles for offshore foundations. However, recent studies have identified limitations of this method when used for rigid short monopiles, such as those used for offshore wind turbines (Hald et al. 2009, Hokmabadi et al. 2012). Further optimisation of the design method is needed to account for the larged diameter piles, so that savings can be made. For example Hald et al. (2009) show that the stiffness of measured pile response is greater than design estimates.

The research described in this paper aims to further investigate monopile behaviour under lateral loading in undrained clay, using three-dimensional finite element modelling. The aim of the work is to provide a basis for developing a more advanced *p-y* method that more accurately captures wind turbine monopile response.

2 NUMERICAL MODEL

2.1 *Model geometry and material parameters*

A 3D finite element model was developed based on the soil properties for the Cowden test site, which is being used for field testing of large diameter piles in the PISA joint industry research project. For the research described here a monopile with a diameter (D) of 5 m and an embedded length (L) of 30 m was analysed.

Due to the symmetry of the problem, only half of the monopile and semi-cylinder seabed soil was considered, as presented in Figure 1. The model consists of two parts, an open-end tubular steel pile modelled with 8-noded quadratic shell elements and the seabed clay soil represented by 20-noded hexahedral quadratic solid elements. The size of the soil mesh was based on previous publications (Abdel-Rahman and Achmus, 2005). In the model the soil outer diameter was set as 15 times the diameter of the pile, and the bottom was 15 m beneath the pile end. These dimensions were chosen to minimize the effect of the boundary conditions on the pile movement. A soil plug inside the pile was assumed to exist along the pile length below the seabed level, as shown in Figure 1. The elements chosen are considered to balance the quality of result against the computational cost, for each analysis.

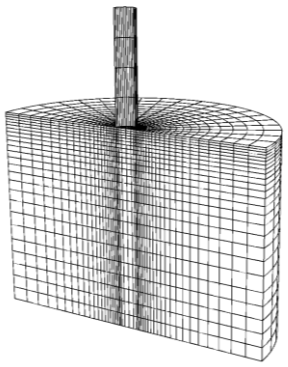

Figure 1. Mesh of the discretised model.

The horizontal force H was applied at the pile top shell edge in Figure 1, at a height, h, of 25 m above the seabed level. The bending moment at seabed level is given by $M = H \bullet h$. The load was increased gradually in 20 steps from 0 MN to 20 MN. Previous work found that vertical loading on the pile had a negligible influence on the performance of the monopile during horizontal loading, and so it was not included for these analyses.

The friction between the monopile and the soil was simulated using contact pairs approach. The mesh for the master and slave surfaces was set to be the same. The coefficient of friction used to calculate the tangential component for contact forces was chosen as $\mu = 0.4$.

The steel pile was modelled as an elastic material, with Young's modulus $E = 200$ GPa, and a Poisson's ratio $\nu = 0.3$. The thickness of the pile $t = 45$ mm was an input parameter of the shell element, and is not visualized in the discretised model shown in Figure 1. The installation effect was not taken into account so that the pile was wished into place.

Ground is not uniform in nature, and its properties vary with depth. By using the subroutine USDFLD, it was possible to simulate the linear or nonlinear variation of material parameters with depth. The soil profiles of the undrained shear strength (Su) and the initial shear stiffness (G_0) are given in Figure 2. These represent the Cowden field testing site, which are considered

very typical for offshore surface clays in the North Sea. The ground comprises only of stiff overconsolidated clay, with a saturated bulk unit weight of 21.2 kN/m^3. A geostatic step was placed before the loading steps to steady the initial stresses of soil without the monopile. The earth pressure coefficient at rest (K_0) was 1.0.

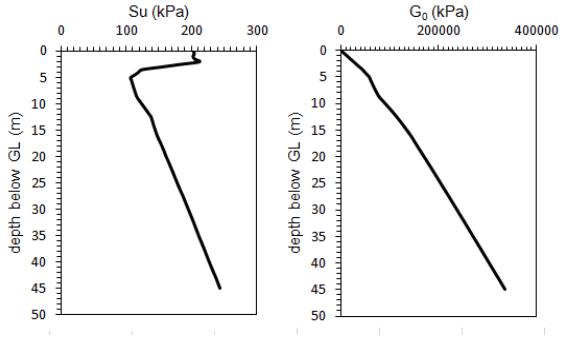

Figure 2. Soil profiles varied with depth. (G_0: Initial shear module, *Su*: Undrained shear strength from triaxial compression test)

2.2 *Kinematic multiple yield surfaces (KMYS) soil model*

The constitutive model of the soil plays a vital role in geotechnical modelling. It is necessary to choose suitable soil models for the simulations. The model adopted in this research is a multiple yield surface kinematic hardening plasticity model for undrained clay (Houlsby, 1999). It is designed to model the variation of soil stiffness with strain, including the small strain stiffness and the dependence of stiffness on recent load history. Non-linearity of soil response at low strain levels was achieved by introducing a number of initially parallel cylinders Von Mises yield surfaces. As the stress point moves in total stress space, the surfaces translate with it according to a set of linear strain hardening relationships. Further details of the model can be found in Houlsby (1999).

Table 1. Input values of non-dimensional constants

Surface	c_i	g_i
1	0.0050	0.9
2	0.0952	0.7
3	0.2264	0.5
4	0.3537	0.3
5	0.5358	0.15
6	0.6768	0.075
7	0.7679	0.030
8	0.8708	0.0075
9	0.9420	0.0006

The nine sets of parameters in Table 1 were derived by fitting stiffness data obtained from laboratory and field testing of soil taken from the Cowden site. These parameters determine the tangent stiffness and the corresponding stress for each yield surface from outside to inside in total stress space, while the outer surface is fixed to the undrained shear strength s_u.

The analyses were carried out by embedding the soil profiles in the subroutine UMAT and implementing this subroutine on the geometry model set up in Abaqus.

2.3 *Isotropic hardening plasticity*

The isotropic hardening plasticity model that is built in to Abaqus was chosen to produce a preliminary validation for the KMYS soil model. This model is based on Von Mises plasticity. By adding a series of yield stresses and plastic strains, the variations of size of the Von Mises yield surface was achieved. The required input data for the isotropic hardening soil model were calculated from the degradation of the soil stiffness from the site investigation.

3 RESULTS

Ideally large scale test data would be used to validate the various analyses, however this is not available. Therefore the focus is on comparing predicted pile response using the different soil models.

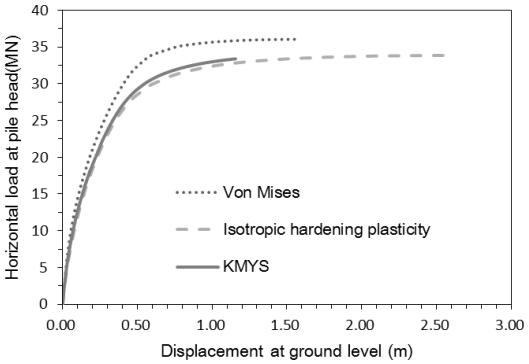

Figure 3. Comparison of the numerical results using three different soil models.

As shown in Figure 3, there is excellent agreement between the results for KMYS and isotropic hardening plasticity, which is expected in this one-way loading case. Also, they both show larger displacements than the Von Mises model due to the continuous stiffness degradation during loading. As the same undrained shear strength profile was used for these three analyses, the curves should show a clear tendency of reaching the same yielding limit.

4 FUTURE WORK

The future work will include derivation of *p-y* curves based on the results of the finite element modelling, and further calibration of the KMYS soil model. Further work will involve the modelling of cyclic loading of the monopile as this is a key design problem.

5 ACKNOWLEDGEMENTS

The results and the soil data presented in this paper were developed within the PISA research project funded by a consortium of wind farm developers and led by DONG Energy. The work is being supervised by Prof B. W. Byrne and Prof H. J. Burd. Their support is gratefully acknowledged.

6 REFERENCES

Abdel-Rahman, K., and Achmus, M. 2005. Finite element modelling of horizontally loaded monopile foundations for offshore wind energy converters in Germany. *Proceedings of the international symposium on frontiers in offshore geotechnic (ISFOG)*, Perth, Australia, 391–396.

Hald, T., Mørch, C., Jensen, L., LeBlanc Bakmar, C., and Ahle, K. 2009. Revisiting monopile design using p-y curves results from full scale measurements on Horns Rev. DONG Energy A/S, *Proceedings of European Offshore Wind Conference and Exhibition*.

Hokmabadi, A.S., Fakher, A., and Fatahi, B. 2012. Full scale lateral behaviour of monopiles in granular marine soils. *Marine structures* 29 (2012), 198-210.

Houlsby, G.T. A model for the variable stiffness of undrained clay. 1999. *Proceedings of the International Symposium on Pre-Failure Deformations of Soil.* Torino, Balkema: Rotterdam, 1999; 443–450.

Numerical Modelling of Rod Buckling in Cone Penetration Testing

J.O. Ejezie
School of Mechanical, Aerospace and Civil Engineering, the University of Manchester.

ABSTRACT: The cone penetration test (CPT) is widely regarded as an accurate method compared to other methods used in measuring ground resistance, frictional resistance and pore water pressure all at once. However, the delicate nature of the cone penetration test-rod system restricts the ground exploration limit of this state-of-the-art equipment. The CPT rod is attached to a 60° cone and pushed into the ground at a constant speed of 20 mm/sec, and with an increasing penetration depth and a slender steel member subjected to forces of varied magnitudes, buckling is inevitable. This study investigates the buckling of CPT push rods numerically in a bid to improve our understanding of the CPT system, where not only geology, but also the geometry of the rod thread, diameter of the rod, and metallurgy come into play. It was found that the buckling of the push rod is governed by the critical slenderness ratio, soil confining pressure and the embedment depth ratio of the push rod.

KEYWORDS: buckling; cone penetration test; embedment depth ratio; slenderness ratio; soil confining pressure

INTRODUCTION

The cone penetration test is a large capacity, quality, and real time based method of obtaining the engineering properties of the soil. These advantages make the cone penetration test a useful ground investigation technique amongst clients and contractors seeking to embark on civil engineering projects.

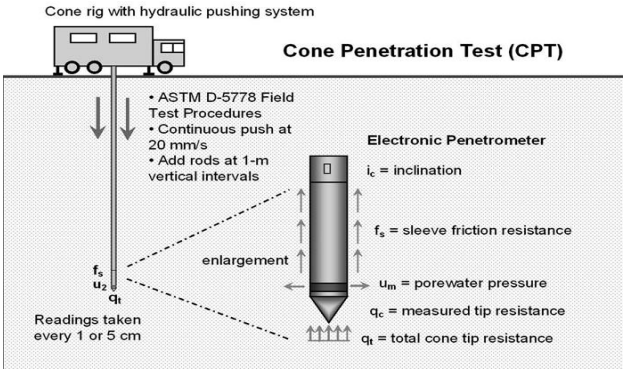

Figure 1: Modern CPT machine, (Mayne, P. 2007).

A CPT test is conducted by pushing a string of hollow rods (36mm and 16mm in outer and inner diameter) attached to a 60° cone statically into the ground at a constant speed of 20 mm/sec. The Gouda Geo-Equipment CPT manual specifies, among other signals, a sudden change in sound during ground penetration, water gushing out of the sounding rods, enormous shaking of the hydraulic system, and when a ballasted unit lifts itself, as termination points during ground investigations (Gouda Geo-Equipment, 2012). However, these termination points are based on observations and the instinct of the CPT machine operator rather than on laboratory/numerical investigations on rod-soil interaction. This study uses a numerical technique in idealizing the problem of rod buckling as it is important that proper knowledge of the buckling potential of the CPT-rod system be known to ensure best results are obtained during ground investigations.

1.1 *FE model idealization*

Abaqus provides unique options for simulating soil/structure interactions. The CPT rod was modelled as a 3-D coherent steel section and the elastic foundation option in Abaqus was used to represent the stiffness effect of an elastic homogeneous soil.

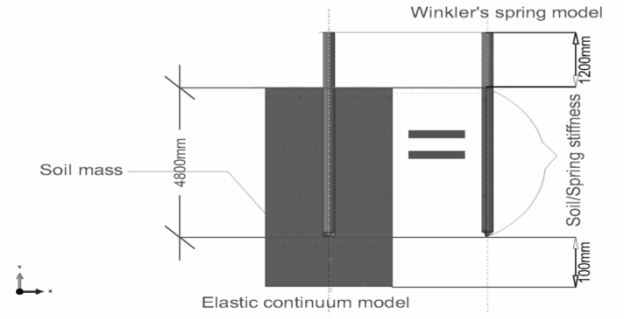

Figure 2: An elastic continuum model simplified using the elastic foundation option in Abaqus.

A cylindrical hollow rod which had an internal and external diameter (**D**) of 16 mm and 36 mm respectively was first modelled. A 60° cone having a 10 cm^2 cross sectional area was modelled separately and attached to the hollow rod using the assembly tool in Abaqus. The assembled rod had a Young's modulus of 200 GPa and a Poisson's ratio (**υ**) of 0.3. The top of the rod was fixed while the bottom was allowed to move laterally. The boundary condition applied at the base of the assembled rod reduced the total height of the push rod by a few millimetres. This was necessary to avoid instability of the model caused by restricting the movement of the rod at the tip of the cone. The soil parameters used are summarised in the table 1. Twice the Vesic's modulus of subgrade reaction equation was used in calculating the stiffness of the soil (Klar et al, 2005).

Table 1: Range of modulus of subgrade reaction, **K**

Type of Soil		Young's Modulus, **E** (MPa)	Modulus of Subgrade Reaction 2 x Vesic's equation (**K**) MPa
Clay	Very Soft	2-5	0.0473-0.1276
	Soft	5-25	0.1276-0.729
	Medium	15-50	0.419-1.545

Table 2: Comparisons between buckling load calculations using Euler's equation and Abaqus.

Rod Length (mm)	Euler's Buckling Equation $\mathbf{P_E}= \boldsymbol{\pi^2 EI/4L^2}$ x 10^{-3} KN	Eigenvalue Analysis in Abaqus ($\mathbf{P_C}$)	
		Mode **n** (1-2)	
		1 x 10^{-3} KN	2 x 10^{-3} KN
5000	1563.96	1563.3	1563.7
10000	390.989	390.81	390.85
15000	173.77	173.70	173.71
20000	97.75	97.71	97.76
30000	43.44	43.42	43.56
40000	24.44	24.41	24.48
50000	15.64	15.62	15.69

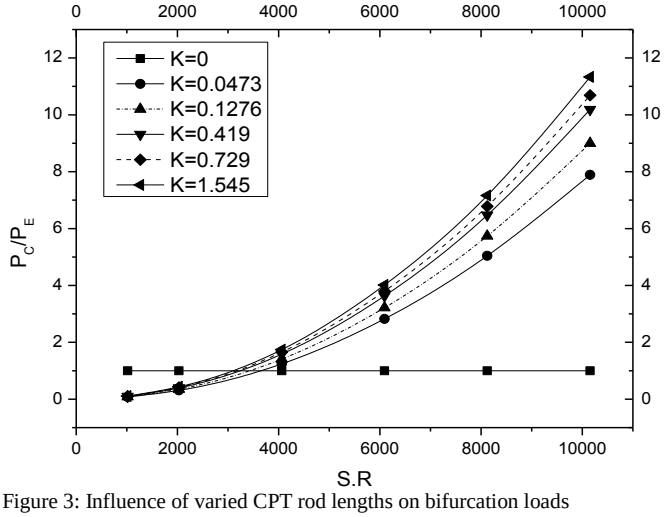

Figure 3: Influence of varied CPT rod lengths on bifurcation loads

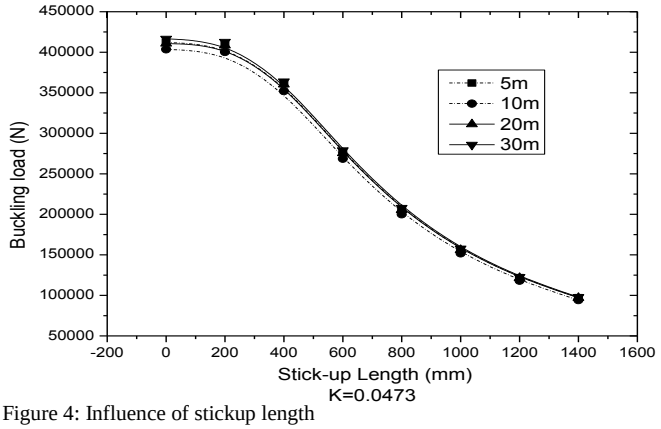

Figure 4: Influence of stickup length

DISCUSION

The Abaqus software suite was used to simulate the static buckling of CPT rods in a homogeneous soil. The proficiency of Abaqus in executing bifurcation analysis was verified by modelling and analysing a cone-less rod. The results of the buckling analysis using both Euler's equation and Abaqus are denoted by P_E and P_C respectively, in table 2. A comparison between both methods revealed an acceptable maximum error of 0.04% when computing the buckling load of the 5000 mm rod length. A non-dimensional plot is used in Figs. 3 to describe the relationship between the slenderness ratio (S.R) of the rod, the bifurcation load and the confining pressure of soils. The buckling loads are converted to non-dimensional values by dividing P_C by P_E. At zero lateral soil support the CPT rod conformed to Euler's buckling equation which does not account for a lateral support. However, when the CPT rods were supported laterally, the load required to buckle the rod increased non-linearly with an increasing slenderness ratio. Fig. 3 also shows that varying the soil stiffness from very-soft to medium will not significantly change the buckling load of a CPT rod at varied penetration depths, provided the critical slenderness ratio of the rod is not exceeded. This simply means that at low depths of penetration, the stick-up length governs the bifurcation load while at high penetration depths; the confining pressure of the soil governs. The critical slenderness ratio of the standard CPT rod ranges between 0 to 2000 and it is governed by the unsupported length of the CPT rod. The Stickup or unsupported length, which is customary to both the 10 and 20-ton equipment, affects the buckling load as shown in Fig.4. The results of the stick-up length investigation presents a closer look at the relationship between the bifurcation loads, the unsupported lengths of CPT rods and the penetration depth. It is seen in fig.4 that the change in bifurcation load becomes significant when the unsupported length is greater than 200 mm. This simply means that at a very low embedment ratio the CPT rod will behave like a fully embedded rod. This observation is in line with the previously discussed results of Fig.3, which identified the stick-up length as the buckling governing factor at low embedment depths. In view of the above findings, there is a need for the redefinition of the word 'Refusal Depth'. The results show that the buckling of a CPT rod is governed by the critical slenderness ratio, soil confining pressure and embedment depth ratio.

CONCLUSION

A study has been conducted on the buckling of cone penetration test rods. The result describes the relationship between buckling load, soil stiffness and the slenderness ratio of the CPT tubes. The results will be useful to CPT operators and manufacturers of the CPT equipment.

REFERENCES

Gouda Geo-Equipment B.V (2012), Manual: CPT sounding tubes, p.6.

Klar, A., Vorster, T. E. B., Soga, K., and Mair, R. J. (2005a). "Soil-pipe-tunnel interaction: Comparison between Winkler and elastic continuum solutions." Geotechnique, 55(6), 461-466.

Mayne, P. (2007). Synthesis 368 on Cone Penetration Test, National Cooperative Highway Research Program (NCHRP), Transportation Research Board, National Academies Press, Washington, DC.

Finite element limit analysis of skirted shallow strip foundations

H.P. Dunne
Department of Engineering Science, University of Oxford

ABSTRACT: Skirted shallow foundations are often used to support subsea structures. Sometimes it is necessary for such foundations to be situated on a sloping sea bed. This paper uses computational limit analysis techniques to investigate how the ultimate bearing capacity of such skirted foundations is affected by a seabed inclination, footing interface roughness and depth of the footing skirts. The geometry is idealized as two-dimensional (plane strain) and the soil response is assumed to be undrained, with an associated flow rule. OxLim Finite Element Limit Analysis (FELA) software was used to undertake the analyses. OxLim uses adaptive mesh refinement to calculate closely bracketed lower and upper bound plasticity solutions. This study considers combined vertical and horizontal (V-H) loading, as well as combined vertical and moment loading (H-M). The results are reported in the form of normalized failure envelopes.

1 INTRODUCTION

Skirted shallow foundations are often used to support subsea structures. These are generally steel, and the skirts are designed to penetrate into the sea bed in order to confine the soil between them, creating a beneficial soil plug. Subsea structures such as pipeline line end terminals (PLET's) and pipe line end manifolds (PLEM's) are commonly supported on such foundations, and in some occasions it is necessary for their installation on an inclined sea bed.

The bearing capacity of shallow foundations can vary depending on a number of factors, including the base roughness, and the tensile capacity at the interface. The shear resistance at the interface (τ_o) is:

$$\tau_o = \alpha S_u \quad (1)$$

Where *Su* is the undrained shear strength of the soil, and α is the roughness factor, ranging from 0 (for a smooth footing) to 1 (for a fully rough footing). The assumption of a fully rough interface is common in finite element analysis studies. At the interface, the soil can have no tensile capacity in the normal direction (T = 0), resulting in the breakaway of the footing from the soil if upwards movement occurs. Conversely, if the interface has infinite tensile capacity (T = ∞), the soil at the base of the foundation can be pulled upwards if there is upwards movement of the footing.

The vertical bearing capacity (q_{ult}) for a strip footing on flat ground is well-established, and is conventionally calculated using modified versions of the classical Terzaghi (1943) bearing capacity equation:

$$q_{ult} = \frac{Vult}{A'} = N_C S_u S_c i_c \quad (2)$$

Where the plane strain bearing capacity factor, *Nc*, is the exact solution 2 + π, for both fully rough and fully smooth foundations where there are no skirts on the footing. An exact solution for pure horizontal loading is equal to the shear strength at the interface multiplied by the footing width, αBSu. Similarly, moment loading (M) on a footing with no skirts has an exact solution for the bearing capacity of $0.69B^2Su$ (Murff & Hamilton, 1993).

Hansen (1961) and Vesic (1975) have expanded on this equation to include empirical factors for foundations near sloping ground. Although there is much research into footings near slopes, and slope stability in itself, there is minimal research into footings on sloping ground.

1.1 *Finite element limit analysis*

The analysis was carried out using the OxLim FELA program, which was developed at the University of Oxford. OxLim differentiates from traditional finite element analysis programs in that it calculates strict upper and lower bounds, bracketing the exact solution.

OxLim employs an adaptive meshing technique, recalculating the mesh size after each iteration based on the computed strains. This allows for the calculation of a highly accurate bracketing of the solution, while the slip line of the failure mechanism can generally be determined by upon visual inspection of the solution. The lower bound is determined from obtaining the highest stress state while still satisfying the equilibrium equations, whilst the upper bound solution requires maintaining a collapse mechanism, by ensuring the rate of work of the external forces is greater than or equal to the rate of internal energy dissipation.

OxLim generates a vector plot for each analysis, allowing for the visualisation of the upper bound displacements and lower bound stress fields.

The underlying theory behind OxLim is explained by (Makrodimopoulos & Martin, 2006, 2007a, 2007b).

2 PROBLEM DESCRIPTION

This paper is addresses the problem of a shallow footing on flat and sloping ground inclined at Θ = 5 degrees (see Figure 1). Undrained soil conditions and an associated flow are also assumed. The footing width over the depth of the skirts (d) was considered for B/d = 0 and B/d of 0.1 (see Figure 1). The thickness of the skirts is 0.005B.

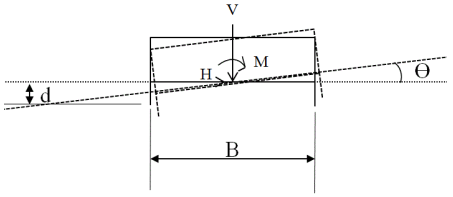

Figure 1. Loading arrangement for footing

Roughness factors (α) of 1.0, 0.5 and 0 were considered for the base and skirts of the footing. The interface tension capacity was considered for the cases of infinite tension capacity (T = ∞).

The footing was loaded using combined horizontal (H) and vertical (V) loads, as well as combined horizontal and moment (M) loads. Failure envelopes for V-H loading and H-M loading were generated using Oxlim bricked solutions to 1.0%. The solutions are generated from probing outwards at a specified ratio of loads. Each probe provides one point on the envelope, and each envelope comprises thirty six probes.

3 RESULTS

The results are displayed are for normalised load envelopes (see Figures 2-5). The loads are normalised by dividing by the footing width the undrained shear strength (Su). The results match the benchmark results discussed earlier for horizontal, vertical and moment load. It can be seen that the roughness factor contributes significantly to the capacity, particularly when d/B=0.

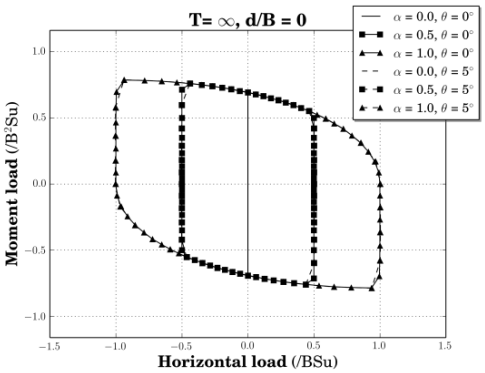

Figure 2. H-M failure envelopes for d/B = 0, T = ∞

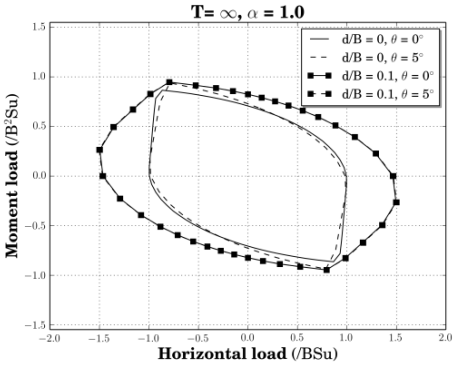

Figure 3. H-M failure envelopes α= 0, T = ∞

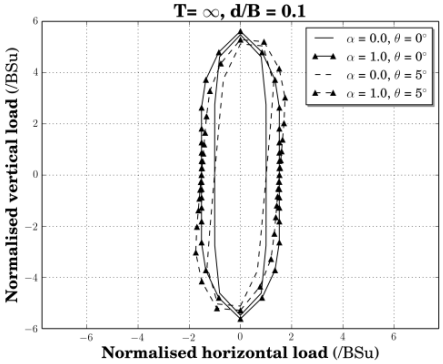

Figure 3. H-M failure envelopes for d/B = 0, T = ∞

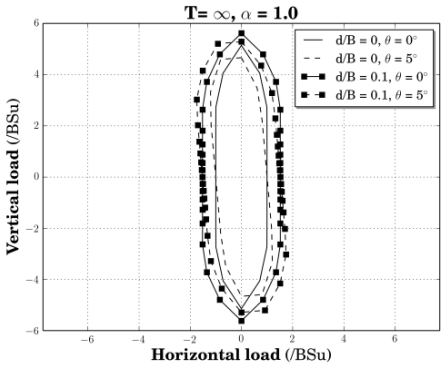

Figure 5. V-H failure envelopes with varying d/B and Θ

4 CONCLUSION

It can be seen that the results compare closely with exact known solutions for vertical load, horizontal load and moment load given in Section 1. The roughness factor can significantly alter the bearing capacity, and its inclusion in analysis of shallow foundations is important.

5 FUTURE WORK

This research is part of a DPhil currently in its first year. Future research will include development of the OxLim FELA software from a two dimensional analysis package to a three dimensional analysis package. The results obtained will be verified using traditional Finite element software.

6 ACKNOWLEDGEMENTS

I would like to thank Subsea7 for providing the funding for this project and my supervisor Chris Martin for his continued guidance and expertise.

7 REFERENCES

Dimmock, P., Clukey, F., Randolph, M. F., Murff, D., & Gaudin, C. (2013). Hybrid Subsea Foundations for Subsea Equipment. *Journal of Geotechnical and Geoenvironmental Engineering*, *139*(December), 2182–2192. doi:10.1061/(ASCE)GT.1943-5606.0000944.

Hansen, B. J. B. (1961). A general formula for bearing. In *Bulletin No. 11. Danish Geotechnical Institute* (pp. 38–46). Copenhagen, Denmark. doi:624.131.5:624.15

Makrodimopoulos, A., & Martin, C. M. (2006). Lower bound limit analysis of cohesive-frictional materials using second-order cone programming. *International Journal for Numerical Methods in Engineering*, *66*(4), 604–634. doi:10.1002/nme.1567

Makrodimopoulos, A., & Martin, C. M. (2007a). Upper bound limit analysis using discontinuous quadratic displacement fields. *Communications in Numerical Methods in Engineering*, *24*(11), 911–927. doi:10.1002/cnm.998

Makrodimopoulos, A., & Martin, C. M. (2007b). Upper bound limit analysis using simplex strain elements and second-order cone programming. *International Journal for Numerical and Analytical Methods in Geomechanics*, *31*(6), 835–865. doi:10.1002/nag.567

Murff, J. D., & Hamilton, J. M. (1993). P-ultimate for undrained analysis of laterally loaded piles. *ASCE Journal of Geotechnical Engineering*, *119*(1), 91–107.

Terzaghi, K. (1943). *Theoretical soil mechanics*. John Wiley and Sons, Inc.

Vesic, A. S. (1975). Bearing capacity of shallow foundations. In H. F. Winterkorn & H. Fang (Eds.), *Foundation Engineering Handbook* (1st ed.). New York: Van Nostrand Reinhold.

An simple strategy for soil structure interaction problems

N. Bux
Coffey

ABSTRACT: This paper describes the assembly of a "production line" of relatively simple analyses to model a complex soil structure interaction problem. It discusses the features of the method in relation to the features of a finite element formulation. It is considered that the method has several advantages over the use of finite elements and it is likely to give results of equal or better reliability.

KEYWORDS: Structural assessments, soil structure interaction, Finite Elements.

1 INTRODUCTION

Finite element programs (FE) are typically used to assess the geotechnical impact of construction activities on sensitive structures. However, they can have significant limitations. For example it is well known that finite elements have difficulty in modelling the settlement trough above tunnels, and hence the effect on structures.

This paper describes an alternative method, which was used to assess the effects of an embankment on an adjacent sensitive piled structure. The method consists assembling a "production line" of relatively simple and stand-alone analyses. The method has a number of advantages over finite element techniques, as discussed below.

2 PROJECT OVERVIEW

The proposed scheme comprised a new dual lane road embankment up to about 5 m high on soft ground overlying Till. It passes close to a sensitive structure founded on piles within the Till. Concern was expressed about the effect of the embankment construction on the structure foundations and hence on the fabric of the structure itself. Table 1 shows a summary of ground conditions.

Table 1 Ground model & soil properties used

Strata	Depth to base	γ	s_u	ϕ′	m_v
	m	kN/m^3	kPa	deg	m^2/MN
Made ground / Alluvial deposits	6-11	17	30	26	0.3
Glacial Till	40	20	150	28	0.05
Sandstone	n/a	22	n/a	n/a	n/a

3 OUTLINE OF METHOD

The stages of the analysis were as follows;

1. Calculate embankment settlement from conventional one dimensional theory.
2. Calculate elastic soil movements at the pile locations using software FLEA 5 (Small 1986), calibrated against consolidation settlement.
3. Calculate pile and pile group movements using the soil pile interaction program EMPIG (Poulos 1994).
4. Adjust the pile group movements using the individual pile group stiffness relationships obtained from EMPIG and the known structural connections between them.

Some work was necessary to construct a production line of software by manipulating the output from FLEA 5 to produce suitable input for EMPIG. This was carried out in spreadsheets.

Output in graphical form could be generated at each stage of the analysis as a means of checking the reasonableness of the results. A typical example is shown in Figure 1, which presents a profile of horizontal ground movement and corresponding horizontal pile movement.

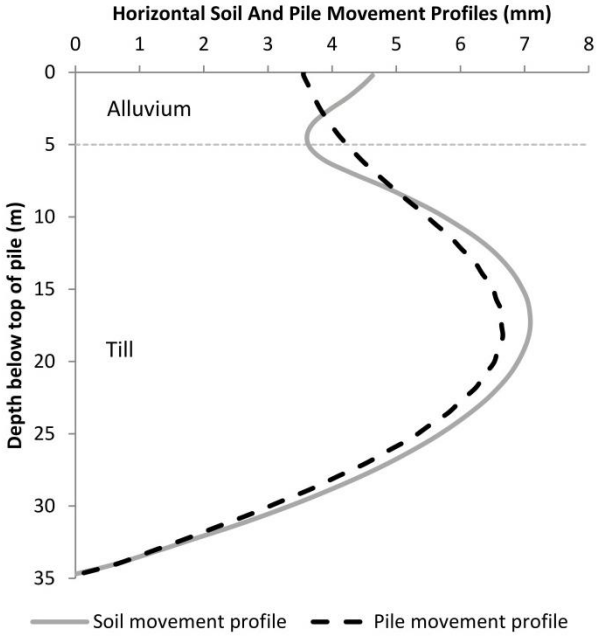

Figure 1. Horizontal soil and pile movements.

It can be seen that, in the stiff Till, the curvature of the pile follows the soil profile quite closely whereas movement of the soft Alluvium have little effect on the pile movements.

4 ASSESSMENT OF "PRODUCTION LINE" METHOD

The "production line" method is considered to have a number of advantages over finite element techniques. In the first place,

each individual software package was relatively simple and required very little input data. Consequently it was possible very easily to carry out sensitivity analyses. Also, as described above, it was a simple matter to create graphical representations of output.

One of the features of the embankment was that its geometry varied considerably close to the structure. It was therefore not appropriate to treat the problem as one of plain strain. The loading had to be modelled in three dimensions. This was a fairly simple procedure in FLEA 5, which allows the loading to be applied as a number of discrete rectangles and then uses superposition to combine the various solutions. It is considered that development of a 3D finite element model would have been very complex and time consuming.

It is accepted that the representation of the loading as discreet rectangles is an approximation. However, the approximation is at least explicit and hence should easily be recognised by the user. Assumptions in finite element formulations e.g. the location of the far boundary or the formation of the mesh may be less easily recognised and taken account of.

As stated above, finite element formulations of the effects of tunnels are known to be difficult to implement. It is considered that a finite element model of the effect of ground movement on piles might have similar difficulties. In addition, interaction between a pile group and the soil could be modelled in finite elements only by using a 3D formulation.

It is therefore considered preferable to use software specifically designed to model soil pile interaction such as EMPIG. Such software has the advantage of incorporating explicit models of such features as bending of the piles.

Another feature of EMPIG is that it is possible to derive a complete stiffness matrix for a pile group. This can be used to model structural connections between pile caps (Figure 2). In the case shown, the two pile caps were connected by a very substantial beam which was modelled as being rigid. The free field ground movements and subsequent pile group movements were first modelled independently, then the implication of the rigid connection modelled in a spreadsheet that incorporated the equations modelling the connection.

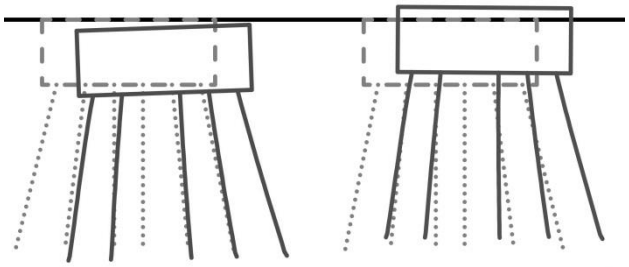

(a) Graphical output of the results from the "production line" assessment for two pile groups assessed separately due to imposed ground movements from adjacent construction activities.

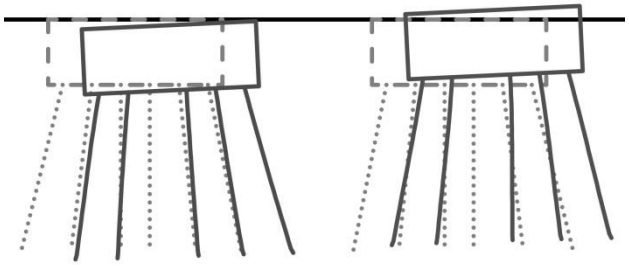

(b) Graphical output and results of the same two pile groups assessed with a rigid structural connection between the pile groups due to the same imposed ground movements from (a).

Figure 2. A graphical representation of pile group movements with rigid connections.

5 CONCLUSIONS

This paper has described the assembly of a "production line" of relatively simple analyses to model a complex soil structure interaction problem. It is considered that the method has several advantages over the use of finite elements and it is likely to give results of equal or better reliability.

6 ACKNOWLEDGEMENTS

Dr. AKC Smith for his encouragement, support and mentoring.

7 REFERENCES

Poulus, H,G, March, 1994
Design of piles through embankements, Phasee 5: Development of computer program 'EMPIG'. Report No. S9711/5-A. Coffey Partners International Pty Ltd.

Small, J.C, 1986
User manual, program FLEA, (Finite Layer Elastic Analysis). School of Civil and Mining Engineering. The university of Sydney

Experimentally accelerated weathering of Mercia Mudstone (MM)

F. A. Ibrahim

School of Earth, Atmospheric and Environmental Sciences, The University of Manchester
School of Mechanical, Aerospace and Civil Engineering, The University of Manchester

ABSTRACT: Mechanical properties of Mercia Mudstone (MM) vary with its degree of weathering which makes it problematic in some geotechnical applications. This technical note describes a set of simulated accelerated weathering experiments using MM as a substrate. The purpose of this study is to investigate weathering-induced chemical and mineralogical changes in MM with time. To simulate accelerated weathering, de-ionised water (DIW) and HCl (pH4 and pH2.5) were reacted with MM in batch and flow-through experiments. Solid substrates were characterised before and after using X-ray fluorescence (XRF) spectroscopy and X-ray diffractometry (XRD). Leachates were analysed using ion chromatography (IC) and inductively coupled plasma (ICP) spectometry. Results indicate that carbonate and sulphate components (calcite, dolomite and gypsum) of MM are the least stable and most susceptible to dissolution weathering. In contrast, the clay mineral assemblage is physically and chemically stable. Future work includes triaxial testing of compacted MM to examine the impact of experimentally accelerated weathering on its hydraulic and shear strength parameters.

KEYWORDS: Mercia Mudstone, Weathering, Mineralogy, Experimental dissolution

1 INTRODUCTION.

Weathering can be defined as the mechanical and chemical processes that act at or near earth surface causing the degradation of its materials. Chemical weathering involves different types of reactions led by water and/or weak acids. These two agents are responsible for one of the most common weathering process which is dissolution. In that water and/or weak acids react with unstable minerals, with temperature and active surface area being the key physical variables. Gislason et al. (2008) found that chemical weathering is boosted by an increase in annual mean temperature. A rise in the average global air and ocean temperature has already been observed (ICCP, 2007), and weathering processes are likely to be accelerated.

MM has been considered a problematic material for geotechnical applications since its mechanical properties significantly vary with the degree of weathering (Chandler and Forster, 2001). It has, though, been used in the foundations of dams and embankments or as a construction material. MM obtained from a reservoir embankment near Lincoln, UK, is the substrate selected for this study. Two experiments, one batch-leaching and the other flow-through, were performed to accelerate the weathering of MM using DIW and dilute HCl at pH4 and pH2.5. This note includes the initial characterisation of MM, a description of the experiments and a discussion of the results.

1.1 *Material characterisation*

The initial MM was first characterised in terms of chemical composition using XRF (Table 1), mineralogy using XRD (Table 2) and index properties (Table 3).
For XRD analysis, the presence of large crystals or highly-crystallised phases such as quartz results in high peaks patterns leaving less well-ordered components such as clay minerals under represented. Clay-size particles were, therefore, separated out by sedimentation and examined independently in the flow-through experiment.

Table 1.Major components of MM obtained by XRF

Major component	**Concentration (%)**
SiO_2	*43.81*
Al_2O_3	*14.86*
CO_2	*11.88*
MgO	*10.11*
CaO	*6.46*
Fe_2O_3	*6.04*
K_2O	*4.23*
H_2O	*1.08*
TiO_2	*0.65*
Na_2O	*0.32*
P_2O_5	*0.18*

Table 2.Identified phases in XRD patterns of MM and clay-size fraction

Phase	**Chemical formula**
Quartz	SiO_2
Dolomite	$CaMg(CO_3)_2$
Calcite	$CaCO_3$
Albite	$NaAlSi_3O_8$
Pyrite/Hematite	FeS_2/Fe_2O_3
Muscovite	$KAl_2Si_3AlO_{10}(OH)_2$
Orthoclase	$KAlSi_3O_8$
Illite	$(K,H_3O)Al2Si_3AlO_{10}(OH)_2$
Chlorite	$Mg_{2.5}Fe_{1.65}Al_{1.5}Si_{2.2}Al_{1.8}O_{10}(OH)_8$
Sepiolite	$Mg_4Si_6O_{15}(OH)_{2.6}(H_2O)$

Table 3.Index properties of MM and associated procedures

Index property	**Value**	**procedure**
Plastic limit (%)	*20.75*	*BS 1377-2:1990*
Specific gravity	*2.725*	*flask method (Akroyd, 1957)*
Gravel content (%)	*15*	*wet sieving (BS 1377-2:1990) and sedimentation*
Sand content (%)	*21*	
Silt content	*36*	
Clay content (%)	*28*	

1.1.1 *Experiments*

Prior to examination, MM was oven dried and powdered to increase the contact surface with the fluids and consequently prompt interaction and potential mineralogical alteration.

Batch-leaching and flow-through experiments involve subjecting a small amount (less than a gram) of the substrate to a high volume of an aggressive fluid to optimise the likelihood of leaching. In the flow-through experiment (Figure 1), a thin film of powdered MM was set in small cells and a flow of DIW, pH4 HCl or pH2.5 HCl was flushed through regulated by a peristaltic pump. Reacted film samples were removed at regular time intervals, left to air-dry and then characterised using XRD.

In the batch-leaching experiment, MM was dispersed in the three fluids at a high ratio of 1:45 and left in a tumbler for 2 to 4 weeks. Specimens were sampled from the suspensions at regular time intervals, centrifuged, filtered and then analysed for solutes using IC and ICP respectively.

Figure 1.Flow-through experiment set

1.1.2 *Discussion of analysis results*

A comparison between XRD data for MM before and after flow-through experiment showed that silicates were not affected by the used fluids but carbonate components including calcite and dolomite were found to give smaller peaks with increasing acidity until they can be no more detected in XRD patterns of MM weathered by pH2.5. This indicates the dissolution of these components which are the main cementing agents in MM (Hobbs et al., 2002). Looking at ICP analysis of leachates sampled from the batch-leaching experiment, it was found that Ca^{2+} concentration increased with time while there was not a considerable change in the lower concentration of leached Mg^{2+}. This may indicate that the main dissolved component was calcite rather than dolomite which was found before to be not or slightly degraded in weathered MM near earth surface (Pearce et., 1996). However, there is another possible source of Ca^{2+} in MM which is gypsum. Although it was not detected in XRD patterns of MM, Gypsum was seen on site while collecting the samples; large bulks were founds in the surrounding area.

XRD patterns of clay-size fraction, before and after the flow-through experiment, did not show any significant changes neither with time nor with increasing acidity. The detected minerals maintained the same peak intensities and revealed no significant changes in the peak widths. Relative peak intensity is related to chemical composition and crystallinity, while the width of the diffraction peak at half its height is related to the size of the phase domain (Moore and Reynolds, 1989). The XRD data suggest that no significant physical or chemical changes have occurred and the clay assemblage in the tested MM is stable.

IC analyses of the different solutes revealed a loss of sulphate during batch experiment. Leaching of sulphate from MM occurred gradually in DIW and pH4 HCl, whereas it was quicker and had higher concentration with pH2.5 HCl. In the later, the average concentration detected by IC was 11 mg/l leached in 24 hours (or less) and this concentration was relatively constant within the following two weeks of reaction. XRD patterns of the initial and weathered MM showed no sulphur-containing phases. However, gypsum was seen on site when the testing material (MM) was collected. Gypsum, therefore, is probably present in MM at concentrations below the detection limits (5%) of the XRD. In addition, sulphur trioxide was detected when analysing the chemical composition of initial MM using XRF.

2 CONCLUSION

Results suggest that weathering of MM by DIW and HCl causes the dissolution of carbonate and sulphate and does not impact the clay minerals assemblage, or other silicates, significantly. Therefore, potential weathering-induced changes in the mechanical behaviour of MM are likely to be a consequence of dissolution of the carbonate cementing components and sulphate only. These changes will be explored in the future work on triaxial testing of compacted specimens of MM.

3 ACKNOWLEDGEMENTS

The access to Lincoln reservoir and collecting testing material was not possible without the help of keen professionals, especially Laura Jarvis (Mott MacDonald) and Andrew Smith (Galliford Try), who worked on that site. Geochemical experiments and analyses and lab geotechnical work have been supported by many friendly technicians. Thanks are always to my supporting supervisors; prof. Colin Hughes, Dr. Carlos Lam and Dr. Ahmad Syed.

4 REFERENCES

Akroyd, T., 1957. Laboratory testing in soil engineering. Geotechnical Monograph, No.1. Soil Mechanics LTD.

Chandler, R.J. & Forster, A., 2001. Engineering in Mercia Mudstone. CIRIA Report C570.

Gislason, S. R., Oelkers, E. H., Eiriksdottir, E. S., Kardjilov, M. I., Gisladottir, B. S., Snorrason, A., Elefsen, S., Hardardottir, J. Torssander, P., Oskarsson, N., 2008. Direct evidence of the feedback between climate and weathering. Earth and Planetary Science Letters, 277(1-2), pp213-222.

Hobbs. P. R. N., Hallam, J.,R., Forster, A., Entwisle, D., C., Jones, L.,D., Cripps. A., C., Northmore, K., J., Self, S., J., Meakin, J., L. (2002). Engineering Geology of British Rocks and Soils. Mudstones of Mercia Mudstone Group. Urban Geosiences and Geological Hazards Programme (UGGH). British Geological Survey. Reseach Report.

IPCC, 2007: Climate Change 2007: The Physical Science Basis. Contribution of Working Group I to the Fourth Assessment Report of the Intergovernmental Panel on Climate Change [Solomon, S., D. Qin, M. Manning, Z. Chen, M. Marquis, K.B. Averyt, M.Tignor and H.L. Miller (eds.)]. Cambridge University Press, Cambridge, United Kingdom and New York, NY, USA.Moore, D.M. and Reynolds, R.C. (1989) X-ray Diffraction and the identification and analysis of clay minerals, Oxford University Press, Oxford

Pearce, J M, Kemp, S J, and Hards, V L. 1996. A petrographical and mineralogical study of clay minerals in the Mercia Mudstone. British Geological Survey Technical Report, WG/96/22R.

Changes to small strain stiffness with time in reconstituted white chalk specimens

G. A. Bialowas and A. Diambra
Department of Civil Engineering, University of Bristol, UK

ABSTRACT: This paper presents preliminary results from an experimental characterisation of the small strain stiffness of remoulded chalk and investigates its changes with time. The preliminary results using Bender Element (BE) measurements have shown that an increase in speed of propagation of shear wave can be observed with time. The triaxial tests performed after different duration of the constant effective pressures applied to the sample have also shown a variation to the initial stress-strain behaviour. Further research is in progress to quantify effects of creep and eventual re-cementation of the remoulded material.

KEYWORDS: English chalk, reconstituted samples, small strain stiffness, bender elements measurements.

1 INTRODUCTION

The deformation of weakly cemented sedimentary rock during intensive compaction and/or shearing, typically results in a formation of an annulus of remoulded chalk around the piles which indeed governs the performance of in-chalk foundations (CIRIA 2002). Clayton (1990) has shown that the cohesion of the remoulded chalk might alter with time, suggesting some re-cementation of the soil (CIRIA 2002). Re-cementation of remoulded chalk around the piles was also reported in CIRIA PR 86 (Lord et al., 2003).

Naturally re-cemented carbonated sediments are very weakly bonded (Clayton 1990). This calcite and/or aragonite crystal bond typically breaks before material reaches a region of normal consolidation response (Coop 1993). As a consequence, ordinary testing method for cemented soils, such as: 1-D compression test or conventional triaxial test will require instrumentation for measurements in small strain domain.
The object of the research is to characterise and investigate changes with time in both strength and small strain behaviour of remoulded chalk.

2 MATERIAL TESTED AND EQUIPMENT

2.1 *English upper chalk*

Margate chalk collected from the outcrop quarry in Kent is investigated in this paper. In accordance with CIRIA (2002), Margate chalk is classified as a grade B2, B3 upper chalk with a typical intact porosity around 44%. On average, specific gravity of the material is about 2.69, which is similar to the specific gravity of a pure calcite 2.72 (Bell. 1999).

Clayton (1990) has shown that the in-situ crushed material during earthworks is almost entirely composed of silt and clay size particles, with less than 5% of particles larger than 0.1mm. This Particle Size Distribution curve corresponds fairly accurate with depositional grain sizes of the bioclasts during chalk formation (Bell. 1999). As a consequence, Margate Chalk excavated from quarry was oven dried in temperature of 105˚C for 24h before crushing. Subsequently, chalk rocks larger than 30mm (longest diameter) were crushed using the plastic mallet and further grinded using the hand disc grinder. Next, gravel size material was passed through the Jaw Crusher BB 100 at the specific Jaws arrangements for further crushing. The Liquid Limit (*LL*) measured for the crushed chalk is equal to 31%.

2.2 *Triaxial tests equipment*

The 50kN maximum capacity loading frame equipped with water tight triaxial cells designed to withstand 2000kPa of water pressure is used for experiments. The cell was modified to accommodate 50mm diameter and 2:1 height to diameter ratio samples (TC-29 2005). The system is instrumented with an External Linear Displacement Transducer (LDS), Volume Gauge (VG) and Pressure Transducers (PT) for both cell and back pressure.

2.3 *Bender Elements equipment*

Initial shear modulus (G_{max}) testing method, based on shear wave propagation velocity measurement, is applied for the experiment (Dyvik 1986). Pizo-ceramic materials in form of Bender Elements (*BE*) are incorporated within the triaxial cell to investigate a G_{max} value (see Figure 1) (Dyvik 1986, Pennington 1999, TC-29 2005)

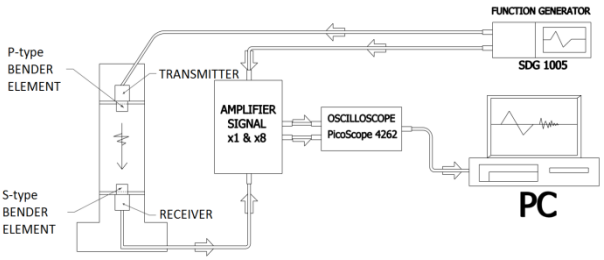

Figure 1. Bender elements and signal acquisition arrangement.

3 SAMPLE PREPARATION & TESTING PROCEDURE

3.1 *Reconstituted chalk samples*

Reconstituted samples with 50mm diameter are prepared based on the technique described by Feron (2000) and Pennington (1999). This technique involves K_0 – consolidation of the chalk slurry in an external consolidometer device (Pennington 1999). To obtain the pouring slurry, fully dried material is mixed for 20mins with de-ionised and deaerated water until reaches 2.2 times (*LL*). Then the slurry is carefully poured into a bottom closed funnel and placed into a deaerating chamber for 60mins to remove entrapped air bubbles. Small rhythmical vibrations are applied to facilitate air removal. After deaeration, the sample is poured into 50mm inner diameter consolidometer tube and an initial 10kPa of normal stress is applied. Normal pressure increments are than applied in successive stages, upon completion of consolidation. This process is continued until the desired consolidation pressure is achieved. The consolidometers used for the test are of the floating cylinder type to minimise the effects of the shaft friction (Pennington 1999). Finally, wet chalk sample is extruded from the consolidation tube, moved on the pedestal of the triaxial cell where rubber membrane is slid on over.

3.2 *Testing procedure*

Before conventional triaxial test commence, both porous discs are flashed with deaerated water to remove entrapped air bubbles from sample placing. The back pressure is then increased to 400kPa with constant mean effective stress kept at 20kPa for further sample saturation. When desirable Skempton B value is achieved, isotropic consolidation is applied and the sample is left to cure at a constant pressure condition.

Wave propagation velocity, using *BE*, is periodically measured during curing period. This value is then processed to evaluate the G_{max} vale for further data analysis (see Eq. 1).

$$G_{\max} = \rho V_s^2 = \rho * \left({l_p}^2 \Big/ t^2 \right) \quad (1)$$

Where ρ is a bulk density of a chalk sample and V_s is a velocity of the wave propagation through the distance (l_p) over time (t).

Finally, monotonic Consolidated-Drained (*CD*) compression test is applied to the sample to complete the test.

4 INITIAL OBSERVATIONS AND RESULTS

Results of a series of 3 triaxial compression tests cured over different periods of time are reported here. Figure 2 shows the deviatoric stress ratio ($\eta=q/p'$) – deviatoric strain (ε_q) trends. It can be observed that the samples cured for longer duration of time (*tests1&3*) show a stiffer initial response when compared with the sample not cured at all (*test2*). The samples from *tests1&3* have a higher and more defined yield point than the non-cured sample. This corroborates other experimental observations on the behaviour of weakly cemented calcareous soils (Coop 1993).

On the other hand, all tested samples achieved similar maximum deviatoric stress ratios at large strains. This corresponds to a friction angle (φ) of about 34 °.

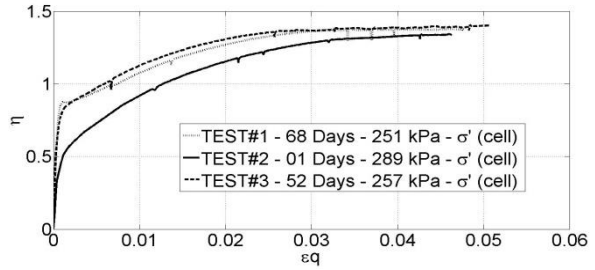

Figure 2. Plot of stress ratio versus deviatoric strain for 3 reconstituted chalk samples obtained from *CD* conventional Triaxial Test.

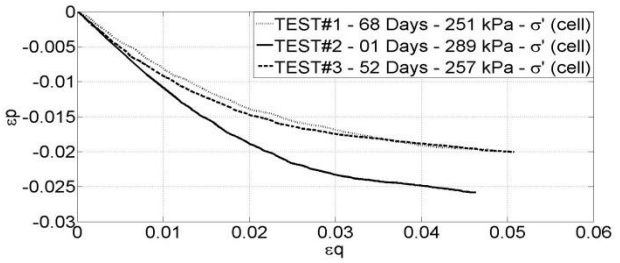

Figure 3. Plot of Volumetric Strain versus deviatoric Strain for 3 reconstituted chalk samples from *CD* conventional Triaxial Tests.

Figure 3 reports the measured volumetric (ε_p) - deviatoric strains (ε_q) trends for the three samples. It is visible that constant volume conditions are reached at large strains which may suggest that critical state conditions have been achieved. The non-cured sample shows a more compressive behaviour than the other two which agrees well with the observed stress-strain behaviour in Figure 2.

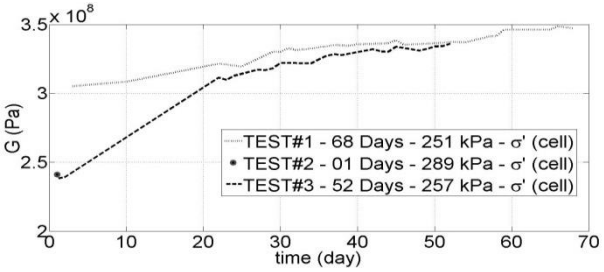

Figure 4. Increase in soil stiffness with time measured using Bender Elements under constant effective cell (σ') pressure.

Figure 4 presents the change in small strain stiffness measured via *BE* during samples curing. The observed data is in agreement with the increased initial stiffness observed in Figure 2. It can be seen that the biggest change to the stiffness modulus has taken place during first 20days. This could be affected by either creep or re-cementation (Clayton 2011), thus further study is required on this issue. After this first major change, the sample stiffness continues to increase at slower rate.

5 CONCLUSION & FUTURE TESTS

The preliminary tests have shown that the small strain stiffness of remoulded chalk is changing with time while it appears that the strength is not so affected. *BE* and triaxial test measurements have proven to be effective in detecting changes to the chalk stiffness at different strain ratios.

Since both creep and re-cementation may influence these changes to the chalk stiffness, the Linear Variable differential transformers (*LVDTs*) will be incorporated inside the testing cell for more sensitive strain measurements. *LVDTs* will be also used to validate the stiffness measurements recorded via *BE*.

Future research will also attempt to characterise the changes to small strain stiffness with time for isotropic and anisotropic stress levels. Moreover, as the water chemistry might have an effect on the degree of re-cementation, water fully saturated with calcite mineral will be used for data comparison.

6 REFERENCES

Bell, F. G. C., M.G. Cripps, J.C. (1999). "A review of selected engineering geological characteristics of English Chalk." Engineering Geology **54**(3-4): 237-269.

CIRIA (2002). Engineering in chalk. J. A. C. Lord, C.R.I. Mortimore, R.N., CIRIA - Publication C574.

Clayton, C. R. I. (1990). "The mechanical properties of the Chalk." Chalk: proceedings of the International Chalk Symposium

Clayton, C. R. I. (2011). "Stiffness at small strain: research and practice." Géotechnique **61**(1): 5-37..

Coop, M. R. A., J. H. (1993). "The mechanics of cemented carbonate sands." Géotechnique **43**(1): 53-67

Coop, M. R. A., J. H. (1993). "The mechanics of cemented carbonate sands." Géotechnique **43**(1): 53-67.

Dyvik, R. A. M. (1986)."Lab measurements of G max using bender elements." Norges Geotekniske Institutt (NGI) publikasjon **161**: 6.

Feron, R. E. C., M.R. (2000) "Reconstitution: what makes an appropriate reference material?" Géotechnique **Vol.50**(No. 4): 471–477.

Lord, J. A. (2003). Shaft friction of CFA piles in chalk. Project report (Construction Industry Research and Information Association) ; 86. London : CIRIA, 2003Pennington, D. S. (1999). The anisotropic small strain stiffness of Cambridge Gault clay. Department of Civil Engineering, The University of Bristol.**Phd Thesis**.

TC-29 (2005). International Parallel Test on the Measurement of Gmax Using Bender Elements Organised by TC-29. Japanese Domestic Committee for TC-29**:** 76.

Geotechnical sampling and testing of geological materials containing sulfur-species

T. W. St. John
University of Bristol

ABSTRACT: Sulfur-species in geological materials can be responsible for a wide range of geotechnical problems, including sulfate attack on concrete, sulfate-induced heave and subsidence. A wealth of guidance exists for the classification of materials, however some aspects of sampling and preparatory testing have received relatively little attention. This paper considers the geochemical behaviour of sulfur-species, with a focus on oxidation, dehydration and solubility. The implications for geotechnical engineering are considered and it is recommended that sampling for sulfur-species be undertaken by profiling at short vertical intervals. The samples should be stored under refrigerated conditions and tested as soon as possible. A new approach to oven drying is proposed whereby samples are dried at 40 °C to prevent gypsum dehydration and minimise the dehydration of other hydrous sulfates.

KEYWORDS: sulfate, sulfur, gypsum, pyrite, sampling, testing.

1 INTRODUCTION

Sulfates and sulfides account for the majority of sulfur-species encountered in soils and rocks. Pyrite is the most common sulfide and is often found as cubic grains and/or microscopic framboids. The iron sulfides marcasite and pyrrhotite as well as other metal sulfides may be present, particularly in mineralised regions. Gypsum is the most abundant sulfate and is typically present as well-formed crystals, especially in clay soils. It may also be found as veins and beds. Other sulfates include the magnesium sulfate epsomite and sodium sulfate mirabilite, both common in evaporite deposits, as well as the iron sulfate melanterite, a common pyrite oxidation product.

2 ENGINEERING PROBLEMS

Problems stem from the oxidation of sulfides, which typically generates acidity and various sulfates depending on the host material chemistry. Low pH conditions can be corrosive to cementicious materials whilst the reaction of sulfates with concrete can lead to sulfate attack and thaumasite and/or ettringite formation. The volume increase associated with the precipitation and growth of sulfates can generate pressures sufficient to cause the heave of floor slabs (Hawkins 2013). Heave may also occur when sulfide-sulfate bearing clays are lime stabilised (Snedker 1996) or when anhydrite ($CaSO_4$) hydrates to gypsum ($CaSO_4.2H_2O$) (Alonso et al. 2013).

Further problems include sinkholes in areas underlain by soluble sulfates (Cooper and Saunders 2002) and the potential accumulation of H_2S gas in excavations (Nash et al. 1997). Waste materials with high sulfate contents may exceed the limit for inert landfill. Although guidance exists for the classification of geological materials containing sulfur-species, some fundamental aspects of sampling and testing are not sufficiently considered. This paper explores the geochemical behaviour of sulfur-species during geotechnical investigation.

3 GEOCHEMICAL CONSIDERATIONS

3.1 Sampling

UK guidance has focused on the regional distribution of sulfur-bearing strata (BRE 2005). Within these deposits, the vertical distribution of sulfur-species is non-uniform and in greenfield sites on clays the sulfate profile tends to show depletion near the surface, with enrichment around the transition (mottled zone) into unweathered clay. Concentrations are low in the upper and unweathered zones due to leaching and lack of sulfide oxidation respectively. Sulfate precipitation in the capillary fringe of the water table causes enrichment peaks, where values of up to 9-10 % acid-soluble SO_4 have been reported (Hunt 2013).

Hawkins and St. John (2013) showed that multiple peaks are possible and that the sulfate content of samples taken at only 1 m depth intervals could differ by up to 1.8 gSO_4/l. This is significant considering that many UK earthworks specifications permit a maximum water-soluble sulfate content of 1.5 gSO_4/l for materials placed within 0.5 m of concrete. At the same site a 1.5 % acid-soluble SO_4 difference was noted between samples taken only 0.2 m vertically apart. The non-uniform vertical distribution of sulfates has important implications for sampling. In many cases, the recommendation of a single test for 1 m deep foundations and two for 3 m deep foundations (BRE 2005) will be incapable of accurately assessing the worst-credible conditions. Testing at sample intervals of 0.5 m or less may be more appropriate, particularly at or around the mottled zone.

3.2 Storage

Research has shown that sulfide-bearing geological materials undergo oxidation once recovered from the ground. Open storage in laboratory conditions can cause a 100 % increase in sulfate in only 15 weeks whilst increases from 0.2 to 0.7 % acid soluble SO_4 for sealed borehole core samples have been recorded in only 90 days (Reid et al. 2001, Hawkins 2013). Appropriate storage is essential if conservatism is to be reduced. Unfortunately, there is variation in guidance (Table 1). General consensus is that sealed refrigerated conditions are suitable.

Table 1. Storage conditions for sulfur-bearing geological materials.

Temperature (°C)	Notes	Reference(s)
0-4	Air tight containers	Reid et al. (2001)
2-4	Cool dark place	BRE (2005)
5-10	Away from sunlight	Lombard (2013)

3.3 Sample preparation for testing

3.3.1 Oven drying

Drying at 110 °C can cause loss of crystal-water from gypsum. Dehydration reduces the sample dry mass and any dry mass-based test result will be affected, including moisture content, Atterberg limits, density and chemical properties. The effect of dehydration on sulfate content becomes significant above 10-20 % mineral content by mass of the sample (Figure 1).

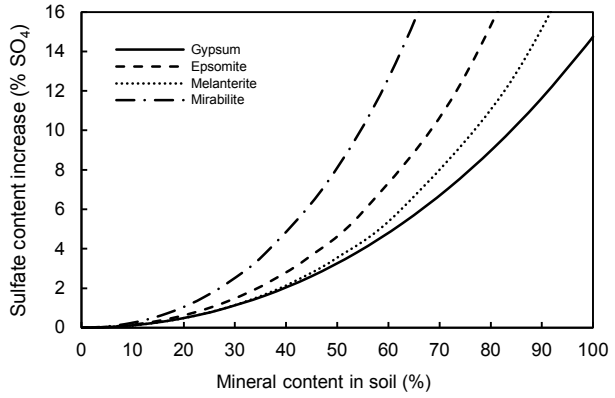

Figure 1. Theoretical increase in sulfate content due to the complete dehydration of various hydrous sulfate minerals.

A number of standards and guidance documents have attempted to minimise gypsum dehydration by outlining lowered drying temperatures (Table 2). It is of note that the standard for chemical testing of aggregates for sulfur-species, BS EN 1744-1, requires drying at 110 ± 5 °C (BSI 2013).

Table 2. Drying temperatures for gypsum-bearing soils in the UK.

Temperature (°C)	Document	Reference(s)
75-80	BS 1377 Part 3	BSI (1999)
60	TRL Report 447	Reid et al (2001)
50	EN 1997 Part 2	BSI (2010)

The range of suggested temperatures can lead to between-laboratory inconsistency as well as varying degrees of hydrous sulfate mineral dehydration. Whilst gypsum dehydration has been studied (Weiser et al. 1937), the dehydration of melanterite ($FeSO_4.7H_2O$) and epsomite ($MgSO_4.7H_2O$) is less understood. To assess the dehydration characteristics of these phases, artificial soil samples containing various proportions of analytical-grade sulfate reagents were dried at 40, 75 and 100 °C (Table 3). The results suggest that the temperatures in Table 2 are appropriate for gypsum-bearing samples but may cause excessive dehydration of melanterite and epsomite.

Table 3. Dehydration tests.

Drying temperature (°C)	Average dehydration (%)		
	Gypsum	Melanterite	Epsomite
40	2	63	14
75	3	86	68
100	100	88	88

Table 4. Rehydration tests. D = desiccated, LC = laboratory cooled.

Drying temperature (°C)	Average rehydration (%)					
	Gypsum		Melanterite		Epsomite	
	D	LC	D	LC	D	LC
40	-	-	2	2	20	11
75	-	-	5	17	10	62
100	28	32	4	29	9	73

After drying, the sulfate-bearing samples were cooled in a desiccator (RH < 10 %) or in the open laboratory (RH c. 60 %). After 24 hours, none of the samples had fully rehydrated, however laboratory cooled samples rehydrated more quickly and to a higher magnitude (Table 4). This incomplete rehydration shows that hydrous-sulfate mineral dehydration is not recovered during typical laboratory drying-testing durations.

3.3.2 Other test and preparation considerations

Wet sieving may dissolve sulfates, which can reduce the retained mass and lead to underestimates of sulfate content. Water should be avoided when preparing thin-sections and SEM samples as sulfates can be degraded, making identification problematic. Oil-based cleaning agents are suitable alternatives. Caution should also be exercised when coarse-grained sulfates are present in samples. Gypsum crystals up to 100 mm in diameter can be present in clays and current guidance is to crush these to < 2 mm (BSI 1999). This may lead to unrepresentative sulfate content results and the need for careful interpretation.

4 CONCLUSIONS

a) The non-uniform vertical distribution of sulfur-species in geological materials is such that sampling by profiling is essential for reliably determining worst-case conditions.

b) To reduce the magnitude of sulfide oxidation, samples should ideally be refrigerated and tested as soon as possible.

c) Samples suspected of containing hydrous sulfate minerals should be dried at 40 °C to prevent gypsum dehydration and reduce melanterite and epsomite dehydration.

d) The use of water should be avoided when dealing with geological materials containing soluble sulfates.

5 REFERENCES

Alonso, E.E., Berdugo, I.R. and Ramon, A. 2013. Extreme expansive phenomena in anhydritic-gypsiferous claystone: the case of Lilla tunnel. *Geotechnique* 63 (7), 584-612.

BRE. 2005. *Concrete in aggressive ground. Special Digest 1*. Building Research Establishment, Bracknell.

BSI. 1999. BS 1377-3:1990. *Methods of test for soils for civil engineering purposes – Part 3*. BSI, London.

BSI. 2010. BS EN 1997-2:2007. *Eurocode 7 – Geotechnical design – Part 2: Ground Investigation and testing*. BSI, London.

BSI. 2013. BS EN 1744-1:2009+A1:2012. *Tests for chemical properties of aggregates. Part 1: Chemical analysis*. BSI, London.

Cooper, A.H. and Saunders, J.M. 2002. Road and bridge construction across gypsum karst in England. *Engineering Geology* 65 (2-3), 217-223.

Hawkins, A.B. 2013. Engineering implications of the oxidation of pyrite: an overview, with particular reference to Ireland. In: A.B. Hawkins (ed.) *Implications of pyrite oxidation for engineering works*. Springer, Switzerland.

Hawkins, A.B. and St. John, T.W. 2013. Importance of understanding the development and significance of sulphates in the London Clay. *Proceedings of the 18th International Conference on Soil Mechanics and Geotechnical Engineering*. Paris, 2013.

Lombard, J. 2013. Sampling potentially pyritiferous materials. In: A.B. Hawkins (ed.) *Implications of pyrite oxidation for engineering works*. Springer, Switzerland.

Hunt. J.R. 2013. The distribution of acid soluble sulfate bands in some British pyritiferous mudrocks and the significance for engineering construction. MSci Thesis, University of Bristol.

Nash, D.F.T., Lings, M.L. and Jefferis, S.A. 1997. Hydrogen sulphide generation beneath a deep basement in Gault Clay. In: A.B. Hawkins (ed.). *Ground chemistry: implications for construction*. Balkema, Netherlands.

Reid, J.M., Czerewko, M.A. and Cripps, J.C. 2001. *Sulfate specification for structural backfills*. TRL Report TRL447.

Snedker, E.A. 1996. M40 Lime stabilisation experiences. In: N. Dixon, S. Glendinning and C.D.F. Rogers (eds.) *Lime Stabilisation*. Thomas Telford, London.

Weiser, H.B., Milligan, W.O. and Eckholm, W.C. 1937. The mechanism of dehydration of calcium sulfate hemihydrate. *Journal of the American Chemical Society*. 59 (8), 1456-1458.

Small scale tests on the progressive retreat of soil slopes

C. Voulgari & S. Utili
University of Warwick

ABSTRACT: Cracks are widely present in soil slopes and can cause a significant decrease in their stability. In this paper, the influence due to the presence of cracks on the morphologic evolution of uniform c and phi slopes subject to weathering is investigated through a laboratory scale test. The characteristics of the soil and the behaviour of a slope model after induced weathering through rainfall simulation were monitored during the test by soil moisture sensors and high resolution cameras. After a short time of rainfall, vertical cracks appeared in the slope model and significant vertical and horizontal deformations started to occur around the crack, until failure was reached. Experimental results indicate that there is a strong connection between moisture content and the occurrence of a landslide.

KEYWORDS: slopes, cracks, failure, weathering, small scale test

1 INTRODUCTION

Cracks can be the result of a variety of phenomena, for instance low tensile resistance, cycles of wetting-drying, desiccation and weathering and are often found in cohesive soils and rock slopes. Weathering turns hard rocks into soft rocks which maintain the structure of the intact rocks, but are characterised by higher void ratios and reduced bond strengths; soft rocks are transformed into granular soils generally called residual soils (Utili 2004). Cracks are widely present in soil slopes and can cause a significant decrease in their stability (Baker, 1981; Michalowski, 2013; Utili, 2013), as they provide preferential flow channels which increase the soil permeability and decrease the soil strength. Moreover, cracks form a part of the critical slip surface that has no shear strength and when water-filled, an additional driving force is applied on the slope. A number of landslides develop in slopes due to weathering which results in the progressive retrogression of the slope face and the further degradation within the weathering zone.

The geological models employed until now are mainly empirical. This paper aims at investigating and developing an engineering model of the morphological evolution of natural cliffs subject to progressive retreat induced by weathering. The deformation response of a slope subject to weathering is not yet thoroughly clarified. In this work, a set of experiment were conducted to investigate weathering induced successive landslides. The weathering was applied to the slope model through rainfall.

Several researchers have tried to study the stability of slopes through experimental procedures. Many of them used centrifuge modelling (Xu et al. 2005; Ling et al. 2009; Zhang et al. 2012) or vibrating boxes (Katz & Aharonov, 2006) to investigate the failure of slopes. The model test is also an important approach, in order to study the behaviour of a slope under certain conditions. In the case of rainfall, it gives the possibility to observe the processes of infiltration, movement of the weathering front, deformation and failure (Wang & Sassa, 2001; Okura et al. 2002; Tohari et al. 2007; Huang et al. 2008; Chen et al. 2011).

2 TEST MODEL

2.1 Apparatus and slope model

The experimental apparatus is illustrated in Figure 1. The main apparatus consists of a soil container made of 10mm thick Plexiglas supported by a steel frame, a rainfall simulation device, six soil moisture sensors and two high speed cameras to record the deformation of the slope model during the tests. The container is 120cm long, 12 cm wide and 50 cm high.

The dimensions of the slope model described in this paper were 15cm high, 12cm wide and 35cm long and the inclination angle of the slope was 90°. The slope model was made of a mixture of 42% w/w calcarenite, 42% w/w glass beads and 16% w/w water. For the construction of the slope models, the materials were manually mixed and layered inside the container in 15 layers of 714g each. Each layer was compacted into 1.00cm to achieve uniformity of the slope model, obtaining a density of 1.7g/cm^3. The soil moisture sensors were buried inside the slope model during the construction phase, so as to cause the least possible disturbance to the soil. Transparent silicon oil was applied on the sides of the container to avoid friction between the slope model and the container.

When the model was prepared, weathering was induced to the model by applying rainfall to the slope's surface through the rainfall device, which was set directly above the slope model. Two M1-mini nozzles (Figure 1) were placed directly above the container and the rainfall intensity was set approximately at 40mm/h.

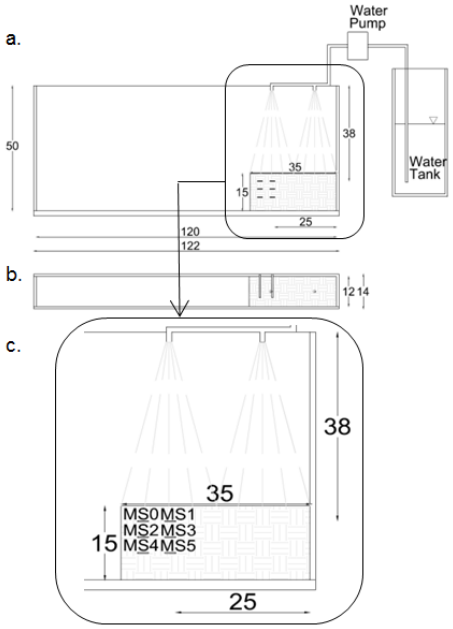

Figure 1. Arrangement of the experimental apparatus: a. front view, b. plan view, c. soil moisture sensors' location

2.2 Measurements

During the event, a high resolution camera (Video Resolution: 1920x1080 pixels) was aimed at one side of the container, to record the process of the test and the movement of the soil. The displacement vectors were obtained by analysing one image per second from the video via GeoPIV. GeoPIV is a Matlab module that implements Particle Image Velocimetry (PIV) in a manner suited to geotechnical testing (White & Take, 2002). The accuracy of displacement measurements, using particle image analysis is strongly dependent on the surface contrast of the soil. For this reason some of the glass beads were painted blue and white to be used as markers, in order to have unique and easy to track patches.

To record the changes in the volumetric water content of the soil over time, 6 soil moisture sensors were buried horizontally in one side of the slope model (Figure 1). When the experiment starts, the readings of every sensor are steady; after some time they start to increase due to the infiltration of the water. This is an indication that the wetting front has reached the corresponding location of the sensor. Uniform weathering is obtained, when the readings become steady again.

3 OBSERVATIONS AND DATA ANALYSES

During the test two cracks were observed causing two successive failures. The first crack occurred after about 3 minutes of rainfall, and significant vertical and horizontal deformations started to take place around the crack, until the first failure was reached and a mass of soil slid away. After that, due to further degradation of the soil's strength caused by the water infiltration, a second crack appeared and the second failure occurred. The displacement rate and the displacement, both horizontal and vertical, of the soil around the first crack at depth 3cm from the slope surface (position of SM0) are illustrated in Figure 2. The first crack appeared at a 3.3cm distance from the slope face and the second one at a 6.2cm distance. Both cracks that appeared on the model were almost vertical and led to the slope's failure a few seconds after their formation.

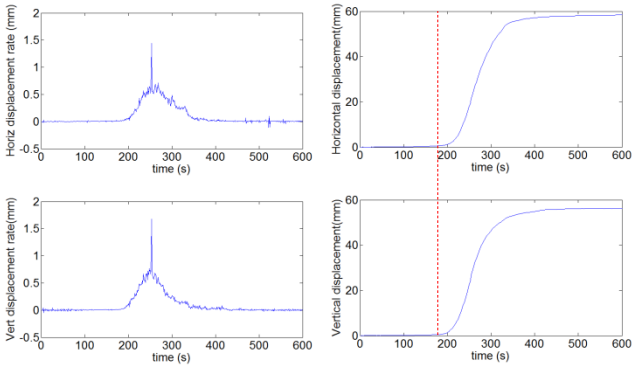

Figure 2. Horizontal and vertical displacement at first failure of a point around MS0.

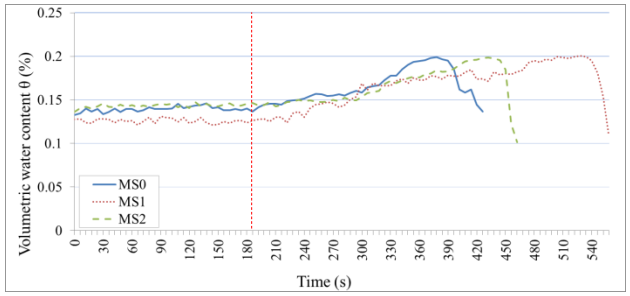

Figure 3. Volumetric water content versus time, obtained from soil moisture sensors MS0, MS1 and MS2.

In Figure 3, the time histories of the volumetric water contents of MS0, MS1 and MS2 are illustrated. The location of each sensor is presented in Figure 1. Three different phases can be observed, the first one when the wetting front has not yet reached the point in question, the second one, where there is a significant increase to the volumetric water content due to the ingress of the wetting front and the third one where a steady moisture level is reached and then the failure occurs. The measured water content of SM0 was compared with the corresponding displacement around it (Figures 2 and 3); a simultaneous increase in the volumetric water content and the displacement of the measurement point was observed. The time histories of soil moisture sensors MS3, MS4 and MS5 are not presented here, as they were buried deeper into the soil and the water front did not reach these measurement points until the end of the experiment.

4 CONCLUSIONS

An experiment on a slope model was conducted to capture its morphologic evolution under induced weathering. Based on the test results presented in this paper, the following conclusions can be drawn:

a) The described setting is satisfying to study the retrogressive retreat of the slope, as two successive failures were observed on the slope model during the test.

b) The displacement started to increase when the wetting front reached the measurement point.

c) A prediction model of slope failures can be introduced based on the observed moisture content response of the slope models.

Pore pressure sensors should also be buried in the slope model in order to obtain the soil suction during the experiment and more tests on slopes with different inclination angles should also be carried out.

5 REFERENCES

Baker R. 1981. Tensile strength tension cracks and stability of slopes. Soils and Foundations 21, Volume 2, pp.1-17, The Japanese Geotechnical Society.

Chen R., Kuo K., Chankg C. 2011. Experiment on the stability of granular soil slopes by rainfall infiltration. Italian journal of engineering geology and environment, 5th International Conference on Debris-Flow Hazards "Mitigation, Mechanics, Prediction and Assessment".

Katz O., Aharonov E. 2006. Landslides in vibrating sand box: What controls types of slope failure and frequency magnitude relations? Earth and Planetary Science, Letters 247, pp.280-294.

Ling H.I., Wu M., Leshchinsky D., Leshchinsky B. 2009. Centrifuge Modeling of Slope Instability. Journal of Geotechnical and Geoenvironmental Engineering, Volume 135, Issue 6, pp.758-767.

Tohari A., Nishigaki M., Komatsu M. 2007. Laboratory rainfall-induced slope failure with moisture content measurement, Journal of Geotechnical and Geoenvironmental Engineering, Volume 133, Issue 5, pp.575-587

Utili S. 2004. Evolution of natural slopes subject to weathering: An analytical and numerical study, PhD Thesis, Politecnico di Milano.

Utili S. 2013. Investigation by limit analysis on the stability of slopes with cracks. Géotechnique, Volume 63, Issue 2, pp.140-154.

Wang G., Sassa K. 2001. Factors affecting rainfall-induced flowslides laboratory flume tests. Geotechnique, Volume 51, Issue 7, pp.587-599.

White, D. & Take, W. 2002. GeoPIV: Particle Image Velocimetry (PIV) software for use in geotechnical testing. Cambridge University Engineering Department.

Xu G.M., Zhang L., Liu S.S. 2005. Preliminary Study of Instability Behaviour of Levee on Soft Ground during Sudden Drawdown. Geotechnical Special Publications, GeoFrontiers, Slopes and Retaining Structures Under Seismic and Static Conditions, Proceedings.

Zhang G., Wang R., Qian J., Zhang J., Qian J., (2012) Effect study of cracks on behavior of soil slope under rainfall conditions. Soils and Foundations, Volume 52, Issue 4, pp. 634–643.

Prediction and determination of soil water retention curves (SWRC) of highly plastic tropical clay soils

Alhaj A, KMA & Standing J R
Civil and Environmental Engineering
Imperial College London

ABSTRACT: Soil-Water Retention Curves (SWRC) are commonly plotted as degree of saturation versus logarithm of suction. When clay is dried from slurry, the curve is referred to as the primary drying curve (PDC). At the end of drying a residual point is reached when the degree of saturation becomes constant. Wetting from this point allows the primary wetting curve (PWC) to be generated (n.b. the PDC and PWC are hysteretic). For very plastic clays, sometimes it is not possible to develop the full SWRC because the maximum suction that can be measured is reached while the degree of saturation is still quite high and still reducing: e.g. with the filter paper technique maximum suction measurements are limited to 30 MPa. This was found to be the case when investigating two plastic clays from Sudan (black and red clay soils). Formulations such as the van Genuchten (1980) expression can be used to extrapolate the PDC down to the residual point using an iterative procedure of trial and error and equally another set of parameters can be used to generate a PWC. This exercise was performed for the black and red clays. This paper presents the results from the filter paper measurements and describes how the curves were extrapolated back to form the full PDC and how the residual point was estimated as part of this process.

KEYWORDS: SWRC, Plastic Clay, Suction.

1 INTRODUCTION.

Many researchers have investigated coupling the hydro-mechanical behaviour of unsaturated soils and several methods have been proposed to predict and estimate their engineering response. The Soil-Water Retention Curve (SWRC), usually plotted as the relationship between degree of saturation, S_r, and logarithm of matrix suction, log *s*, plays a key role in recently proposed constitutive models and has been used to predict the compressibility during virgin loading (Wheeler et al., 2003), shear strength (Tarantino and Tombolato, 2005) and volume change behaviour of unsaturated soil. The general shape of the SWRC is a sigmoid curve having an 'S' shape. The SWRC is generally presented in terms of volumetric water content, θ_w, defined as the ratio of the volume of water to the total volume of soil. To investigate the relationship between the SWRC and the properties of an unsaturated soil, the SWRC should be determined experimentally in the laboratory.

In the laboratory the SWRC can be obtained by taking a sample in its initial state (fully saturated) or a slurry state and gradually drying it in incremental stages and at the end of each stage taking measurements of suction and water content. Once the sample reaches the residual state (constant degree of saturation) the wetting-up process can commence by adding small amounts of water to the sample in incremental stages. From these measurements both drying and wetting curves can be drawn (generally as log *s* versus S_r). If drying starts from slurry, the two curves are considered to be boundary curves (primary drying curve PDC and primary wetting curve PWD) and it is often considered that any sample in any condition should lie within these boundaries. Usually the end of the wetting curve differs from the starting point of the drying curve (i.e. the soil does not return to a fully saturated state). As the PWC does not follow the path of the PDC the process of drying and wetting is hysteretic. If small wetting and drying cycles take place from positions along the PDC or PWC, intermediate 'scanning' curves are created within the primary curves.

For very plastic clays, sometimes it is not possible to develop the full SWRC because of limitations of some suction measurement techniques, e.g. with the filter paper method the maximum suction that can be measured is 30 MPa. In these cases it is not possible to reach the residual value because the soil has reached very high suctions while the degree of saturation is still relatively high. This is particularly the case for highly plastic clays.

A full SWRC can be generated by using a formulation such as the van Genuchten equation, making various assumptions. This can be used for both drying (to residual level) and wetting paths (wetting from residual point). It is then possible to formulate both PDC and PWC.

2 MATERIALS AND SAMPLE PREPARATION

The work presented here forms part of an extensive research study at Imperial College on two natural soils from two locations in Sudan: a black cotton clay and red clay. One of the aims of the research was to generate SWRCs for the 'black' and 'red' soils. Particle size distributions of the two types of soils are presented in Table 1. Values of specific gravity for the clays are 2.72 for black and 2.78 for red soil. Atterberg limits for the two soils are given in Table 2.

The black and red soils were reconstituted from slurry in a consolidometer to a vertical effective stress of 200 kPa. Four discs for each soil were trimmed from the resulting soil cakes and initial water content and volume measured.

The discs were gradually dried and subsequently wetted, measuring both matrix and total suction, in order to obtain the Soil-Water Retention Curve (SWRC) for each soil. The filter paper technique was used to determine the SWRCs.

Table 1. Grain size distribution results.

Type of soil	Gravel (%)	Sand (%)	Silt (%)	Clay (%)
Black soil	4	22	26	48
Red soil	4	8	38	50

Table 2. Atterberg limits results and BSI classification.

Type of soil	LL (%)	PI (%)	Activity (%)	BS classification
Black soil	60	31	0.65	CH
Red soil	87	53	1.06	CV

3 EXPERIMENTAL RESULTS

3.1 Experimental SWRC

The results from reconstituted black and red soil samples in terms of S_r vs log s are presented in Figure 1. The samples were incrementally dried from a fully saturated state at zero total stress. The PDCs are clearly defined but stop at a relatively high degrees of saturation (S_r=45% and S_r=55% for black and red soils respectively), when the suction reached 30 MPa. As the residual point was not reached, the wetting curve from this point constitutes a scanning curve.

3.2 Modelled SWRC

Experimental SWRCs were modelled using the van Genuchten (1980) equation, given as follows:

$$\frac{}{\left(1+(-)\right)} \quad (1)$$

where:

volumetric water content at any point;
= volumetric water content at saturation;
θ = volumetric water content at the residual condition;
α = controls the air entry-value (AEV);
m = controls the point of inflection;
n = controls slope of the SWRC.

The unknown parameters α, n, and m were determined using a trial and error approach and a best fit to the drying and wetting experimental data determined using the least squares method. The best fit van Genuchten curves used to model the SWRCs are presented in Figure 2.

In order to model the full SWRC for these plastic clays, assumptions were necessary since there is a lack of data over a significant range between the limit of filter paper (30MPa) and the residual degree of saturation.

To estimate the residual degree of saturation, samples of both soils were subjected to three different temperatures to assess the resulting water content and hence the degree of saturation, as shown in Figure 3. Head and Epps (1986) state that hydrated, adsorbed and absorbed water within and around the clay particles cannot be removed by oven drying at 100 °C. They are considered to form part of the intrinsic clay particle. However, the mineralogical composition of clay particles can change when they are subjected to temperatures greater than 100 °C. In order to avoid this effect, the residual degree of saturation was taken to be greater than that determined at this temperature (5 and 8 % for the black and red soils respectively). Based on the shape of the curves fitted through the data (as shown in Figure 3), values were estimated to be 10% and 12% for black and red soils respectively. Having fixed the residual degree of saturation, the van Genuchten expression could be used to extrapolate the PDC with greater confidence (and less uncertainty).

It should be noted that the estimated residual point for these plastic clays does not really have practical significance (the suction values are of the order of GigaPascals). However, in order to investigate boundary value problems using numerical analyses, it is necessary to implement a complete formulation of the SWRC.

From this point, the PWC can be generated, again using Eqn. 1, so that it intersects the data from the wetting process in its final stages (when the points should tend to rejoin the PWC) as shown in Figure 2. The figure shows that there is little hysteresis between the PDC and PWC.

Subsequently, as another aspect of the study, suction measurements were performed on statically compacted samples with different water contents and compaction effort. The SWRCs from these samples were found to lie to the left of the PWCs shown in Figure 2. Several authors have shown that the SWRC is void ratio-dependent and it is characterised by a surface in the space (s, e, S_r) (e.g. Huang et al. (1998), Tarantino (2009) and Tsiampousi et al. (2013)). This can explain why this was observed. The SWRCs for the compacted samples are presented and discussed by Alhaj (2013).

4 CONCLUSION

The paper has presented an experimental and theoretical approach to generate the SWRC of two highly plastic clays from Sudan. Particular emphasis has been made on the estimation of the residual degree of saturation. Subsequent SRWCs generated for compacted samples indicate that the PDC and PWC are not unique as they are affected by void ratio, as suggested by other researchers.

5 ACKNOWLEDGEMENTS

Financial support for the first author and this research was provided by the Professor Shawki Saad Scholarship. This support is gratefully acknowledged. The work described was carried out as part of PhD research programme by the first author at Imperial College London, UK

.

6 REFERENCES

Alhaj A, K. M. A. (2013), Mechanical response of two plastic clay soils from Sudan., PhD thesis, Imperial College London, UK.

Head, K. H. and Epps, R. (1986), Manual of soil laboratory testing, Vol. 3, Pentech Press Limited, London, UK.

Huang, S., Barbour, S. L. and Fredlund, D. G. (1998), 'Development and verification of a coefficient of permeability function for a deformable unsaturated soil', Canadian Geotechnical Journal 35(3), 411–425.

Tarantino, A. (2009), 'A water retention model for deformable soils', Géotechnique 59(9), 751–762.

Tarantino, A. and Tombolato, S. (2005), 'Coupling of hydraulic and mechanical behaviour in unsaturated compacted clay', Géotechnique 55(4), 307–317.

Tsiampousi, A., Zdravkovic, L. and D.M. Potts (2013), 'A three-dimensional hysteretic soil-water retension curve', Géotechnique 63(2), 155–164.

van Genuchten, M. T. (1980), 'A closed-form equation for predicting the hydraulic conductivity of unsaturated soils', Soil Science Society of America Journal 44(5), 892–898.

Wheeler, G. L., Trotter, E. W., Dawes, I. W. and Grant, C. M. (2003), 'Coupling of the transcriptional regulation of glutathione biosynthesis to the availability of glutathioneand methionine via the met4 and yap1 transcription factors', Journal of Biological Chemistry 278(50), 49920–49928.

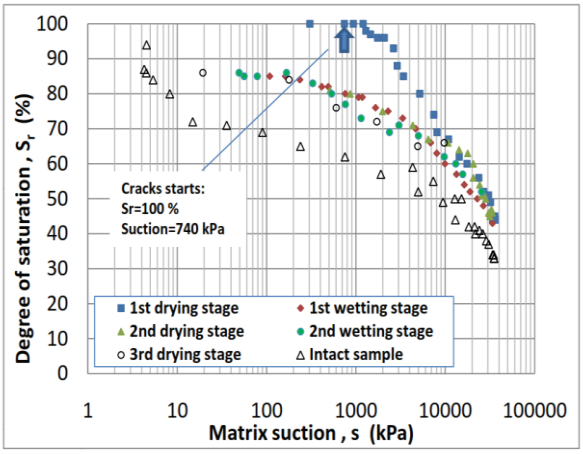

(a)

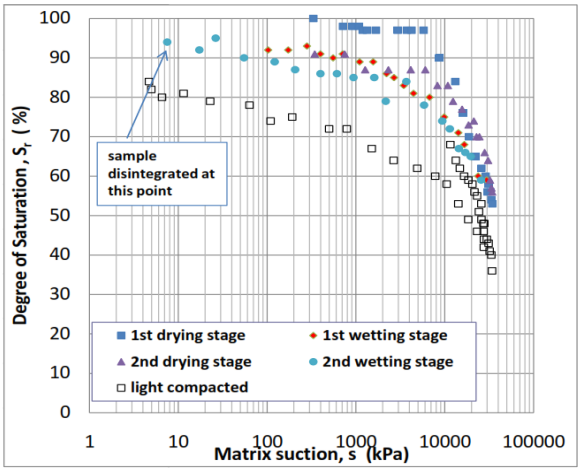

(b)

Fig. 1: Laboratory measurement of SWRC in terms of S_r versus (u_a- u_w) for the (a) black soil and (b) red soil.

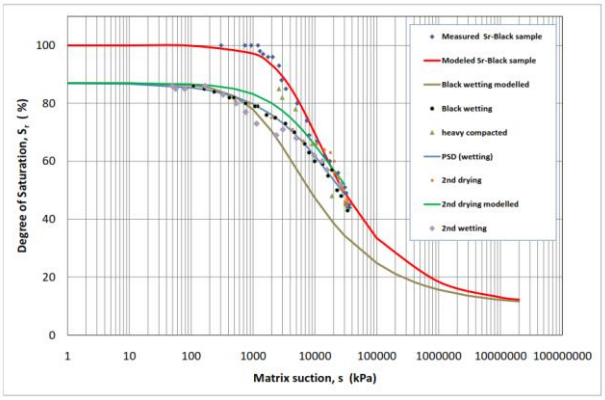

(a)

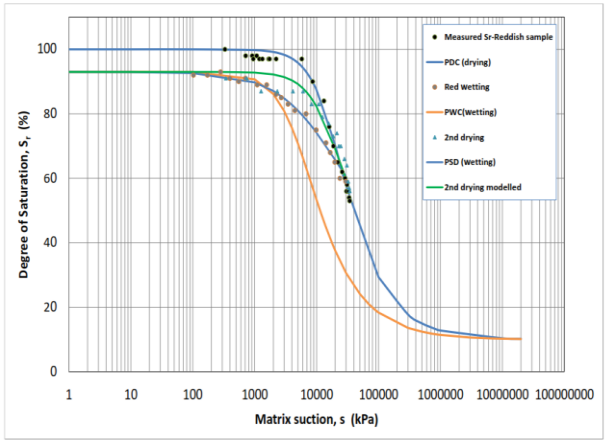

(b)

Fig. 2: Laboratory measurement and modelling of SWRC for (a) the black and (b) the red soil in terms of S_r versus (s= u_a-u_w).

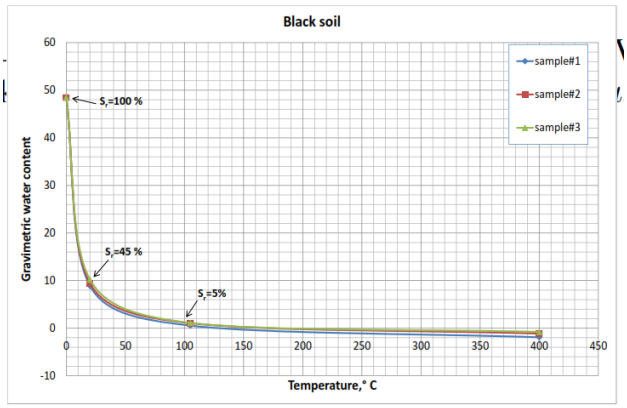

(a)

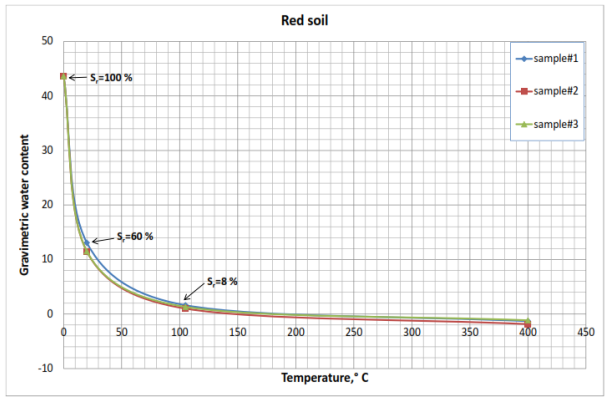

(b)

Fig. 3: Change in degree of saturation with temperature for (a) the black soil and (b) the red soil.

Mechanics of Soft-Rigid Soil Mixtures

S. Rouhanifar
University of Bristol
Supervisor: Dr E. Ibraim

ABSTRACT: Use of rubber particles resulted from shredding of used lorry tyres could a viable alternative for the materials used in construction industries, including geotechnical systems. The study of the mechanical behaviour of the sand-rubber mixture is considered in this research. Triaxial compression tests under drained conditions are performed on various samples with different rubber fractions and under different confining pressures. Stress and volumetric behaviour of the mixtures are analysed.

KEYWORDS: Laboratory; Sand; Rubber particles; Triaxial Test; Sample fabrication.

1 INTRODUCTION

The number of scrap tyres is increasing rapidly in both developed and developing countries due to the increase in usage of vehicles. These materials can be considered as an alternative for conventional materials in construction industries. As far as geotechnical systems are concerned, recent studies show that the use of these materials for backfilling can be an attractive solution that would provide lighter weights on the structure compared to traditional backfilling materials. However, before implementation, further research is required in order to understand the behaviour of the soil/tyre chip mixtures, including internal interaction mechanisms resulted from the combination of two materials, one soft, tyre rubber, and one rigid, granular soil.

2 RESEARCH AIMS AND OBJECTIVES

During this project, two types of granular materials, Leighton Buzzard sand and Hostun sand are mixed with granular rubber particles resulted from a shredding process of used scrap tyres. The novel idea here is to use rubber particles with the same particle size distribution of the Hostun sand and Leighton Buzzard materials. Therefore, the analysis of the effect of rigid/soft mixture will be mainly related to the proportions of the mixture components. While testing rubber/sand composites in the laboratory, one of the main concerns is the segregation phenomenon that can occur in the fabrication process between the two constituents. This aspect appears to be ignored in the literature. In this research, different sample preparation techniques have or are in progress to be assessed in order to explore the best fabrication method for the sand-rubber samples. Experimental behaviour of the sand/rubber mixture will be investigated based on classical triaxial tests but more advanced testing procedures will be considered once the conclusions based on the first series of testing are available.

3 MATERIALS

Two kinds of sand one characterised as fine and the other as coarse have been chosen: Leighton Buzzard fraction A and Hostun RF sand, respectively. According to the particle size distribution (PSD) of these sand materials, two kinds of rubber materials resulted from the shredding process of used lorry tyres have been created to match the PSDs of the two sands following a long and tedious process that involved market investigation, individual assessment of rubber samples sent by various suppliers, sieving and sorting of the particles. As an example, Figure 1 shows the individual PSD of Hostun RF and Leighton Buzzard sands. Various index properties of the materials are given in Table 1.

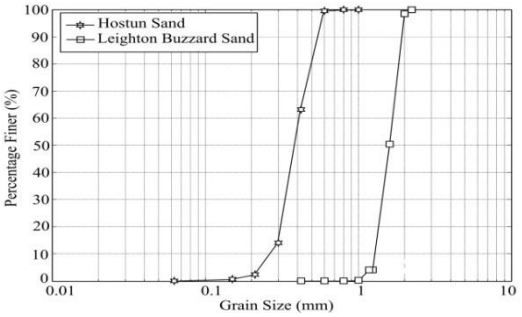

Figure 1-PSD of Hostun Sand and Leighton Buzzard Sand

Table 1-Index Properties of Tested Materials

Used Materials Properties	*Hostun sand*	*Leighton Buzzard Sand*	*Rubber Particles*
Specific Gravity	2.65	2.65	1.04
Minimum Void Ratio (e_{min})	0.62	0.55	-
Maximum Void Ratio (e_{max})	1	0.83	-
Mean Grain Size (D_{50} (mm))	0.38	0.8	0.38/0.8
Coefficient of uniformity (C_u)	1.7	1.27	1.7/1.27
Coefficient of gradation (C_g)	1.1	1.19	1.1/1.19

4 SAMPLE FABRICATION

There are different ways to create rubber-sand samples in laboratory but in general, the process invariably involves the following three stages: mixing, deposition and compaction. Youwai and Bergado (2003) used water content of 7.5% for mixing sand and shredded rubber tire and stored the created samples for 3 days to cure. Rao and Dutta (2006) mixed the

required amount of tire chips and sand together in dry condition and then the mixture was soaked. The sand was then deposited in layers into the mould, each layer being compacted with a rubber tamper. Lee et al. (1999) prepared their samples in three layers by pouring the dry tire chips/sand mixture into a vacuum split mould. Each layer was then vibrated at 60Hz under weights that provided a 14kPa vertical surcharge. Kim and Santamarina (2008) believe that by minimizing any vibration and avoiding granular flow during specimen's preparation, segregation will be reduced. Yang et al. (2002) poured the dry mixture into the mould in three layers each compacted vertically with a spatula.

In this research, cylindrical samples with 70mm in diameter and 70mm in height are made in three equal successive layers. Sand and rubber materials are mixed together with 10% water content and then deposited in three lifts into the mould. Then, each layer is compacted by a steel rod until the specific target void ratio is achieved. Samples are made at the same relative density of 65% for both Hostun sand and Leighton Buzzard sand. Figure 2 shows a schematic view of a sand-rubber sample. Samples with different rubber fractions between 0% and 100% with similar void ratio will be tested during this research.

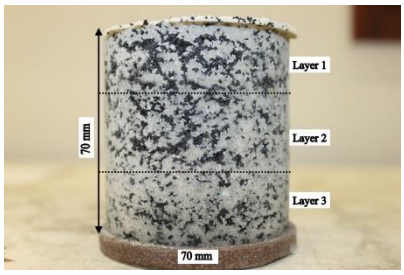

Figure 2-Schematic View of Triaxial Sample

5 TRIAXAIL COMPRESSION TESTS ON SAND-RUBBER SAMPLES

Drained tests in triaxial apparatus are conducted for investigating the behaviour of these composites. Samples are tested under different confining pressures of 50kPa, 100kPa and 200kPa, however, in this paper only the results at 100kPa confining pressure are presented. The deviator stress and volumetric strain evolutions with the axial strain of samples with 0%, 20% and 100% rubber are shown in figure 3 for Hostun Sand and figure 4 for LB sand.

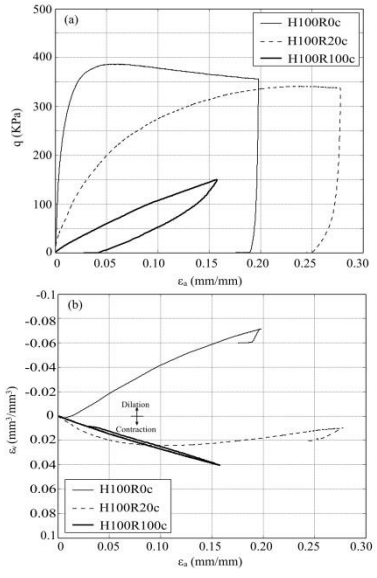

Figure 3-Triaxial Compression Tests on Hostun Sand/Rubber Mixture: (a) Deviator Stress-Axial Strain; (b) Volumetric Strain-Axial Strain

The results depict well the expected behaviours for pure dense sand and pure rubber: pronounced peak strength followed by softening towards a critical state and highly dilative volumetric behaviour for sand and almost linear stress evolution associated with a very contractive response for rubber. The latter result is consistent with the previous investigation of Lee et al. (1999). It is clearly shown that adding rubber to sand generates an intermediate response for both material composites. While the strength of the composites decreases, the strain corresponding to the peak deviator stress increases. The volumetric behaviour for 20% rubber fraction is also closer to pure rubber behaviour.

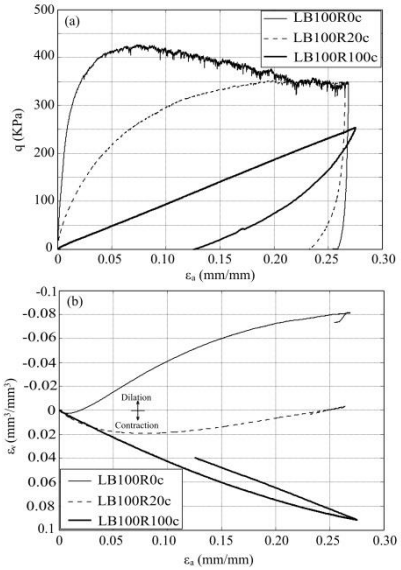

Figure 4-Triaxial Compression Tests on LB Sand/Rubber Mixture: (a) Deviator Stress-Axial Strain; (b) Volumetric Strain-Axial Strain

6 CONCLUSION

An experimental testing program under triaxial conditions was conducted to investigate the behaviour of soil mixtures between two sands, Hostun Sand and Leighton Buzzard sand, and rubber particles resulted from a shredding process of used scrap tyres. While several rubber fractions from 0% to 100% were used, the particle size distribution of the added rubber conserved the particle size distribution of the Hostun sand and Leighton Buzzard sand. While some limited data is presented in this paper and the results offer already an excellent database for studying the influence of the interaction between soft and rigid particles. A constitutive model will also be developed based on these results.

7 REFERENCES

Kim, H. K. and Santamarina, J. C. (2008). "Sand-rubber mixtures (large rubber chips)." Canadian Geotechnical Journal **45**(10): 1457-1466.

Lee, J., Salgado, R., Bernal, A. and Lovell, C. (1999). "Shredded tires and rubber-sand as lightweight backfill." Journal of Geotechnical and Geoenvironmental Engineering **125**(2): 132-141.

Rao, G. V. and Dutta, R. (2006). "Compressibility and strength behaviour of sand–tyre chip mixtures." Geotechnical and Geological Engineering **24**(3): 711-724.

Yang, S., Lohnes, R. A. and Kjartanson, B. H. (2002). "Mechanical properties of shredded tires." stress **1**(79): 1.

Youwai, S. and Bergado, D. T. (2003). "Strength and deformation characteristics of shredded rubber tire sand mixtures." Canadian Geotechnical Journal **40**(2): 254-264.

Analysis of ash clinker waste from historical tipping site

K. A. Ibrahim
School of Earth, Atmospheric and Environmental Sciences, The University of Manchester
School of Chemical Engineering and Analytical Science, The University of Manchester

ABSTRACT: Northwich has been at the heart of the salt mining and salt based chemical industries since the mid-19th century. The study area was selected because it represents an important example of previously derelict land enclosing a very substantial deposit of legacy industrial waste. The wastes were deposited over a period of 200 years before abandonment in the 1960s. Since this time the legacy waste has aged and weathered under the prevailing environmental conditions. Samples of ash clinker were collected from different sites across the tipped area, where relative ages could be determined. Petrographic and geochemical techniques have been used to characterise the samples. Bulk chemical compositions of the ash clinker samples are dominated by slightly varying compositions of silicon, aluminium, calcium, and iron oxides. Sample mineralogy included various proportions of albite, mullite, quartz, and anorthite in a glassy matrix and the presence of iron oxide surface coating, due to weathering oxidation. There is some evidence that the oxide coatings are thicker on older ash clinkers relative to the younger, and that the relative coating thickness could give an indication of sample age and the possibility of a dating technique for other similar ash clinkers.

KEYWORDS: Northwich, chemical industry, salt mining, subsidence, ash clinker waste, aging.

1 INTRODUCTION

All solid wastes produced by industrial activities are termed 'industrial solid waste' (Abduli, 1996). Historically, chemical industries have managed their waste materials by discharging them into the adjacent environment, often without pre-treatment (Casares et al., 2005). This industrial waste constitutes a major component of many contaminated land and brown-field sites and is of concern because of its potential for significant long-term environmental impact. The town of Northwich in the Northwest of England has supported extensive industrial activities for over 200 years exploiting the local salt deposits for the production of soda ash, initially through the Leblanc process and later the Solvay process (Clapp, 1994). The legacy of salt mining is clearly evident in the landscape with widespread subsidence (Wallwork, 1956) and brine seeps. This paper reports on a programme of analysis of ash clinker wastes from historical waste tips close to Northwich.

1.1 *Industrial History of Northwich*

The major part of the UK salt industry is situated around Northwich with a long history of salt mining which in turn led to the flourishing of salt based chemical industries (Ashmore, 1982). Initially extracted in Roman times, rock salt deposits were rediscovered by accident in 1670 whilst prospecting for coal (Evans et al., 1968). The poor mining practice often resulted in flooding and the development of extensive uncontrolled brine pumping in the area. This caused yet more water to penetrate into the mines and halite strata ultimately leading to severe subsidence on large scale, causing the formation of large ponds known as 'flashes'. The flashes and the surrounding poor quality land became tipping sites for the huge volumes of waste produced by salt based chemical industries.

Initially alkali (soda ash) was produced by the "Leblanc" process, invented by Nicolas Leblanc in 1791, which required large amounts of sodium chloride, concentrated sulphuric acid, coke and limestone, and involved the discharge of hydrochloric acid gas and the calcium sulphide as an industrial solid waste, known locally as 'galligu'. However, by the 1870s, a new method for converting salt into soda had been developed; the Solvay process. This industrial process, rediscovered and improved by Ernest Solvay in 1861, is based on inputs of common salt of sodium chloride, limestone, ammonia and thermal energy (Speight, 2002).

Figure 1 Gravel-size ash clinker particle with colourful bands (photograph taken at Northwich tipping site, Cheshire).

2 CHEMICAL AND MINERALOGICAL CONTENT OF ASH CLINKER

The ash clinker waste samples were analysed for their key constituents by X-ray florescence spectrometry (XRF). The key chemical constituents are SiO_2, Al_2O_3, Fe_2O_3 and CaO. Table 1 provides the chemical composition of the example of ash clinker in Figure 1. The silica content is around 55%. The aluminium oxide content can be as high as 23%. Iron oxide content is around 11%. The crystalline components have been identified by X-ray diffractometry (XRD) as including anorthite, mullite, quartz and albite.

Table 1. Chemical composition of ash clinker sample (Oxides, mass %)

CaO	SiO_2	Fe_2O_3	Al_2O_3	MgO	Na_2O
2.4	55.2	10.5	23.1	1.6	0.5
K_2O	TiO_2	SO_3	P_2O_5	LOI	Total
4.8	0.6	0.2	0.1	0.5	99.6

3 SCANNING ELECTRON MICROSCOPY (SEM) OBSERVATIONS

SEM data suggest that some ash clinker samples have rims of iron oxide coating enclosing some of the perimeter of the sample. It is noticed that the samples of older age have a thicker film of iron oxide when compared to younger samples. Figure 2 shows an example of fringes of iron oxides. The approximate thickness of the film in Figure 2A is around 5 µm whilst in Figure 2B is around 10 µm.

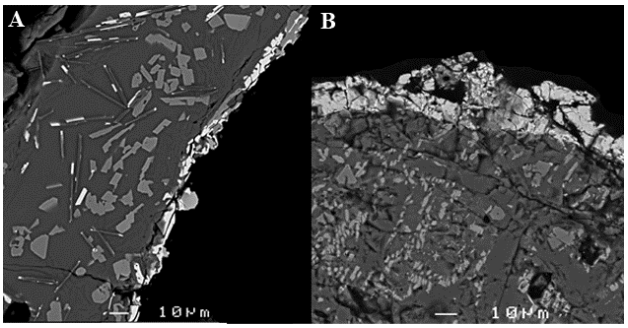

Figure 2. A plate of SEM micrographs under magnification of X500 showing: A. younger (~50yrs) and B. older (~100yrs) sample of ash clinker with 2 different thicknesses of iron oxide coating rim.

A different example is also shown in figure 3. It is observed that both matrices exhibit a microcrystalline texture. Vesicles are also present in both samples. A thin film of iron oxide which has been confirmed using energy dispersive spectrometry (SEM-EDS) is also enclosing the perimeter of both sections. Some vesicles in the older sample have a rim of iron oxide.

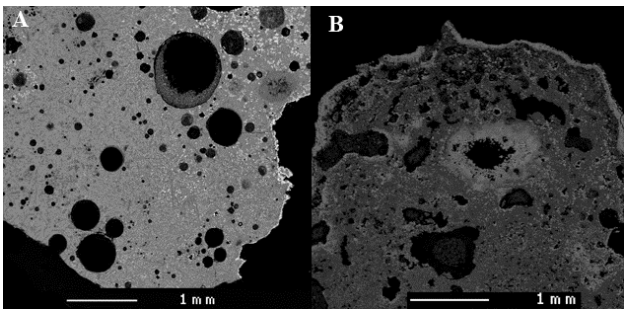

Figure 3. A plate of SEM micrographs under magnification of X20 showing A. younger (~50yrs) and B. older (~100yrs) ash clinker sample with 2 different thicknesses of iron oxide rims.

4 CONCLUSION

The morphological, mineralogical and chemical constituents of ash clinker samples collected from the abandoned tipping sites in Northwich were analysed by XRD, XRF and SEM. Bulk chemical compositions of the ash clinker samples are dominated by slightly varying compositions of silicon, aluminium, calcium, and iron oxides. Sample mineralogy included various proportions of albite, mullite, quartz, and anorthite in a glassy matrix and the presence of iron oxide surface coating. There is some evidence that the oxide coatings are thicker on older ash clinkers relative to the younger, and that the relative coating thickness could give an indication of sample age. Therefore, the primary application of scanning electron microscopy to studies of ash linker waste revealed important features regarding the aging process. This confirmed SEM as a powerful tool in industrial solid waste studies.

5 ACKNOWLEDGEMENTS

I would like to thank Prof. Colin Hughes and Dr. Alastair Martin for their supervision, unlimited help and support throughout my study at The University of Manchester. Thanks to Tishreen University, Higher Institute for Environmental Research for funding this research project. Thanks to David James of Marbury Country Park in Northwich for his help and invaluable support during the field work. And Alastair Bewsher, Paul lythgoe, John Waters and Cath Davis for their help in the analysis and during the laboratory work at The University of Manchester.

6 REFERENCES

Abduli M.A. 1996. Industrial waste management in Tehran. *Environment International* 22 (3), 335-341.

Ashmore O. 1982. *The industrial archaeology of Northwest England*, Manchester University Press, Manchester. UK

Casares M.L., Ulierte N. Mataran A. Ramoas A. Zamorano M. 2005. Solid industrial wastes and their management in Asegra (Granada, Spain). *Waste Management* 25 (10), 1075-1082.

Clapp B.W. 1994. An environmental history of Britain since the Industrial Revolution. Longman, UK.

Evans W.B. Wilson A.A. Taylor B.J. Price D. 1968. *Geology of the country around Macclesfield, Congleton, Crewe and Middlewich.* Natural Environment Research Council, Geological Survey of England and Wales.

Speight J.G.2002. *Chemical and process design handbook.* McGraw-Hill, New York, USA.

Wallwork, K.L. 1956. Subsidence in the Mid-Cheshire Industrial Area. *The Geographical Journal* 122 (1), 40-53.

Rheology of sand-foam mixture used in EPB tunnelling: a review

Q. Zhang
School of Mechanical, Aerospace and Civil Engineering, The University of Manchester

ABSTRACT: The use of earth pressure balance machines (EPBMs) has become increasingly popular in tunnelling over recent decades. This method was first developed for ideal soils, which have low inner friction, plastic flow characteristics, low permeability and appropriate compressibility. However, natural soils do not usually have these ideal properties, therefore, soil conditioners such as foams, bentonite slurries and polymers are mixed with original soils to improve the performance of EPBMs. The rheological properties of conditioned soils are of great importance for their influence on flow behaviours of spoils in working chambers and screw conveyors. The aim of this paper is to provide a review of soil conditioning in tunnelling through soft ground, particularly the rheological properties of sand-foam mixtures.

KEYWORDS: EPB tunnelling, conditioned sands, rheological properties.

1. INTRODUCTION

EPBMs could be considered the most commonly used tunnelling equipment in soils ranging from coarse sands and gravels to stiff clays. The increasing number of applications of EPBM thank not only the improvement of mechanical technology, but also widely used soil conditioners.

Soil conditioners are often injected into the working chamber, ahead of the cutterhead, or along the screw conveyer to optimise EPBM performance. In the context of tunnelling through sand strata, Milligan (2000) indicated that the ideal soil conditions for EPBMs are a low permeability (less than 10^{-6} to 10^{-5} m/s) and a favourable plastic consistency which makes it easy to extrude soils through the screw conveyor.

Therefore, for the purpose of improving EPBM working conditions, research on the plastic flow properties of conditioned soils is necessary. Nevertheless, very few studies on soil conditioning could be found in the literature, especially for cohesionless soils. The operation of the soil conditioning process on job sites is usually based on trial and error, which could cause poor efficiency and extra costs. In this paper, the results of recent research along with the newly designed laboratory equipment are presented.

2. FOAM AS CONDITIONER IN EPBM

The underlying principle of EPBM is using the excavated soils in a working chamber to provide continuous support by balancing the forward pressure of the machine and earth pressure. This balance is achieved with the help of a screw conveyor, which extrudes the same volume of spoils as the soils excavated by cutting wheel. As the support medium of EPBM is the excavated material itself, soil conditioners (for examples: foams, bentonite slurries and polymers) which could make the soil more ideal become of great significance. These conditioners could be used separately or in combination, and their effects vary on different soils.

Foam is a mixture in liquid phase, consisting of water-based surfactant solution, water and compressed air. Compared with bentonite slurries, foam benefits from the extremely small amount of extra liquid which must be added to the excavated soil (Psomas, 2001), the lower price of the agents and the simplicity of the system required for its generation. The effects of foam on excavated soils depend on many factors, for instance, the solution chemistry, the concentration of surfactant, the foam injection ratio (FIR), the foam expansion ratio (FER) and the bubble size. Recent research by Merritt (2004), Peña Duarte (2007), Zumsteg *et al.* (2013) and Gharahbagh *et al.* (2014) on foamed soils have shown that foam could act as an effective conditioner with various types of soil. In clayey soils, foam is mainly used to reduce adhesion and stickiness of the soil, leading to fewer possibilities of clogging. In granular soils, foam could give the soil a plastic consistency, increased compressibility, and reduced torque and wear. In hard rocks, a significant reduction of wear is achieved by adding foam. Furthermore, foam also acts as a dust suppressant in hard rock tunnelling.

To date, investigation into the effects of foam on the properties of soils in EPB tunnelling are limited. Further studies on the direct relationship between the amount of foam and its performance with different soils would help in saving time and costs in tunnelling projects.

3. SAND FOAM MIXTURE RHEOLOGY

Rheology is the study of flow and deformation. Flow properties have great influence on the performance of conditioning agents and their mixtures with soils.

3.1 *Rheological properties of sand foam mixture*

The flow behaviours of soil are governed by general rheology theories. In order to investigate the rheology of a material, it is necessary to study flow properties over a range of shear rates and shear stresses, which are usually presented in a flow curve. Five of the most common relationships between shear stresses and shear rates are shown in Figure 1.

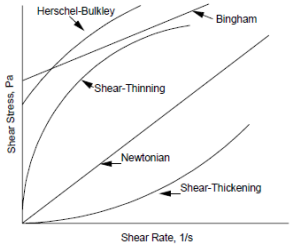

Figure 1. Common relationships between shear stresses and shear rates.

Bingham fluids are viscoplastic materials which behave like solids at low stresses but flow as viscous fluids when the yield stress is exceeded. The Bingham model is a common

mathematical model in drilling engineering and in the handling of slurries.

Viscosity is defined as the relationship between shear stress and shear rate (Milligan, 2000). Viscosity is affected mainly by factors such as temperature, pressure and time and can be measured with the use of viscometers or rheometers. For example, in the case of the Bingham fluid, the viscosity can be calculated from at least two readings of shear stress at different shear rates.

The phenomenon of yield stress is often observed in multiphase fluids. The yield stress is associated with the force required to initiate flow. In the case of sand-foam mixtures, interaction between sand particles can form a three-dimensional network structure, which resists flow at low stresses. In tunnelling projects, the yield stress of the soil may be an important model parameter regarding the economical application of the EPBMs.

Meng et al. (2011) studied conditioned sands aiming to determine their rheological parameters under varying pressures. The sand samples were conditioned with foams and bentonite slurries, and were tested using a modified vane shear apparatus which applied pressures ranging from 0-500 kPa to the soils. It was found that the conditioned sands followed the Bingham fluid model, and showed shear-thinning properties, which meant that the viscosity decreased with increasing shear rate. The values of the viscosity and yield stress were observed to be 9.1-53.5 kPa·s and 1.5-10.2 kPa, respectively. This data can be a good reference to further research on sand-foam mixtures. More importantly, this new apparatus could be used to investigate direct rheological parameters of conditioned soils in pressurised conditions, and its design will be introduced in the following section.

3.2 *Development of testing methods*

Rheological properties can be measured by tube viscometers or rotational rheometers. In general, tube viscometers are better at measuring precise viscosity. On the other hand, rotational rheometers provide the advantages of being able to measure the changes in shear stress and shear rate over time, making them preferable for conditioned soils in tunnelling. However, due to the large particle sizes of conditioned soils and complex conditions in the working chamber and screw conveyor, most commercially available viscometers or rheometers cannot be used without modification.

Most recent studies on flow properties are based on slump tests (Quebaud et al., 1988; Peila *et al*, 2009; Thewes and Budach, 2010), shear box tests (Psomas, 2001; Peña Duarte, 2007), large scale fall cone tests (Merritt, 2003), or model tests (Merritt, 2003; Peña Duarte, 2007; Vinai et al., 2008). However, most of these methods suffer from one drawback: the residual strength and its rate dependency cannot be investigated simultaneously.

In the rheology literature, the vane shear test is a simple test that provides investigation of both residual shear strength and its rate dependency. This method has gained increasing attention in soil rheology because of its two main advantages: minimum disturbance to the tested soils, and an effective reduction of wall slip effects. Recently, efforts have been made to simulate the pressurised conditions in an EPB working chamber. Messerlinger *et al.* (2011) and Meng *et al.* (2011) developed two vane shear apparatus which allowed applications of pressure on the tested soils. Since the main structure of these two apparatus are similar, only one structure diagram by Meng *et al.* (2011) is presented in Figure 2.

This device is used to determine the viscoplastic properties of conditioned sands. As shown in Figure 2, it consists of a test container, a vane impeller, a torque sensor, a loading system and a motor with two reducers. The pressure is applied through a gasbag at the bottom of the container, aiming to provide a comparable pressure in the working chamber of the EPBMs. Compared to this device, Messerlinger *et al*. (2011) placed the torque sensor inside the container, which is believed to offer a more accurate torque measurement by minimising machine friction. The test results from the new apparatus were proven to be reliable by comparative measurements with a commercially available rheometer.

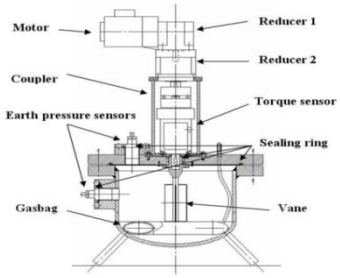

Figure 2. Structure diagram of the vane shear apparatus (Meng et al., 2011).

4. CONCLUSION

Due to the rapid development of the EPB tunnelling method, the rheological properties for conditioned soils have become of great value for optimising machine performance in excavation processes. A modified vane shear device provides a new method of investigating the behaviour of conditioned soils under pressurised conditions. Further efforts might be required in the systematic characterisation of conditioned soils to improve the behaviour of mixtures for different soils with various conditioners; the correlation between results from slump tests and those from vane shear tests; and considerations of other factors affecting rheological properties of conditional soils, for example temperature and time.

5. REFERENCES

Gharahbagh, E. A., Rostami, J. and Talebi, K. (2014) Experimental study of the effect of conditioning on abrasive wear and torque requirement of full tunnelling machines. *Tunnelling and Underground Space Technology*, 41, pp 127-136.

Meng, Q., Qu, F. and Li, S. (2011) Experimental investigation on viscoplastic parameters of conditioned sands in earth pressure balance shield tunnelling. *Journal of Mechanical Science Technology*, 25, pp 2259-2266.

Merritt, A. S. (2004) *Conditioning of clay soil for tunnelling machine screw conveyors.* PhD. University of Cambridge.

Milligan, G. W. E. (2000) *Lubrication and soil conditioning in tunnelling, pipe jacking and micro-tunnelling: A state-of-the-art review.* London, UK: Geotechnical Consulting Group.

Peña Duarte, M. A. (2007) *Foam as a soil conditioner in tunnelling: physical and mechanical properties of conditioned sands.* PhD. Thesis, University of Oxford.

Peila, D., Oggeri, C. and Borio, C. (2009) Using the slump test to assess the behavior of condioned soil for EPB tunnelling. *Environmental & Engineering Geoscience*, 15, pp 167-174.

Psomas, S., (2001) *Properties of foam/sand mixtures for tunnelling applications.* Msc. Thesis, University of Oxford.

Quebaud, S., Sibaï, M. and Henry, J. P. (1998) Use of chemical foam for improvements in drilling by earth-pressure balanced shields in granular soils. *Tunnelling and Underground Space Technology*, 13, pp 173-180.

Vinai, R., Oggeri, C. and Prila, D. (2008) Soil conditioning of sand for EPB applications: A laboratory research. *Tunnelling and Underground Space Technology*, 23(3), pp 308-317.

Zumsteg, R., Plötze, M. and Puzrin, A. M. (2013) Reduction of clogging potential of clays: new chemical applications and novel quantification approaches. *Géotechnique*, 63, pp 276-286.

An investigation into the disaggregation of soil during slurry tunnelling

N.S Phillips, S.E Stallebrass, R.J Goodey, S. Jefferies
Geotechnical Engineering Research Group, City University, London, UK

ABSTRACT: The research concerns the development of test procedures and methods of soil classification that will enable improved predictions of the degree to which soils/weak rocks will disaggregate during the slurry tunnelling process. This will facilitate the prediction of the rate at which the transportation slurry will increase in density and allow economic specification of surface separation plant.

1 BACKGROUND

Soil slurry has been used as a support and transportation mechanism within tunnelling and pipe jacking since the 1970's. The slurry used is water based and depending on the ground conditions bentonite or/and synthetic polymers may also be added. For efficiency and environmental reasons this slurry is reused in a closed loop system, resulting in the need to remove all excavated solids from the slurry. This is most challenging with the suspended solids sub 63µm.

The majority of particles larger than 63µm are removed from the slurry using a series of shaker screens and hydrocyclones. The remaining particles require separation using a decanting centrifuge and flocculant treatment. In order to specify the processing capacity of the centrifuge(s) the quantity of sub 63µm particles must to be known.

Significant advances have been made in tunnelling machine technology and the surface separation plant. However, the breakdown of the excavated solids, due to the machine action and slurry solid interaction during transportation is not widely understood.

The industry has expressed a need to understand how different soils and rocks react to the processes being applied to them during tunneling, with the aim of accurately predicting the plant required for surface separation. Inaccurate prediction can lead to high off-site processing costs or the loss of a contract at tender stage; this has led the Pipe Jacking Association to commission this research.

2 INTRODUCTION

The research being undertaken will characterise samples from a range of different soils using both existing tests for soil properties and new methods that imitate the mechanical action applied to the slurry. Hence it will be possible to develop a link between the properties of the intact soil and the degree to which the soil will disaggregate in slurry during tunnelling. The aim is to quantify the particle size distribution that the slurry separation plant will have to process.

The first stage of the research is concerned with a systematic evaluation of how excavated soil, which initially exists in centimetre sized lumps, disaggregates or breaks down to its constituent particles. In particular, those particles which are smaller than 63µm.

A repeatable test regime has been developed to examine the effect on degree of disaggregation of varying the water content of the slurry, time spent in the slurry, agitation of the slurry and soil type. The initial soils tested were Speswhite Kaolin, London clay and Mercia Mudstone. Further tests have been carried out with weathered London clay and glacial clay from Fleetwood. The reasons for choosing the materials are as follows.

- Speswhite kaolin; Well characterised standard clay with a narrow range of particle sizes, clay-fine silt size. The voids ratio and moisture content can easily be varied.
- London clay; Well characterised natural clay, with a relatively narrow grading curve, but natural fabric and structure. Heavily over consolidated, with a low voids ratio
- Mercia Mudstone; Very variable deposit, but the particular formation used has been comprehensively characterised, (Seward & Stallebrass, 2011), larger spread of particle sizes, starting at sand sizes, heavily overconsolidated and cemented in its natural state

Additional soil samples have been added to the data set along with other soils samples planned.

3 TEST DEVELOPMENT

The initial test regime looked at the effect on disaggregation of varying the time spent on mixing or agitating the slurry. The experimental method was as follows:

The soil is divided into 50-60g samples of soil or weak rock. These are then mixed with 4.5 l of distilled water. This produced realistic water contents, which was determined from a typical slurry flow rate to excavation rate ratio found within the pipe jacking industry. The choice of particle size and quantity was taken from typical cutting size from a 1.2m ID pipe jack tunnel. It is also the size and quantity used within the slake durability test (ASTM D4644-08, 2008).

The water and soil samples are placed in a Hobart planetary mixer and mixed for a set time that will be varied over the course of the research. Initial mixing times were 1, 2, 5 and 10 minutes, this is later extended with intervals up to 120 minutes. The paddle height was set close to the base of the bowl, leaving a gap of 1.5mm between the two parts. The original test methodology removed the slurry mixture and sieved for one minute through 4.75, 1.18, 0.6, 0.063 mm sieves. This represents typical cut sizes within the separation plant. The sieving time is not to BS1377-2 (1990) as the material being sieved is often clay that sticks and extrudes through the sieve if longer shaking times are used. Minimal disturbance to the samples is required to give a representative picture of the effects of mixing. For consistency a 6 minute pause is allowed between the end of mixing and the start of sieving.

The sub 63µm particle slurry was collected in an adapted tray that allows the slurry to flow into a jug. All sieves and the material in the jug were then oven dried and the proportions of different sized dry solids was determined.

After analysis of the initial test results the test procedure was adapted to improve repeatability and accuracy. The first change was to increase the gap between the paddle and the mixing bowl. This ensured that clay cuttings no longer smeared and stuck to the base of the bowl. A small study was carried out in which the paddle height was varied from 1.5- 40 mm. This showed a big change in amount of clay cuttings stuck to the bowl and the apparent disaggregation when the gap was increased from 15-20 mm, showing that 20 mm is a more appropriate gap to use.

Secondly, due to extrusion of clay during shaking and the 63 µm sieve blinding with silty sandy soils, stacking and shaking the sieves was removed from the procedure. Instead the mixed slurry was poured over each sieve individually. Passing the slurry between two jugs with the individual sieve placed on top.

In order to find the solids content in an accurate and representative way a cone splitter was manufactured. (Christina, Pitt & Clark, 2008) The 10-way splitter (Figure 1) allows for manageable samples of slurry to be oven dried and not the entire volume, which is in excess of 5 l.

Due to small dimensional variations arising from manufacture of the splitter, a series of tests were required in order to calibrate it and identify the variation in split quantity and error at each port. The port with most repeatable results had a range of 0.82% and the port with the least repeatable results had a range of 2.66%. The error associated with port 7 (the least repeatable) would result in the volume of sieved slurry varying up to 13.6ml when splitting the proposed 4.5l (plus wash water and solids) of slurry from the mixing tests. With a slurry density of 1.02sg this could equate to an approximate variation of 0.42 g of dry solids.

Figure 1. Cone splitter

Although the test was primarily designed to estimate the volume of sub 63µm particles in the slurry, sedimentation test were carried out on a representative sample of 63µm slurries to get a better feel for how the clay and silt size distributions. This proved valuable information of the detail of the disaggregation process. A method adopted from BS1377-2:1990 (1996) was adapted. Two of the collection beakers are placed in to sedimentation tubes immediately after the slurry is passed through the splitter. The tubes are then left in the water bath until they reach 25°C. Each tube is then shaken end-over-end for 120 cycles in two minutes. The following test procedure is that of BS1377-2:1990 (1996). Critically stages like adding sodium hexametaphosphate are omitted from the procedure so that's it is possible to give an accurate understanding of what the mechanisms of disaggregation includes clay or silt sized aggregates of clay. Comparisons can be made to fully dispersed particle size distributions undertaken in accordance to BS1377-2:1990 (1996).

4 SOIL CLASSIFICATION

The aim is to link the disaggregation behavior to standard soil properties. Consequently simple classification tests have been undertaken for all soils, including fully dispersed particle size distributions, liquid and plastic limit test. In addition simple triaxial and oedometer tests have been carried out to include strength and permeability.

5 CONCLUSIONS

A methodology has been developed that allows the disaggregation potential of a variety of soils to be determined. These soils are representation of a wide range of clays and weak rocks that might be encountered during tunneling. Thus the results provide a database, which should enable the particle size distribution of slurries to be predicted more accurately and in particular the percentage of particles sub 63µm.

REFERENCES

ASTM D4644-08, (2008), Standard Test method for slake durability of shales and similar weak rocks, ASTM International, USA

BS1377-2:1990, (1996), Methods of test for Soils for Civil engineering purposes- Part 2 classification tests, London, BSI

Christina, S,U. Pitt, R. & Clark, S,E, (2008), Errors associated with sampling and measurement of solids: Application to the evaluation of stormwater treatment devices, 11th International Conference on Urban Drainage, Edinburgh, Scotland

Stallebrass.S.E, Seward. L.J, (2011), The effect of mechanical remolding and strength characteristics of a Mercia Mudstone, *Proc.* 15th Soil Mechanics and Geotechnical Engineering, pp. 281-286, IOS Press, Athens

ACKNOWLEDGEMENTS

The Pipe Jacking Association along with the Pipe Jacking and Tunnelling Research group are gratefully acknowledged for both their funding and valuable input in to this project.

A critical review of existing design charts for bored pile shaft resistance in clay

Z. M. Habbi

School of Mechanical, Aerospace and Civil Engineering

The University of Manchester

ABSTRACT: Many researchers have recommended a variety of practices for designing deep foundations. The selection of the pile design parameter adhesion factor (α) is an important matter in designing any pile because it is influenced by both the behaviour of the soils and the effects of pile installation on shaft resistance. The adhesion factors have already been identified in different charts and equations related to the construction of piles in undrained conditions, which are now extant in the literature; however, they do not discriminate among the different pile construction methods: dry, wet or casing. To address this issue, it is essential to combine the data points of those existing charts showing the same pile construction methods into one curve. These data points refer to full-scale piles loaded in soft to hard cohesive soils, often involving casting of concrete in unsupported ''dry'' boreholes at different sites and times. For better design purposes, a database of 188 field load tests collected from the literature is used to create a new trend (fitting) between undrained shear strengths of clayey soils and adhesion parameters. This compound curve is recommended for estimating alpha values from known undrained shear strengths of cohesive soils for piles installed in dry conditions. To conclude, alpha values can be improved, at least for dry construction techniques, in such a way as to be accessible to geotechnical engineers. This is necessary to achieve a successful foundation design, taking into account the methods of pile construction.

KEYWORDS: bored piles, adhesion factor (α), case history, existing charts, database, unsupported borehole.

1 INTRODUCTION

Alpha values in terms of total stress as a function of unit shaft resistance (f_s) and undrained shear strength (S_u) are dependent on factors such as the pile construction technique and soil conditions. The alpha values were also recommended (i.e. Tomlinson, 1970; Weltman and Healy, 1978 and Bowles, 1997) to be within the range of less than unity for all piles in cohesive soils and they decrease as undrained shear strength increases ($\alpha = f_s/S_u$).

Pile construction methods can be classified into three broad categories. These are: (1) the dry method, (2) the casing method, and (3) the wet method. In current methods, there is no evidence that the construction method is taken into account in finding alpha value. A possible issue is that the limited values of alpha for one construction method, such as dry, are not equivalent to those values for the other construction techniques, wet and casing

This paper contains a brief review of the most widely used charts in recent decades (e.g., Weltman and Healy, 1978; Coduto, 1994; Lin et al, 2007) and also analyses the results of some of their case histories (see Table 1) for the evaluation of the adhesion parameters of a pile that take into account the relationship between S_u and α. The data mostly deal with bored piles which have different lengths and diameters and which have been conducted in cohesive soils.

2 THE ADHESION PARAMETERS OF PILE IN CLAYEY SOILS

2.1 *General Review*

The relationship between α and S_u has been widely investigated and the back analyses of loading tests on instrumented bored piles mostly located in the UK are summarised in Table 1. The table contains geotechnical data which have been collected from over 15 authors researching in clayey soils over 11 sites. This table can be used in estimating α value but in some conditions, for example, for designing a pile in boulder clay in the UK, the existing alpha limit which was proposed by Weltman and Healy (1978) should be applied. The authors reviewed numerous pile foundations in cohesive and granular till in 1978 and back calculated the alpha parameter of bored piles in function of S_u based on analysing several load test results in glacial till for bored and driven piles, as shown in Figure 1. The alpha values for bored piles which may be seen in the figure range from 0.3 to 0.9 and this range is recommended by many researchers. Alpha values for bored piles are generally smaller than those of driven piles, since these parameters are influenced by the construction method and soil conditions.

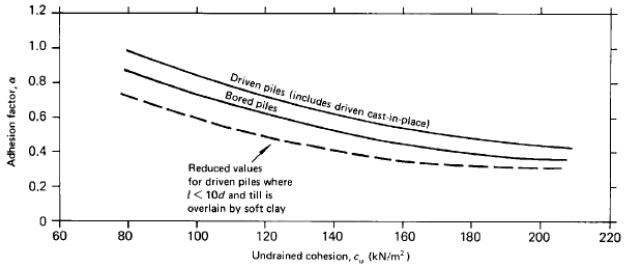

Figure 1 Adhesion factor and undrained shear strength of soil relation by Weltman and Healy (1978).

Nevertheless, this method of analysis has a number of limitations, in that the piles, whether bored or driven, are constructed under specific conditions. These are presented in the table. This approach needs to be improved to evaluate the adhesion parameters for each construction technique separately. The alteration could be presented through carefully selecting the data points for one construction technique, which is dry, as described in Section 2.2.

2.2 *Database*

The database consists of 188 data points collected from six sources (Weltman and Healy, 1978; Fearenside and Cooke, 1978; Stas and Kulhawy, 1984; Patel, 1992; Bowles, 1997; Akbar et. al., 2008) as shown in Table 1 and inserted in a new sheet to plot a new fitting curve, which is shown in Figure 2. The figure shows a clear trend between the alpha values and the undrained shear strength, the alpha values apparently increasing from 0.38 to 1.0

with a decrease in the undrained shear strength from 25 to 300 kPa. It is interesting to note that in 182 cases the alpha values range from 0.1 to 1.0; this range has been recommended by many researchers such as Kerisel (1965) and Tomlinson (1957). This finding cannot be extrapolated to all piles in this area which links α and S_u. However, surprisingly, alpha parameters in six shafts, which reproduce large unit side resistance, are found to be higher than unity. This observed increase in alpha values could be attributed to the residual loads in the piles. These loads are caused by three mechanisms: 1) recovery of the soil at the pile-soil interface after disturbance caused by the installation, which includes the drilling process and the heat and pressure from the fresh concrete; 2) change in the volume of concrete during curing; 3) reconsolidation of the cohesive soils due to dissipation of excess pore water pressures (Fellenius, 2002).

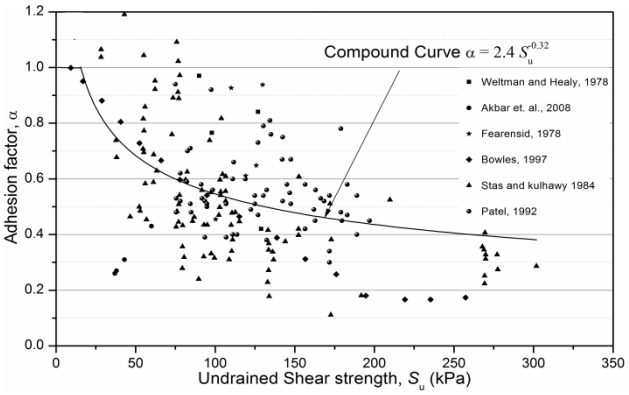

Figure 2 Developed relation between undrained shear strength and adhesion parameters for dry construction method.

2.3 *Variation of α value with respect to the pile installation*

Bored and driven piles are commonly installed in the UK and throughout the world. In this review, the driven piles showed higher adhesion factors than those for the bored piles. Fleming and Sliwinski (1977) and Weltman and Healy (1978) observed that the alpha values of driven piles were high compared with those for bored piles constructed under dry conditions. This is to be expected, since these parameters are influenced by the construction method and soil conditions. A number of studies (McCarthy, 1977; O'Neill and Reese, 1999) have reported the same conclusion, but the limitation of the alpha values is different, as presented in Table (1). Therefore, in view of all that has been mentioned so far, alpha values for piles driven in clayey soils are higher than those for bored piles.

2.4 *Variation of α value with respect to the bored pile construction methods*

Various investigators have reported the adhesion parameter values of piles. For instance, the relation shown in Figure 1, for bored piles, has been used for many years. Because the piles have been constructed under dry methods, the curve should be applied in the same conditions. Comparing two different construction methods, Fleming and Sliwinski (1977) and Fearenside and Cooke (1978) investigated bored piles under dry and bentonite construction methods. The alpha values are different even though the piles were constructed in similar conditions, the same soil and location (London Clay), and remain in the range of less than unity as seen in the table. It can be seen that the adhesion of the bond between the pile material and the soil is developed by the use of a stabilising liquid. This is an indication that the method of construction has an influence on the skin friction, or adhesion parameters, which has been developed between the soil and pile shaft and a special type of analysis design is required.

3 CONCLUSIONS AND RECOMMENDATIONS

The application of an adhesion factor to pile design has been used successfully in the engineering industry. However, choosing an appropriate α value is not always easy and erroneous analyses can result. This is because the adhesion parameter is dependent on several factors, such as soil conditions, pile construction method, and pile location.

This paper has reviewed the variation of alpha values based on several charts and equations which have been identified in the literature and summarised in Table 1. A new relationship between adhesion parameters and undrained shear strength has been proposed and is given as Equation 1. This equation can be used instead of the charts currently available for design bored piles.

$$\alpha = 2.4\, S_u^{-0.32} \quad (1)$$

Further research is being conducted to establish the relationship between the adhesion factor and undrained shear strength for construction techniques involving the use of support fluids and steel casing.

4 ACKNOWLEDGMENTS

The author offers thanks to the supervisor Dr Carlos Lam for his support and valuable suggestions throughout the period of this work.

5 REFERENCES

Akbar A., Khilji S., Khan S.B., Qureshi M.S. and Sattar M. 2008. Shaft Friction of Bored Piles in Hard Clay. *Pak. J. Engg. & Appl. Sci.* 3:54-60.

American Petroleum Institute (API) 2002. Recommended practice for planning, designing and constructing fixed offshore platforms-working stress design. *API Recommended Practice 2A-WSD*, 21st Edition, American Petroleum Institute, Washington, D.C., USA.

Bowles J. E. 1997. *Foundation Analysis and Design* (5th edition). McGraw-Hill, New York.

Coduto, D.P. 1994. *Foundation Design: Principles and Practices*. Prentice Hall, Upper Saddle River, NJ.

Fearenside G. R. and Cooke R. W., 1978. The skin friction of bored piles formed in clay under bentonite. Report 77, *Construction Industry Research and Information Association, London*, UK.

Fellenius B. H. 2002. Determining the resistance distribution in piles. Part 1: Notes on shift of no-load reading and residual load. *Geotech. News*, 20(2):35-38.

Fleming W. K. and Sliwinski Z. J. 1977. *The use and influence of bentonite in bored pile construction*. Construction Industry Research and Information Association, UK.

Lin, S. Wang, K., Hsieh, H., Yu-Herng C., and Huang, C. 2007. Field Testing of axially loaded drilled shafts in clay/gravel layer. *Journal of Geoengineering 2*, pp. 123-128.

McCarthy, D. F. 1977. *Essentials of soil mechanics and foundations*. Reston Publishing Company, Reston, Virginia.

O'Neill, M. W. and Reese, L. C. 1999. *Drilled shafts: construction procedures and design methods*. Federal Highway Administration, U.S. Department of Transportation.

Patel, D. C. 1992. Interpretation of results of pile tests in London Clay. *Proceedings of a Conference on Piling: European Practice and Worldwide Trends, Institution of Civil Engineers*, London, 1992, pp. 100–110.

Sladen, J. A. 1991. The adhesion factor: applications and limitations. *Canadian Geotechnical Journal*, 29:322-326.

Stas, C.V. and Kulhawy, F.H., 1984. *Critical Evaluation of Design methods for Foundations under Axial Uplift and Compression Loading*. Report EL-3771, Electric Power Research Institute.

Tomlinson, M.J. 1957. The adhesion of piles driven in clay soils. *Proceeding of the 4th International Conference on Soil Mechanics and Foundation Engineering*, London, vol. 2, pp. 66-71.

Tomlinson, M. J., 1970. *Adhesion of piles in stiff clays*. CIRIA Report 26. London.

Weltman, A.J. and Healy P.R. 1978. *Piling in 'Boulder Clay' and Other Glacial Tills*. CIRIA Report PG5, London.

Woodward, R. J., Lundgren, R. and Boitano, J. D. 1961. Pile loading tests in stiff clays. *In Proceeding of the 5th International Conference on soil mechanics and foundation engineering*, Paris, vol.2, pp. 177-184.

Table 1 Summary of adhesion parameters based on several sources

Sources	Pile Location	Soil Conditions	Pile type and construction method	S_u (kPa)	Adhesion factor (α) Limitations & Equations
Tomlinson (1957)	UK	Clayey soils	Driven piles	$40 \leq S_u \leq 150$	$0.25 \leq \alpha \leq 0.9$
Tomlinson (1970)	UK	London Clay	Driven pile	$75 \leq S_u \leq 140$	$0.4 \leq \alpha \leq 1.0$
Fleming and Sliwinski (1977)	UK	London Clay	Dry bored pile	$50 \leq S_u \leq 100$	$0.74 \leq \alpha \leq 1.0$
			Bentonite bored pile		$0.86 \leq \alpha \leq 1.78$
McCarthy (1977)	US	Clay	Driven Pile	$33 \leq S_u \leq 287$	$0.2 \leq \alpha \leq 1.0$
Weltman and Healy (1978)	UK and Canada	Boulder clay	Dry bored pile	$80 \leq S_u \leq 210$	$0.37 \leq \alpha \leq 0.87$
			Driven pile		$0.42 \leq \alpha \leq 1.0$
Fearenside and Cooke (1978)	London, UK	London clay	Dry bored pile	$37 \leq S_u \leq 60$	$0.26 \leq \alpha \leq 0.43$
			Bentonite bored pile	$37 \leq S_u \leq 65$	$0.26 \leq \alpha \leq 0.46$
Stas and Kulhawy (1984)	USA	Cohesive soils	Bored piles	$28 \leq S_u \leq 302$	$0.3 \leq \alpha \leq 1.1$
Sladen (1991)	Canada	Cohesive soils	Driven pile	$50 \leq S_u \leq 400$	$\alpha = 0.5 \left(\frac{S_u}{\sigma'_v}\right)^{-0.45}$
Patel (1992)	London, UK	London Clay	Dry Bored piles	$75 \leq S_u \leq 142$	$0.4 \leq \alpha \leq 0.94$
Coduto (1994)	New York, USA	Clayey soil	Dry bored pile	$S_u \leq 51$	$\alpha = 1.0$
				$S_u > 51$	$\alpha = 0.32 + 250\, S_u^{-1.5}$
			Driven pile	$S_u \leq 32$	$\alpha = 1.0$
				$S_u > 32$	$\alpha = 0.35 + 170\, S_u^{-1.6}$
Bowles (1997)	USA	Cohesive soil	Dry Bored pile	$9 \leq S_u \leq 257$	$0.2 \leq \alpha \leq 0.9$
O'Neill and Reese (1999)	USA	Clayey soil	Dry bored pile	$1.5 \leq S_u/P_a \leq 2.5$	$\alpha = 0.55 - 0.1(S_u/P_a - 1.5)$
				$S_u/P_a \leq 1.5$ *or* $S_u/P_a \geq 2.5$	$\alpha = 0.55$
API (2002)	USA	Cohesive soils	Driven pile	$S_u/\sigma'_v \leq 1.0$	$\alpha = 0.5\,(S_u/\sigma'_v)^{-0.5}$
				$S_u/\sigma'_v > 1.0$	$\alpha = 0.5\,(S_u/\sigma'_v)^{-0.25}$
Lin et. al. (2007)	Taiwan	Silty clay soils	Polymer bored pile	$41 \leq S_u \leq 53$	$0.7 \leq \alpha \leq 0.95$
Akbar et. al. (2008)	Pakistan	Hard clay	Dry bored pile	$\delta \geq 12$ mm, $90 \leq S_u \leq 127$	$0.84 \leq \alpha \leq 0.97$
				$\delta < 12$ mm, $98 \leq S_u \leq 129$	$0.42 \leq \alpha \leq 0.76$

S_u = average undrained shear strength; σ'_v = effective vertical stress; P_a = atmospheric pressure (101 kPa); δ = pile settlement

Development of a Laboratory Model to Investigate the Thermo-Mechanical Behaviour of Thermal Piles

A. Rafiei, C. Arya
Dept. of Civil, Environmental and Geomatic Engineering, UCL, Gower Street, London, WC1E 6BT

R. Fuentes
School of Civil Engineering, University of Leeds (formerly UCL)

ABSTRACT: The UK 2020 target is to supply 12% of heat from renewable sources. Thermal piles are one possible solution of the low-carbon emission systems currently available that could help meet this demand. Despite an increasing number of applications in recent years, knowledge of the thermo-mechanical behaviour of thermal piles is still limited. The overall aim of this project is to investigate the effect of cyclic thermal loading on the bearing capacity of thermal piles under different boundary conditions including varying end restraint conditions, thermal loading amplitude and the number of cyclic loading. A 1g small scale model has been designed and developed to perform a series of mechanical, thermal and thermo-mechanical loading tests. A novel monitoring technique is also used in this study based on Fibre Bragg Gratings to monitor the strain and temperature changes along the pile surface and the surrounding soil. A brief description of the design and development of the apparatus is presented.

KEYWORDS: Thermal pile, thermo-mechanical behaviour, cyclic thermal loading, small scale model, monitoring

1 INTRODUCTION

At the moment, the UK's commitment for 2020 is to supply 12% of heat from renewable sources (Renewable Heat Incentive, 2011). The Ground Source Heat Pump (GSHP) system is considered as one of the rapidly growing low-carbon emission technologies. This research deals with a specific type of GSHP system known as Thermal Piles. Thermal piles have the dual responsibility of carrying the structural weight to the ground and also providing heating and cooling of the building. Hence, they undergo seasonal heating-cooling cycles and understanding the effects of combined thermo-mechanical loading on thermal piles has become a major issue in recent years.

The aim of this project is to investigate the effect of cyclic thermal loading on the bearing capacity of thermal piles. In order to achieve the project aims, a 1g small scale model has been designed and developed and a series of monotonic and cyclic mechanical, thermal and thermo-mechanical loading tests with different boundary conditions devised. A novel monitoring technique is also used in this study using Fibre Bragg Gratings (FBG) to monitor the strain and temperature changes along the piles surface and the surrounding soil. The pile is heated in controlled increments of temperature and then allowed to recover to room temperature;the procedure is repeated subsequently at other temperatures. The framework proposed by Bourne Webb et al (2012) is used to predict the behaviour of thermal piles.

This summary presents a brief description of the experimental set-up that has been developed. To justify the dimensioning, scaling laws and non-dimensional analysis were applied but due to limitations of space, only the apparatus development is described. A brief description of the results obtained by the numerical model is also presented.

2 THERMO-MECHANICAL LOADING

The load transfer mechanism used in this study is the same as that described in Thermal Pile Standard; GSHPA 2012, which is based on the framework proposed by Bourne-Webb et al (2012). When a pile is heated or cooled, it expands or contracts resulting in changes to the soil-pile interaction. From the structural point of view, thermal loading is expected to induce additional strains and consequently additional axial loads and stresses inside the pile. At the soil-pile interface, movement of the pile due to heating and cooling will cause the shaft resistance mobilisation to vary. Additional induced axial load and stress means that the margin of safety may be reduced. It is found by Laloui et al (2006) that the induced thermal loading could be twice the initial mechanical loading and consequently twice the induced stress. This reduces the safety factor from 3 to 1 which could endanger the integrity of the structure.

3 EXPERIMENTAL EQUIPMENT

3.1 *Tank and pile Design*

The apparatus consists of a cylindrical steel tank made of 3mm-thick steel plate (See Figure 1.a). The outer diameter and height of the tank are both 500mm. Steel grade S275 was used which is suitable for welding. Container dimensions were chosen to make sure that the results obtained would not be affected by the boundary conditions.

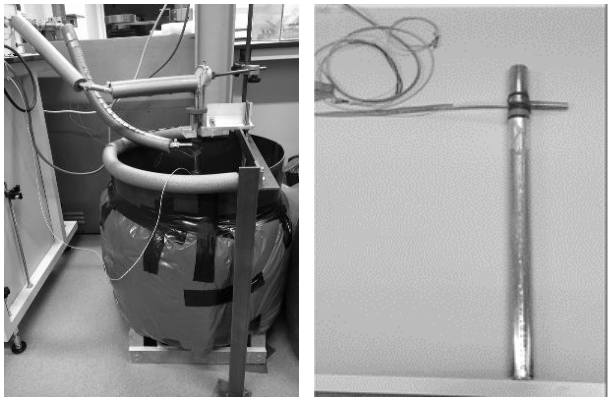

(a) (b)

Figure 1. (a) Experiment set-up (b) Pile instrumentation.

An insulation jacket is provided around the container to minimise heat transfer between the container and the surroundings. The container is placed on the ground on top of a wooden box which will allow enough space for the pile to travel downwards as the shaft resistance of the pile is mobilised, hence no bearing resistance is present. A wall bright polished round stainless steel (304) tube is used as a model pile with outer diameter, height and thickness of 28, 535 and 1.5mm respectively (See Figure 1.b). The bottom of the model pile is closed by welding a base plate of the same material to make it a close-ended pipe pile.

3.2 *Loading Mechanism*

Different techniques have been used in the literature for applying mechanical loading to piles. There as three possible options as follows:

1. Using a dead load (i.e. weights) to apply a static load
2. Using a hydraulic jack to provide incremental loading
3. Using an actuator

In this study, weights are used as it is closer to the situation in the field where the superstructure acts as a dead load resting on the thermal piles. The amount of axial load applied on the pile head is a percentage of the maximum bearing capacity of the pile i.e. are 25%, 50% and 75%.

3.3 *Temperature Control System*

The pile is heated using a Techno C-400 water/oil circulator. A compact circulator is used which recirculates thermostatically-controlled water through tubes connected to the pile head. The circulator allows the temperature to be varied in the range of -20˚C and +80˚C.

3.4 *Sand Characteristic Properties*

The soil used in this study is a Uniform fine sand (poorly graded) having uniformity coefficient of 2.32 and the effective grain size D_{10} of 0.086 with an average specific gravity of 2.64 g/cm^3 and maximum and minimum dry densities of 1.658 and 1.349 g/cm^3 respectively. The soil friction angel for the sandwas calculated as 34˚ for the peak shear resistance using BS 1377:Part 7:1990:4 for shear box tests.

3.5 *Novel monitoring technique*

In this study, the pile behaviour,the soil behaviour and temperature/strain on the container wall will be monitored. For the pile, strain and temperature variations are recorded and for the soil mass the temperature changes will be recorded. Strain monitoring will be carried out on the pile surface using 5 Fibre Bragg Gratings (FBG). Temperature monitoring consists of:

1) pile surface monitoring using 5 FBG sensors,
2) soil mass at five different depths using 4 FBG in each layer (See Figure 2),
3) container wall.

For the container wall monitoring, 2 thermocouples type T are installed at the bottom and wall of the. An extra thermocouple is also placed at the middle of the pile surface which provides a comparison and redundancy to the measurements obtained by the fibre optic sensors. Moreover, one single FBG strain sensor is also placed on the container wall to assess the effects of strain changes during thermal loading on the boundaries. A summary of the monitoring instruments are given in Table 1.

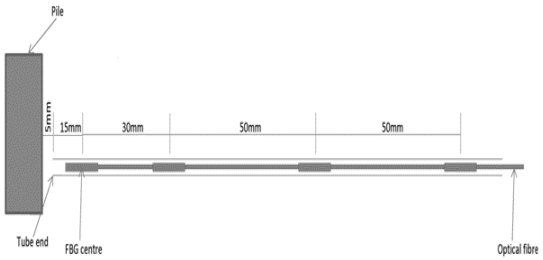

Figure 2. Fibre optic placed in the sand bed with 4 FBGs at different spacing

Table 1. A summary of the applied monitoring instruments

Monitoring instrument	*Number of sensors*
FBG Temperature sensors on the pile	5
FBG strain sensors on the pile	5
FBG strain sensors on the container wall	1
FBG Temperature sensors in the soil	20
Thermocouple Type 'T'	3

3.6 *Numerical model*

A Matlab code is developed to predict the temperature distribution inside the soil using the two-dimensional transient heat conduction method. It is found that the temperature dissipates quickly radially away from the pile. The pile is heated up to 50˚C and at 150mm away, the temperature is 35˚C after 8 hours, which means that most of the monitoring points were placed within this distance (See Figure 3). Most of the heat propagation occurs during the first 4 hours, after which only small variations occur before reaching steady state. Information found by the numerical model has helped to allocate the critical monitoring points.

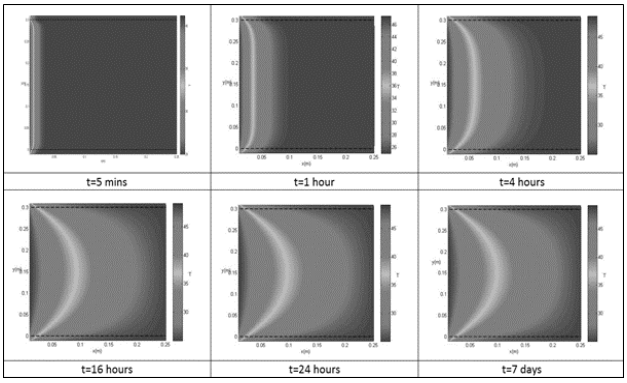

Figure 3. Heat diffusion in the sand bed for different time steps

4 SUMMARY

This note discusses the effects of thermo-mechanical loading on pile behaviour. A laboratory apparatus has been developed to study the soil-pile interaction and temperature distribution in the surrounding soil. Moreover, a numerical model developed to support the experiment assumptions is presented. The developed physical model is part of an on-going project and the test results will be presented in the future.

5 REFERENCES

Bourne-Webb, P.J., Amatya, B., Soga, K. 2012. A framework for understanding energy pile behaviour. *Proceedings of the ICE - Geotechnical Engineering*, 166(2). 170 –177.

British Standards Institution, 1999. BS 1337-7: 1990. Methods of test for Soils for civil Engineering purposes - Part 7: Shear strength tests (total stress).Milton Keynes: BSI.

Department for Energy and Climate Change, 2011. Renewable heat incentive. London: Department for Energy and Climate Change.

Ground Source Heat Pump Association, 2012.Thermal Pile Design, Installation & Materials Standards. Milton Keynes. GSHPA.

Laloui, L., Nuth, M., Vulliet, L. 2006. Experimental and numerical investigations of the behaviour of a heat exchanger pile. *International Journal for Numerical and Analytical Methods in Geomechanics*, 30(8). 763–781.

Automatic detection of secondary consolidation in computer controlled oedometer tests

D. C. Teles
GDS Instruments

ABSTRACT: Oedometer tests are one of the most widely used methods to evaluate consolidation behaviour in soils. Reliable, fully automated testing using currently available computer controlled equipment has been hindered by the inherent variability of soils, a function of their nature and geotechnical context. Using Analysis of Variance statistical models, applied to consecutive data clusters of deformation and time for a single vertical load increment, a method was developed which allows virtual shape quantification of a typical log time-deformation plot for individual load increments during an oedometer test. This was achieved by testing the variability of deformation in relation to the variability of time within consecutive data clusters using the F-Test, and establishing the relation between its value and the rate of consolidation for a load increment. It was concluded that at the end of primary consolidation there was a sudden decrease in the values returned by the F-Test, followed by stabilization at a lower value during secondary consolidation. This behaviour constitutes an objective indicator for the onset of secondary consolidation during oedometer testing, independent of the soil being tested, which can be used within an algorithm to automate the transition between two consecutive loading increments.

KEYWORDS: Oedometer, consolidation, computer controlled, automated testing, testing software, ANOVA.

1. INTRODUCTION

Recent years have brought us a wide range of testing apparatuses which allow computer control of test procedures, providing users with decreased operation complexity and increased reliability. Automated one-dimensional consolidation systems do away with the need for bulky weights, replacing them with pneumatic or motorized systems for the application of vertical load during a test. However, despite their name, full automation of incremental loading and unloading for a complete oedometer test is still difficult to achieve in a reliable way. Testing specimens of different soil types and geotechnical contexts implies variability in consolidation behaviour, which in turn means that the same automation trigger may not be applicable for different specimens.

Standardised oedometer test methodology requires the incremental application of a vertical load on a laterally confined specimen. To be able to determine the coefficient of consolidation for each load increment, time-deformation readings will be recorded for that increment, plotted to a square root or logarithmic scale and analysed using a curve fitting method (Craig and Knappett 2012). Automation of the transition between loading increments requires the identification of a conditional state indicative of the end point of a load increment. This point can be defined as the time when enough data has been recorded for determination of the coefficient of consolidation. To ensure repeatability and applicability of the automation method, this conditional trigger must not be affected by the variability between test specimens.

2. DEFENITION OF A TRIGGER CONDITION

To avoid dependency between soil properties and trigger conditions, the selected approach focused on statistical analysis of the theoretical data distribution for points defined by time and deformation data. During consolidation of a soil specimen under a given loading increment these parameters will vary in magnitude according to the characteristics of the soil being tested, but they will keep the same type of data distribution expressed by the theoretical curves for oedometer consolidation.

Discrete specimen behaviour during consolidation (initial compression, primary and secondary consolidation) can be related to intervals within the time-deformation data distribution. Standardised test methods rely on this relation for the determination of the coefficient of consolidation (BS1377-Part 5, 1990 and ASTM D2435, 2011) by means of the curve fitting methods. When a specimen fully enters secondary consolidation after application of a vertical load increment during standardised oedometer testing, enough registered data will be available for the application of at least one of the curve fitting methods. Thus it was considered the onset of secondary consolidation would constitute a reliable condition to trigger the transition for the next loading stage.

2.1 *Graphical definition of secondary consolidation*

Casagrande's curve obtained by plotting deformation data against time in minutes on a logarithmic scale (Casagrande, 1936) was used to identify secondary consolidation during incremental loading oedometer trial tests performed on remoulded clay. This theoretical curve was chosen because it typically requires a longer increment duration than Taylor's root of time curve, providing a larger data set for the same data acquisition frequency (Alshenawy 2007).

2.2 *Adaptation of theoretical one-dimensional consolidation behaviour for software development*

Curve fitting methods are practical and easy to use. However, the design of an algorithm capable of performing the conceptual shape analysis associated with these methods, which comes naturally during direct human interaction, can be very challenging and resource consuming. To circumvent this issue a numerical approach was adopted to virtually quantify the shape of the theoretical consolidation data distribution. This was achieved by splitting test data from the loading increment into consecutive pairs of corresponding clusters of time and deformation data, creating different non-overlapping and statistically comparable populations. The time clusters contained a constant number of consecutive observations with a difference of one second between them.

Each deformation data cluster was compared to its corresponding time data cluster, providing a numerical indicator of consolidation behaviour for that time interval. The analysis of consecutive cluster pairs provides a numerical indicator which can be plotted against time (using the largest time value for each

cluster) on a logarithmic scale, and directly comparable to the shape of the corresponding theoretical consolidation curve. Using this data grouping methodology, Analysis of Variance (ANOVA) statistical models were used to assess the available data.

Linearity analysis was conducted by testing the applicability of a linear regression model through the determination of the coefficient of determination (R^2) for each pair of data clusters.

The F-Test was also used to test the variability of deformation readings and the respective time readings. Having control of time data means that the result of ANOVA's F-Test will constitute a good numerical indicator of the variability of deformation data in relation to time.

Figure 1 compares the results of both models with data from a consolidation loading increment on a clay specimen, in which the vertical stress was increased from 400 kPa to 800 kPa.

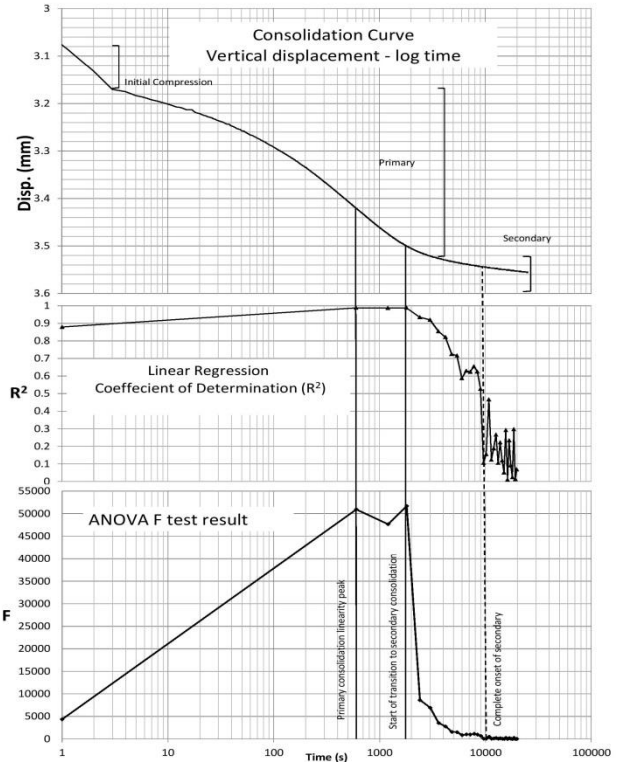

Figure 1.Relation between consolidation curve, R^2 and ANOVA F-test cluster analysis.

The graphical comparison shows a discernible relationship between the behaviour of the statistical indicators and time-deformation data distribution. The same analysis was repeated, with identical results, for different loading increments on different soil specimens. There is an increase of the test parameter value as the consolidation curve approaches linearity during primary consolidation, progressing to an accentuated drop in the statistical test results during the transition between primary and secondary consolidation, and a final stabilisation at a lower value when secondary consolidation is ongoing. Although this behaviour is observed for both indicators, the coefficient of determination shows a milder reaction to changes in the consolidation curve than ANOVA's F-test, in addition to an increased variability during secondary consolidation.

This association between the onset of secondary consolidation and stabilization of F-Test at a lower value relative to a previously identified maximum constitutes an objective indicator useful for viable software implementation during the automation of the transition between load increments.

2.3 *Experimental test results*

The F-Test trigger condition was implemented within the software used to control an oedometer system. Tests conducted on clays showed a consistent automated transition between load increments occurring at the start of secondary consolidation. Manual data analysis using the log time method confirmed there was enough data for each stage for accurate determination of the coefficient of standardized consolidation parameters. Additionally, it was observed that the trigger condition was also applicable for unloading stages, as the inverted time-deformation distribution obtained during unloading produced similar results under clustered F-test analysis.

Further data obtained from automated increment transition tests showed a decrease in total test time without loss of relevant data. Testing is still being conducted to quantify this decrease in duration. It will be difficult to reach a specific value as the beginning of secondary consolidation will change according to specimen characteristics. However, at this early stage of testing, results obtained showed an average duration decrease of 42 % in relation to the 24 hour increments suggested by BS 1377 part 5 1990. Given its nature, the ANOVA F-test trigger should activate on the onset of secondary consolidation, even for specimens requiring longer consolidation times (i.e., above 24 hours), unless a user defined duration limit is established.

3 CONCLUSION

To automate computer controlled oedometer tests, the onset of secondary consolidation was selected as the condition triggering the transition between vertical load increments.

A study of time-deformation data relying on variance analysis and linearity tests was used to identify an indicator of secondary consolidation, independent of the characteristics of the specimen being tested. The coefficient of determination R^2 and ANOVA's F-Test were used to quantify the linearity and variance, respectively, of the test data. It was observed that, independent of the specimen being tested, statistical test values decreased at the end of primary consolidation, stabilising at lower values during secondary consolidation. The F-Test provided better results than R^2 after primary consolidation. Its behaviour was then used as a conditional trigger in test control software, successfully automating transitions between both loading and unloading increments during oedometer testing, resulting in an average decrease of 42 % in test duration.

4 ACKNOWLEDGEMENTS

The author would like to thank GDS Instruments for providing the resources needed for development of this work, David Pallet and Ben Hutt for their support and software applicability assessment of the method here presented and Nick Warren and Sean Rees, for the technical review of this work.

5 REFERENCES

Alshenawy A. O. 2007, *"Determination of the coefficient of consolidation using different methods and study the effect of applied pressure for different types of soils"*. King Saud University.

ASTM Standard D2435, 2011, "*Standard Test Methods for One-Dimensional Consolidation Properties of Soils Using Incremental Loading*" ASTM International, West Conshohocken, PA,

British Standard BS1377, 1990, Soils for Civil Engineering Purposes, Part 5, *"Compressibility, Durability and Permeability tests"*. British Standards Institution, 2-8

Casagrande, A., 1936 *"The Determination of Pre-Consolidation Load and its Pratical Significance".* Proceedings 1st ICSMFE, III. P.60

Craig, R. F., Knappett, J.A. 2012. *Craig's Soil Mechanics*. Spon Press, 121-124

Compensation grouting to control ground movements around deep excavations

H. Halai and A.M. McNamara
Geotechnical Engineering Research Centre, City University London, UK

ABSTRACT: This research will investigate the application of compensation grouting around deep excavations to limit ground movements using the geotechnical centrifuge at City University London. The equipment developed to model the excavation process and the development of the apparatus for modelling the compensation grouting is described. Results showing excavation induced ground movements without the presence of grouting are presented, with a brief discussion of further work planned for modelling and testing compensation grouting and its effect on the retaining wall and ground surface movements.

KEYWORDS: deep excavations, compensation grouting, ground movements, centrifuge modelling

1 INTRODUCTION

Increasing demand for space both commercial and residential and on infrastructure from rapidly swelling populations in urban centres is driving the development of larger and taller structures. As a result engineers are asked to look to available underground spaces through the construction of deep basements.

The construction of these underground structures requires deep excavations. The design of the support and bracing system is often approached conservatively with very large props and stiff retaining walls. Even with these measures ground movements inevitably occur as ground stresses are relieved during excavation. The movements that occur are of significant concern to the engineer owing to the vast array of buried services and surrounding structures often found in urban settings.

One method used successfully and extensively in the past for controlling movements induced by tunnel excavations is compensation grouting. The method first introduced by Mair and Hight (1994) involves the injection of grout between the tunnel and building foundations overhead. The grouting compensates for the ground loss and stress relief created by the tunnel excavation.

To date this method of ground movement control has not been applied to retained excavations. The project aims to understand the limitations of its application and highlight ideal positioning for achieving the most efficient ground movement control.

2 BACKGROUND

A series of 15 to 20 plane strain tests will be conducted using the geotechnical engineering Centrifuge at City University London. The tests will be carried out in a soft to firm overconsolidated speswhite kaolin clay with S_u ranging between 35-60 kN/m^2. All tests will be carried out within a strongbox with a clay sample measuring 550x200mm in plan and 300mm in height. Two reference tests without the presence of grouting have been carried out to establish the pattern of movements developed during the modelling of a deep excavation. The results from these, presented later, have helped to decide on the initial testing parameters for the compensation grouting testing phase of the research.

3 APPARATUS

3.1 *Excavation modelling*

At 100g a 12m deep by 16m half-width excavation with a single stiff prop at the crest will model the deep excavation, illustrated in Figure 1.0. The excavation is supported in flight using a1mm thick latex bag filled with sodium polytungstate, at a specific gravity of 1.778 g/cm^3.

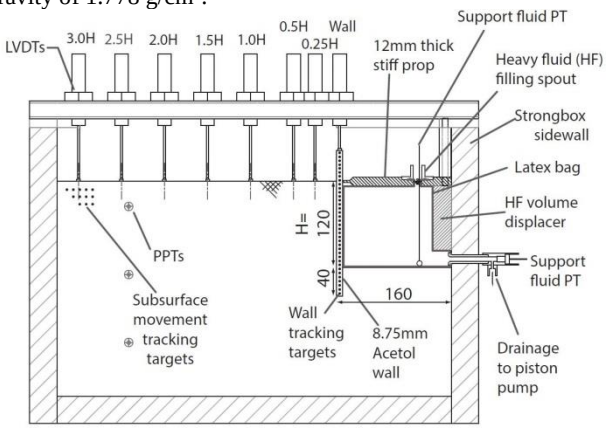

Figure 1.0. Excavation modelling setup

During the test the total volume of support fluid is drained in three equal stages to model the excavation process. Each stage takes approximately 2.5 minutes which equates to 18 days at prototype scale. This is considered sufficiently fast enough to model an undrained event as well as allowing monitoring of surface movements of the clay. The fluid is removed from the latex bag using a custom built piston pump which allows control over the rate and volume of fluid removal.

3.2 *Compensation grouting modelling*

The main phase of testing to investigate the grouting will focus on the effect of position and grout type on the ground and retaining wall movements.

Compensation grouting typically can be sub categorised into two forms; fracture grouting and compaction grouting. Fracture grouting involves hydro fracturing of the soil to form fissure planes along which the grout can flow. Compaction grouting is a process in which grout is injected to form an approximately spherical bulb. Figures 2.0(a) and (b) shows the cross sectional view of the different grouting apparatus setups to allow modelling of the two different processes.

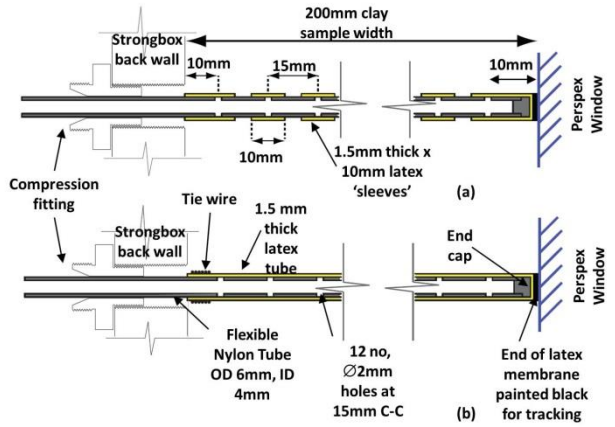

Figure 2.0. Cross sectional view of the compensation grouting injection apparatus setup: (a) for fracture grouting and (b) for compaction grouting.

The latex tubes 'sleeves' around the 6mm diameter nylon tubing has been formed to provide a compressive fit onto and over the grout outlet holes. This will prevent either ingress or egress of pore water or grout when not grouting and will also allow subsequent grouting after initial grouting passes.

A double acting piston will use a compressed air feed to push the grout into the injection setup shown in Figure 2.0. Two pressure transducers and a LVDT connected to the double acting piston will provide instrumentation to the grout injection system.

4 TEST RESULTS

Two reference tests, 2HH and 3HH have been carried out using the excavation modelling equipment without the presence of grouting to establish a baseline for the pattern and magnitude of movements expected with the equipment. Figure 3.0 shows the vertical ground settlement, δ_v logged from the LVDTs. Figure 4.0 shows the horizontal wall displacement, δ_h plotted from the image analysis of the wall tracking targets.

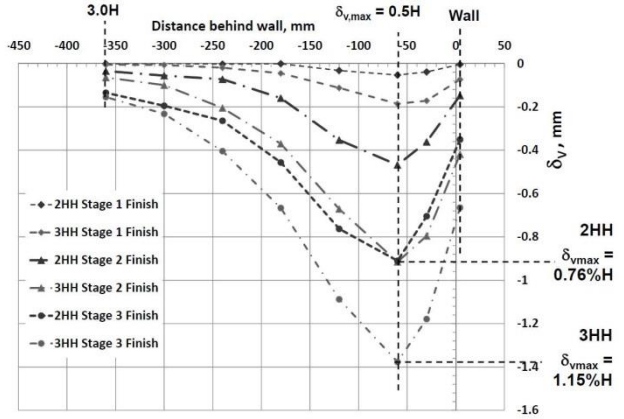

Figure 3.0. LVDT Surface settlement behind the model retaining wall, δ_v plotted against distance behind the retaining wall.

It can be seen from the figure above that maximum vertical settlements, δ_{vmax} occur at a distance 0.5H behind the wall, where H is the excavation depth. At the end of the final stage of excavation, there is 0.5%H difference in δ_{vmax} between the two tests. This could be attributed to a slight difference in the drainage rate and some additional support fluid being left in the latex bag in 3HH. The settlement profiles from both tests and the normalised settlement δ_{vmax}/H values for each test shows good correlation with the expected profiles and values presented by Clough and O'Rourke (1990).

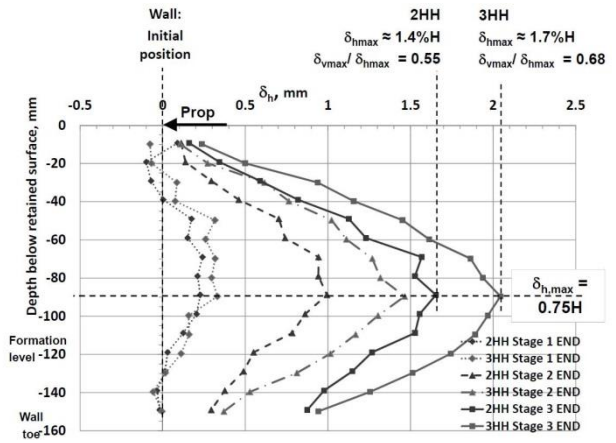

Figure 4.0. Tracking target horizontal wall displacement, δ_h plotted against depth below retained clay surface.

Figure 4.0 shows that the maximum horizontal displacement, δ_{hmax} at the end of each drainage stage for both tests occurred at a depth 0.75H. Normalised δ_{hmax}/H values of 1.4% and 1.7% respectively for test 2HH and 3HH show consistency with the database collated by Long (2001) for a propped wall with a low factor of safety against basal heave of 1.4 used in this model.

5 CONCLUSIONS AND FURTHER WORK

The behaviour observed from the two tests provides confidence in the excavation modelling apparatus and allows progression to the modelling of compensation grouting.

The position of δ_{vmax} behind the wall was consistently 0.5H behind the wall for both reference tests. This provides a good starting point for deciding the positioning of the first grouting tests. The first few tests will look the effect of fracture and compaction grouting at depths of 0.25H, 0.5H and 0.75H at this distance behind the wall. The sequence of grouting relative to the modelled excavation stages will also look in further detail to determine if early control of movement during excavation is more efficient than remedial grouting at the end of excavation.

Water will be used as the grout medium for the first few tests. This is in order to ensure low grout pumping pressures. It is expected that the water grout will be detrimental to the compensation effect in the long term as it will increase consolidation related settlements. However, the short term undrained response of the water injection and subsequent soil and wall movements will provide useful information on the effect of introducing an additional volume into the soil.

A clay slurry grout medium will also be explored which could make use of a custom designed and made inflight grout mixer to keep the particulates in suspension prior to grouting.

6 REFERENCES

Clough G.W. and O'Rourke T.D (1990). Construction induced movements of insitu walls, Proceedings of ASCE Conference on Design and Performance of Earth Retaining Structures, Geotechnical Special Publication, 25, ASCE, New York, pp. 439–470.

Long, M, (2001). Database for Retaining Wall and Ground Movements due to Deep Excavations, Journal of Geotechnical and Geoenvironmental Engineering, Vol. 127, No. 3, pp.203-224.

Mair R.J. & Hight D. (1994). Compensation grouting. World Tunnelling, November, pp. 361-367.

Interaction behaviour of soil and geo-grid reinforcement

A.Tatari
Department of Civil & Structural Engineering, University of Sheffield, UK.

ABSTRACT: Geosynthetic materials are frequently adopted as reinforcement to improve soil properties and geotechnical structural performance. One particular challenge facing engineers when designing soil reinforcement relates to the interface friction that is generated between soil and geosynthetic material. This aspect is not fully understood and current understanding is based on empirical data from laboratory pull-out interface tests. The objective of this research is to investigate fundamental aspects of interface mechanics, evaluating the effect of parameters such as aperture size, soil particle size distribution, embedment length and confining stress to enhance design implementation. The research adopts a novel methodology of non-intrusive modelling using transparent soil in conjunction with laser aided imaging to visually observe soil geo-grid interaction mechanics in a specially designed pull-out test apparatus.

KEYWORDS: Soil reinforcement, Soil-geosynthetic interaction, Transparent soil

1 INTRODUCTION

The use of geosynthetic materials in engineered earthworks has increased significantly in recent years to provide reinforcement to geotechnical earth structures. When designing reinforced earth structures a vital aspect is to understand the interaction between the reinforcement inclusion and the compacted soil as the interaction governs the overall stability. The main function of the inclusion is to redistribute stresses within the soil mass in order to enhance the internal stability of reinforced soil structure. The inclusions undergo tensile strain as they transfer loads from unstable portions of the soil mass into stable soil zone. The most common example of soil-reinforcement interaction research is to investigate pull-out capacity. The lack of knowledge of interaction mechanics between soil and reinforcement has considerable impact on our ability to implement rigorous analytical solutions or assign suitable parameters for interface elements in numerical modelling of reinforcement. It is common that the design will assume a perfect boundary condition between soil and reinforcement assuming that the full soil strength will be mobilised in shear (i.e. interface factor = 1). Previous research using classical pull-out tests have indicated this not the case with interface factors varying between 0.6 - 0.8 (FHWA, 2001); hence, it is likely that many designs over predict the possible resistance that may be generated. Furthermore, in the absence of field validation, there is uncertainty as to how representative small scale pull-out tests reflect the likely behaviour that would prevail in the prototype structure.

1.1 *Research aim*

The main objective of this research is to investigate interaction mechanics between granular soil and geo-grid reinforcement. Fundamental aspects of the investigation will consider:

i. the effect of geo-grid aperture size,
ii. soil particle size distribution,
iii. embedment geo-grid length,
iv. applied boundary confining stress.

For achieving this aim, this research will adopt physical modelling using non-intrusive modelling techniques of transparent soil coupled with Particle Image Velocimetry (PIV). The purpose of using the transparent soil is to enable direct visualisation of interaction mechanics during element pull-out tests between the soil and reinforcing material (Figure 1).

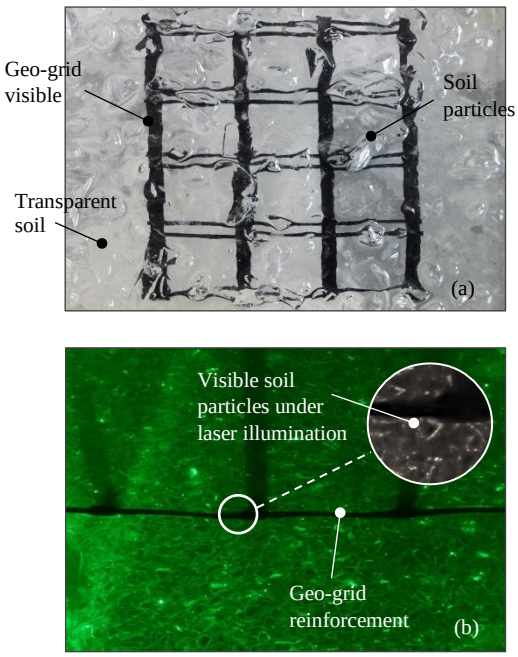

Figure 1. Photograph showing geo-grid in transparent soil; (a) under natural light (plan view), (b) under laser illumination (side view).

2 PHYSICAL MODELLING

Interaction between soil and reinforcement can be evaluated using a pull-out box. British Standard and American Society for Testing Materials codes of practice outline such experiments (configuration and geometry) and note that these are influenced by the particle size of soil and side wall friction characteristics. While these classical testing methods offer the opportunity to evaluate capacity and determine an estimate of likely interface friction, they fail to offer any conclusive evidence as to the localised mechanics, zone of influence or interactions that govern the global response. For this reason a modified pull-out test system has been devised to enable internal visualisation of the soil and reinforcement.

Bathurst (2011) conducted a study using transparent soil whereby a geo-grid was back silhouetted within the soil material. This enabled detection of strain within the geo-grid to

be observed during pull-out. Soil interactions mechanics were not considered as part of this work.

The current research adopts similar methodology but extends this technique by introducing laser aided imaging to illuminate a cross section vertical plane within the soil, which reveals the outline of individual soil particles so that the soil-reinforcement interaction mechanics can be quantified (Figure 2).

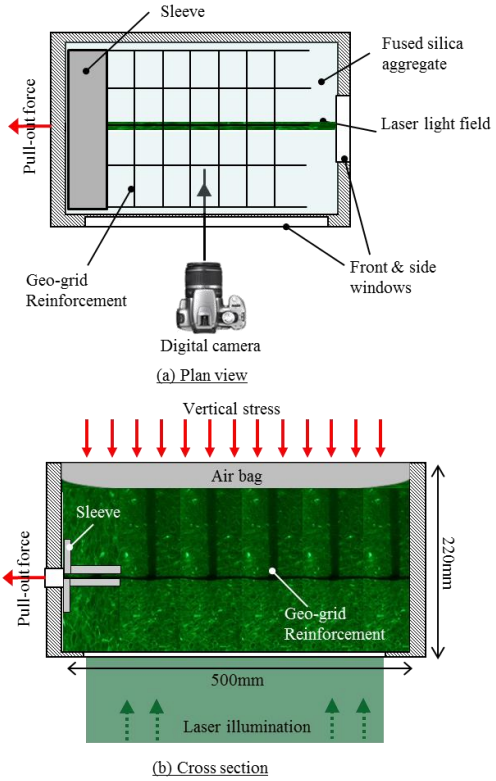

Figure 2. Test concept.

2.1 *Test System development*

According to literature, there are two important parameters which have significant effect on the pull-out force derived from experimental methods: (i) friction between front wall and (ii) the method of applying the vertical stress (i.e. flexible of rigid boundary). Preliminary numerical simulation, using limit analysis software LimitState:GEO, reflecting the proposed test configuration, revealed that a flexible boundary stress condition was necessary to mitigate boundary effects from rigid loading that would impinge on the failure mechanism observed.

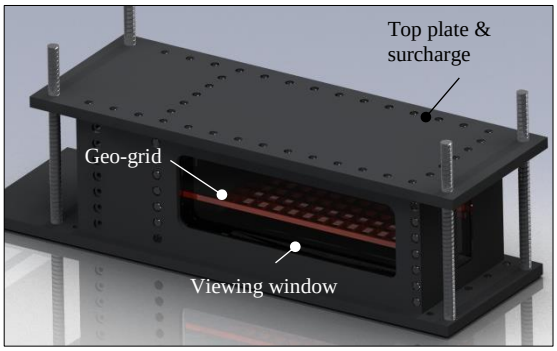

Figure 3. Design of pull-out box test.

Figure 3 shows the design of the pull-out box developed for this purpose. The inner dimensions of the box are 500mm x 200mm x 200mm is made with 20mm thickness aluminium plate and incorporates several Perspex windows that allow introduction of the laser illumination and the camera capture. Vertical load is applied as a flexible boundary condition by using an air bag to make sure the distributed load over specimen is uniform.

2.2 *Transparent soil material*

The transparent soil consists of fused silica aggregate which is mixed with two types of mineral oil that have the same reflective index with fused silica. The fused silica is produced from high purity Quartz Sand which is melted at high temperature between 1800-2000ºC, cooled and crushed to produce a granular based aggregate. The aggregate has a shear friction angle of 40º at a unit weight of 12kN/m^3. Once submerged in suitable refractive matched index fluid the aggregate particles become transparent. The matched RI pore fluid is blended from two mineral oils: technical white oil and Paraffin that are mixed at 77:23 ratio by volume. Optical transmission of the soil is critical to ensure optimum viewing of the particles illuminated by the laser sheet and thus the precise mixture ratios have been carefully calibrated at 20ºC.

3 RESULTS

The test methodology and experimental systems have been successfully developed for this research project. Trial tests using the system confirm the ability to track soil particle movement and grain rotations as mobilisation of the geo-grid commences during tensile pull out. Figure 4 demonstrates the PIV vector displacements for one trial conducted at low confining stress at a pull out rate of 1mm/min. It is evident that mobilisation interaction zone is present that will control the pull out mechanics. An extensive series of tests are currently underway to address the aims of the investigate (Section 1.1) and preliminary analysis is very encouraging that this work with contribute to the broader understanding of geo-grid interactions.

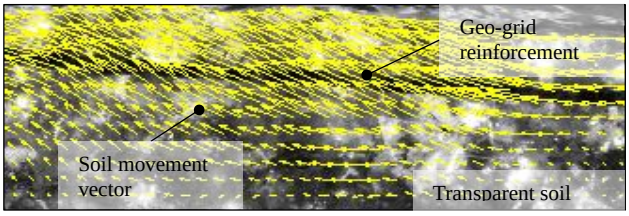

Figure 4. Relative displacement coarse material over geogrid in pull-out

4 ACKNOWLEDGEMENTS

Support from the technical staff in the Dept. of Civil & Structural Eng. to develop the test system is gratefully acknowledged. Supervision is provided by Dr Jonathan Black and Dr Colin Smith.

5 REFERENCES

ASTM D 6706-01 (2001). Standard test method for measuring geosynthetic pullout resistance in soil. ASTM, Philadelphia, PA, USA.

BS EN 13738 (2004). Geotextiles and geotextile-related products-Determination of pullout resistance in soil. British Standard.

Ezzein, F. & Bathurst, R.J. (2011). Development of a geosynthetic pullout test apparatus with transparent granular soil,Geotechnical Conference, Pan-Am CGS

FHWA –NHI-00-0043 (2001). Mechanically stabilized earth walls and reinforced soil slopes. Design and constructions guidelines, U.S. Department of Transportation Federal Highway Administration.

The Effect of Soil Reinforcement on Tunnel Face Stability in Clay

B. T. Le & R. N. Taylor
City University London

ABSTRACT: Adequate face stability is crucial to the safe construction of any tunnel. Insufficient support will lead to ground movements which have the potential to cause damage to existing infrastructure. Congested urban environments have led to a requirement to minimise these tunnelling-induced deformations. Forepoling Umbrella System (FUS) has proved to be a useful soil reinforcement measure for controlling ground movements due to NATM tunnelling in urban areas. Previous research has focused on the effect of having 'spile reinforcement' ahead of an advancing tunnel face. A new series of three-dimensional centrifuge model tests using stiff clay has been conducted using the geotechnical centrifuge facility at City University London. These tests aim to discover reinforcing proficiency in different arrangements of steel pipes in FUS. A pressurised air supported tunnel was adopted and gradual reduction of the air pressure simulated the ground deformation due to tunnelling. The results highlight some interesting effects on the tunnel stability and the spread of ground movements in the vicinity of the tunnel heading.

KEYWORDS: forepoling umbrella system, centrifuge model testing, urban tunnelling.

1 INTRODUCTION

Forepoling Umbrella System (FUS) consists of steel pipes installed from the tunnel face in an umbrella shape around the excavation area (Figure 1) to provide additional support and reduction of ground movement.

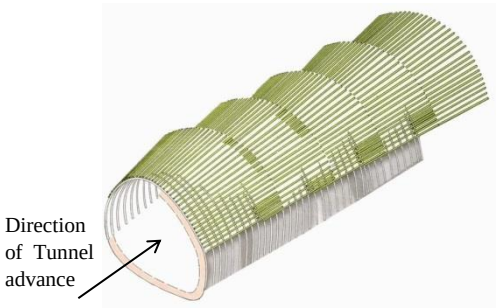

Figure 1. Forepoling Umbrella System – After Carrieri et al. (2002)

Generally, steel pipes are 70mm to 200mm diameter with a wall thickness of 4mm to 8mm. The length of steel pipes varies from 12m to 18m. Figure 2 presents a schematic diagram of a FUS. FUS is normally installed at an insertion angle (β) of from 5^0 to 7^0. The filling angle (α) is from 60^0 to 75^0. The minimum overlap/embedded length between FUS sections varies from 3m to 6m. The spacing between steel pipes varies from 300mm to 600mm centre to centre. Values for the above parameters are determined dependent on tunnel geometry and ground conditions for maintaining sufficient support.

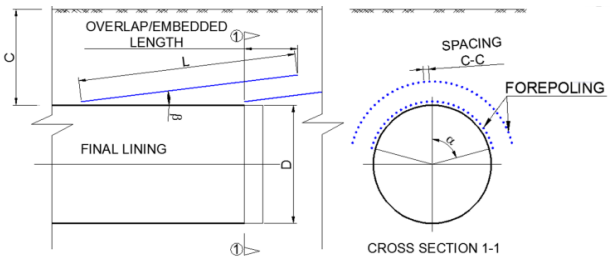

Figure 2. FUS schematic diagram.

2 CENTRIFUGE TESTS

2.1 Methodology

In situ stresses within the soil mass is a key factor in determining ground deformation behaviour. Thus, physical modelling studies generally require the reproduction of a representative self-weight stress regime.

Centrifuge modelling techniques, by the mean of inertial radial acceleration, can create a proper self-weight effect in a small scale model to be identical to a full scale prototype. Hence, soil behaviour prototype scale can be replicated in a model of 1/n scale. Also the structural behaviour of steel pipes can be modelled.

Therefore, with careful selection of dimensions and materials, centrifuge model tests can deliver valuable insights into the effect of soil reinforcement of tunnel face stability in clay.

2.2 Centrifuge model testing setup

A three-dimensional tunnel heading test in kaolin clay was undertaken. The Speswhite kaolin slurry was one-dimensionally consolidated to a vertical effective stress of 175 kPa. Figure 3 shows the diagram of the model apparatus.

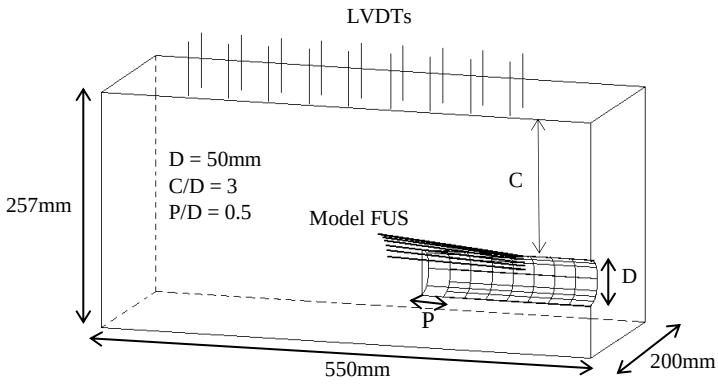

Figure 3. Diagram of model apparatus

Only half of the prototype was modelled. The stiff tunnel lining was modelled by a 50mm diameter semi-circular brass tube. The unlined portion of tunnel (P) was supported by compressed air within a rubber bag. 14 1mm diameter brass rods were inserted in to modelled clay via a guiding device to model steel pipes. Insertion and filling angles are 5^0 and 90^0 respectively. Spacing between brass rods is about 3mm. The embedded length was 25mm (0.5D).

Table 1. Tunnel geometry

Parameter	*Model(mm)*	*Prototype (m)*
Diameter D	50	6.25
Cover C = 3D	150	18.75
Protrusion P = 0.5D	25	3.125

2.3 Testing procedure

The model was accelerated to 125g and left running until the model clay reached an equilibrium state. During the spin up phase, the tunnel pressure was increased to balance the overburdened pressure at tunnel axis level (376 kPa at 125g). After the model clay reached equilibrium, the tunnel pressure was gradually reduced over a period of about 3 minutes to simulate the ground movement due to tunnelling.

Data were recorded and stored continuously during this testing phase.

3 RESULTS

3.1 Subsurface settlement

Subsurface settlements were obtained by image processing program. The targets were inserted into the front side of the clay model and used to monitor the positions and displacement of clay during the test. Images of these targets were captured by a camera through perpex window and processed in a computer program.

Figure 4 shows the overall pattern of subsurface settlements in the vertical plane though the longitudinal axis of the tunnel. The crosses represent the initial positions of targets and the vectors show targets' displacements.

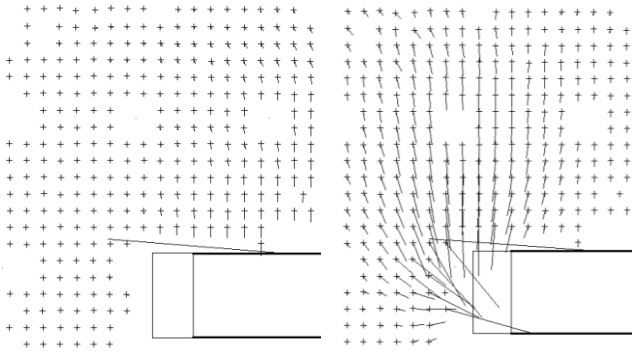

(a) vectors magnified by 10 (b) vectors magnified by 4

Figure 4. Subsurface settlements (a) σ_T from 376 to 210 kPa; (b) σ_T from 376 to 0 kPa

3.2 Vertical surface settlement

Figure 5 shows the vertical surface settlements recorded by LVDTs during the reduction of tunnel pressure.

The effect of FUS is reflected by the development of ground settlement during the test.

Based on image processing and LVDTs records in Figures 4 and 5 respectively, it was found that when σ_T was reduced to 210 kPa, the ground movement mostly occurred in the area behind tunnel heading while the area in front of and above tunnel heading showed negligible deformation. The areas in front of and above tunnel heading were supported by FUS hence negligible movement was observed.

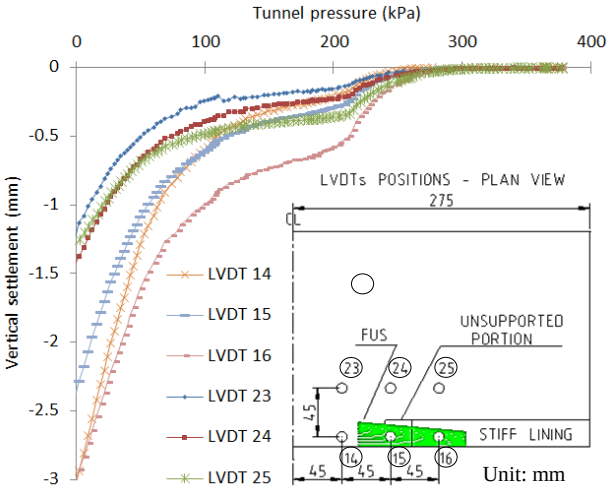

Figure 5. Development of near surface settlement above the tunnel face under the change of tunnel pressure.

From Figure 5, it is evident that the slopes of surface settlements lines when σ_T was reduced from 210 to 100 kPa are less steep than these when σ_T was reduced from 250 to 200 kPa and from 100 to 0 kPa.

The above phenomena did not occur in the similar three-dimensional heading tests conducted by Mair (1979) and Cavello and Taylor (1999) in which no reinforcement and face spiles reinforcement (modelled by plastic rods) were adopted respectively.

Undoubtedly, the presence of FUS gave structural reinforcement to ground nearby. When σ_T was less than about 90 kPa, the FUS seemed to exceed the elastic limit and lose their reinforcing effect which resulted in a large increase in settlement.

4 CONCLUSION

By comparing the test results to works conducted by other authors, it is clear that FUS contributed to reduce the development of settlement.

Post test it was noticed that the top brass rods had larger deformation than the bottom rods. Therefore, focused distribution of steel pipes at the tunnel crown area potentially improves FUS reinforcing proficiency compared to uniformly spaced as the forepoling used in practice.

The effect of the embedded length of steel pipes ahead of tunnel face and focused distribution to FUS reinforcing proficiency will be the subject of the future testing program.

5 REFERENCES

Cavello, M. and Taylor, R.N. 1999. Centrifuge modelling of a spile-reinforced tunnel heading. Proc. 2nd International Symposium on Geotechnical Aspects of Underground Construction in Soft Ground. Tokyo.

Mair, R.J. 1979. *Centrifugal modelling of tunnelling construction in soft clay*. PhD Thesis, University of Cambridge

Mair, R.J. and Taylor, R.N. 1993. *Prediction of clay behaviour around tunnels using plasticity solutions*. Predictive Soil Mechanics. Proc. Wroth Memorial Symposium, Oxford. Thomas Telford, 449-463.

Yeo, CH. 2011. *Stability and collapse mechanisms of unreinforced and forepole-reinforced tunnel headings*. PhD Thesis, National University of Singapore.

The Stabilisation Measures at Beaminster Tunnel, Dorset

V. M. Turner-Weare
Parsons Brinckerhoff Ltd.

Slope failures above the north and south portal entrances to Beaminster Tunnel occurred in July 2012 following a period of exceptionally heavy rainfall. The landslip above the north portal is thought to have caused the portal headwall to fail, resulting in debris falling onto the road below. The tunnel was closed to the public shortly afterwards. Following this catastrophic event, the safe and quick reopening of the tunnel to traffic was critical. Ground investigation and design works were able to start within weeks of the event and construction of stabilisation measures started 6 months later.

KEYWORDS: Slope stabilisation, soil nailing, Upper Greensand Formation, Gault Formation.

1 INTRODUCTION

Beaminster Tunnel is the only pre-railway age road tunnel that is still in daily public use in the UK. This historically significant tunnel, opened in 1832, is located approximately 2 kilometres northwest of the town of Beaminster on the A3066, Crewkerne to Bridport road.

Slope failures above the north and south portal entrances occurred in July 2012 following a period of exceptionally heavy rainfall. The landslip above the north portal is thought to have caused the portal headwall to fail, resulting in debris falling onto the road below. The tunnel was closed to the public shortly afterwards.

2 BACKGROUND

Due to the age of the tunnel, there is no as-built information available. It is approximately 105 metres long and runs underneath Horn Hill with a public right of way (Common Water Lane) running east-west across the top of the site between, and approximately equidistant from, the portals.

A prolonged period of extremely wet weather affected all of England during the months between April and November in 2012. April and June were each the wettest on record in the England & Wales precipitation series since records began in 1766, and the 2012 summer was the wettest since 1912, particularly in the immediate locality of Beaminster.

2.1 *Desk Study Information*

A literature review was undertaken covering several previous projects constructed within the Upper Greensand Formation, and using the following sources of information:

- CIRIA 591 - Infrastructure Cuttings: Conditions Appraisal and Remedial Treatment
- BS 6031: 1981 - Code of Practice for Earthworks
- Geological Survey of Great Britain - Geology of the Country around Bridport and Yeovil

2.2 *Geological Conditions*

According to the British Geological Survey (BGS) geological map of the area, the site is underlain by the Upper Greendsand Formation. An outcrop of the Gault Formation (formerly known as the Gault Clay) was noted immediately south of the site.

A two-phase intrusive ground investigation was undertaken across the site, comprising cable percussive boreholes, window samples, coring of the portal entrance wingwalls and observation pits. The investigation confirmed the ground conditions, *i.e.* the slopes were Upper Greensand Formation, and the Gault Formation was encountered at road level at the south portal. No groundwater was encountered within the slopes above the tunnel portals, but elevated groundwater levels were noted in the area of the south west slopes adjacent to the south portal.

2.3 *Geotechnical Parameters*

The characteristic parameters were determined using the information collated from the literature review, the back analysis and the laboratory testing, particularly from the effective stress testing.

The characteristic geotechnical parameters used in the strengthening measures deigns are shown in Table 1.

Table 1. Characteristic Geotechnical Parameters.

Parameter	*Upper Greensand Formation*	*Gault Formation*
Angle of Shearing Resistance (°)	33.5	23.0
Effective Cohesion (kPa)	0	0

3 STABILISATION MEASURES

The stabilisation measures, designed by Parsons Brinckerhoff, comprised three interlocking facets: geotechnical (*i.e.* the stabilisation of the slopes above the portals), structural (*i.e.* stregnthening of the portal walls and the installation of the concrete saddle) and drainage. Those different aspects were designed to complement and work together as part of the overall stabilisation solution under tight time constraints

3.1 *Slope Stabilisation*

Stabilisation of the slopes was achieved by installing soil nails designed using the effective stress methods detailed in BS 8006-2. The length of the soil nails was varied across the site to control potential deep seated failures. Five metre long dowels, tensile mesh facing and erosion protection matting were also installed in order to prevent shallow transitional landslips, such as those observed during the July 2012 failures, and to enable vegetation to establish itself on the slopes, thereby further aiding stability.

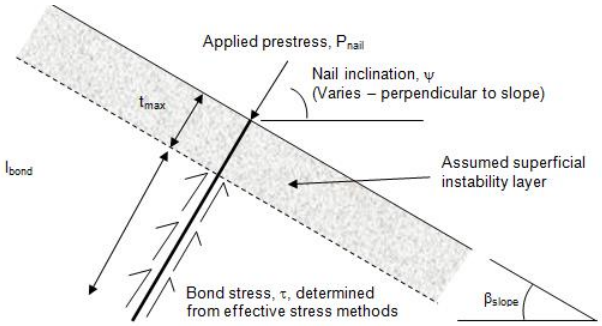

Figure 1. Dowels, Idealised Model

One of the main challenges was the complex geometry of the site requiring stabilisation, which comprised concave bowl-shaped slopes above the portals with continuing side slopes at each tunnel portal.

3.2 *Portal Strengthening*

Structural checks of the portal retaining walls were carried out by the structures team using BD21/01 and BA 55/06 (including CP2) from the Design Manual for Roads and Bridges. Although there were no visible or reported signs of distress to the walls, the stability of the walls was called into question by a quantitative assessment undertaken in accordance with CP2 of BA 55/06. To guard against potential future instability, the walls were strengthened by installing soil nails along their entire length.

As the tunnel portals are Grade II listed structures, alterations of the aesthetics by the strengthening measures had to be minimised. The portal wing-walls were cored prior to soil nail installation, and the cores were replaced over the top of the soil nails after installation to hide the strengthening measures. That incorporation of the existing tunnel portal structure into the strengthening measures, rather than replacement, also provided a sustainable solution that protected the life-long heritage value and architectural significance of the Grade II listed structures.

When designing the wing-wall stabilisation measures, it was assumed that the soil nailed material and the wing-walls would act as a rigid block, *i.e.* as a mass gravity retaining wall.

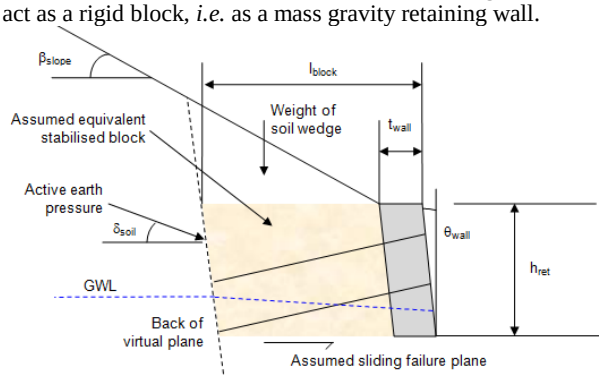

Figure 2. Wing-wall Stability, Idealised Model

The soil nail lengths extended beyond that rigid block by a distance sufficient that overlapping 45° cones from the end of the nails intercepted at the back of the internal mass gravity retaining structure.

The outcrop of the Gault Formation at the south portal required the installation of longer soil to stabilise the portal wing walls.

The design also included reinforced concrete saddles which were constructed on site at the top of wing-walls of the two portals, the saddle at the northern portal enabling rebuilding of the failed headwall. The saddles were provided to strengthen and further protect the existing masonry stone portal entrances.

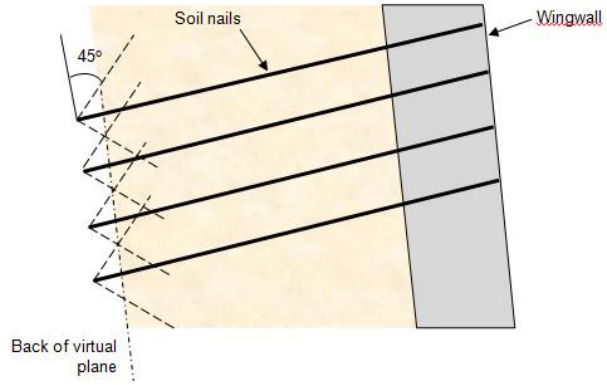

Figure 3. Soil Mass Block, Idealised Model

3.3 *Drainage Measures*

Crest drains and French drains were installed at the toes of the various slopes to prevent water from draining onto the slope faces, and to prevent water pressure build-up behind the wing-walls. Those drainage measures were connected into the existing highway drainage, which was itself refurbished/replaced to cope with the higher volume of water likely to be discharged.

Long-hole drainage was also installed within the slopes at the base of the nails, and at the wing walls in order to further minimise the build-up of water pressures.

3.4 *South West Slopes*

As previously mentioned the elevated groundwater level in the area of the south portal, coupled with the presence of the Gault Formation, necessitated the use of a completely different ground model to that for the north portal. Further modification of the model was required when the sacrificial test nails were found to be unable to take the required test loads.

Long-hole drainage was immediately installed to reduce the groundwater level and to minimise pore water pressures. The original stabilisation design was supplemented with the addition of a gabion mass gravity retaining wall. Granular fill was placed behind the wall to slacken the slope angle.

4 CONCLUSION

A particular challenge for the designers was the need to provide a comprehensive set of interlocking stabilisation measures in a very restricted time-frame, and the necessity to adapt the design as more information became available throughout the construction phase. Following design and construction of stabilisation measures, including inputs from the geotechnical, drainage and structural teams, the tunnel was successfully re-opened to traffic 12 months after it was originally closed.

5 ACKNOWLEDGEMENTS

This paper has been based on the technical aspects of the scheme as presented jointly with Dorset County Council at a number of events.

I would like to thank Ian King and the Geotechnical, Structural and Drainage Teams involved in the project.

6 REFERENCES (TNR 8) (IN ALPHABETICAL ORDER)

BS 8006-2:2011 Code of Practise for Strengthened / Reinforced Soils – Soil Nail Design

BS EN 14490:2010 Execution of Special Geotechnical Works – Soil Nailing

CIRIA C637 Soil Nailing – 'Best Practice Guidance', 2005

Design Manual for Roads and Bridges, Volume 4, Section 1, Part 4, HA 68/94 – 'Design Methods for the Reinforcement of Highway Slopes by Reinforced Soil and Soil Nailing Techniques'

Strength anisotropy of fibre reinforced sands under generalised loading conditions using the Hollow Cylinder Torsional Apparatus

A. Mandolini, E. Ibraim, A. Diambra
Department of Civil Engineering, University of Bristol, UK

ABSTRACT: The results from an experimental campaign which aimed investigate the behaviour of fibre reinforced sand in the multiaxial stress space are shown in the present paper. Using the Hollow Cylinder Torsional Apparatus (HCTA), fibre reinforced samples have been subjected to probing stress paths with different orientation of principal stresses. The observed behaviour was found to be highly anisotropic and strength envelope in the multiaxial stress space will be for the first time provided for this type of material.

KEYWORDS: Hollow Cylinder Torsional Apparatus, Hostun sand, Fibre Reinforced sand, Anisotropy, Fibre

1 INTRODUCTION

Mixing sands with random discrete flexible fibres increases their strength and influences their deformation characteristics (Gray and Ohashi, 1983; Michałowski and Cermák, 2003; Diambra A, 2010 among others). Recent experimental studies on fibre reinforced soils have demonstrated that the reinforcing effect may be highly anisotropic as a result of the preferential horizontal bedding induced by the mixing and compaction processes employed (Diambra et al. 2007 and Ibraim et al. 2012).

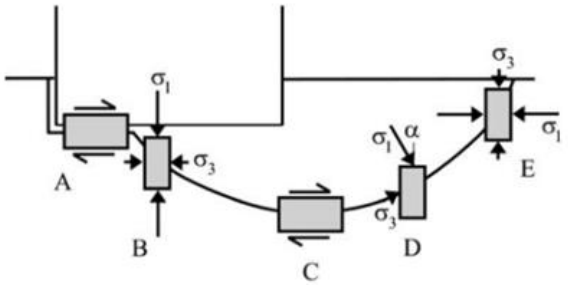

Figure 1 Stress conditions along a potential failure surface.

Considering that the rotation of the principal stress axis almost invariably occurs within a soil mass (for example, see Figure 1), this aspect is of foremost importance for the perspective field application of the fibre reinforcing technique. Thus the present study aims to extend the previous experimental work by investigating the anisotropic behaviour of fibre reinforced sands in the generalised multiaxial stress space using the Hollow Cylinder Torsional Apparatus.

2 MATERIALS AND APPARATUS

2.1 Fibres

For the whole campaign of tests, crimped polypropylene fibres (LoksandTM) have been used as a reinforcing material. These fibres present a circular cross section of 0.1mm diameter and they are 17.5 mm long. This length was selected to have a reasonable fibre to wall thickness ratio while maintaining an easily detectable fibre contribution. A study on the effect of fibre length in triaxial samples was performed by Mandolini (2012), results ensured that 17.5 mm long fibres provide a measurable strength increase.

2.2 Hostun sand

Hostun sand is European standard sand for this laboratory campaign with a high siliceous amount (SiO_2>98%). Its grain shape varies from angular to sub-angular. Its physical properties are as follows: mean grain size D_{50}=0.32 mm, coefficient of uniformity Cu=1.70, coefficient of gradation Cg=1.1, specific gravity Gs=2.65 and minimum and maximum void ratios, respectively e_{min}= 0.62 and e_{max}= 1.00.

2.3 Hollow Cylinder Torsional Apparatus

Traditionally, experimental investigations on fibre reinforced sands have been carried out on conventional triaxial apparatus and direct shear. HCTA provides a greater freedom to explore general variations of stresses and strains. Soil samples tested in the HCTA have a typical hollow cylindrical shape (as shown in Figure 2a) and the apparatus has the capability to control axial load (W), torque load (T) and internal and external pressure (P_i and P_o) independently.

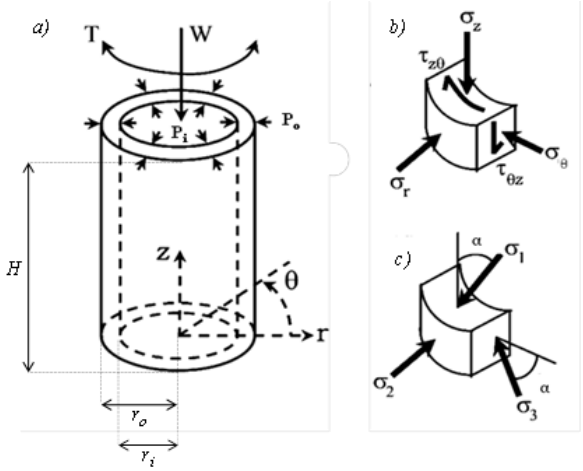

Figure 2 Stress state in hollow cylinder torsional sample. (a) Surface loads, (b) stress components, (c) main principal stresses;

3 EXPERIMENTAL TESTING

3.1 Sample preparation

The Bristol HCTA enables the testing of specimens with the following nominal dimensions: height (H) of 200mm, outer radius (r_o) of 50mm and inner radius (r_i) of 30mm (Figure 2a).

These dimensions respect the recommended dimensions suggested by Sayão and Vaid (1991), in order to minimize the sample curvature and restraint effect which may lead to stress and strain non-uniformities. To obtain an acceptably uniform distribution of fibres and fulfil the repeatability requirements a new sample fabrication was developed. Fibre reinforced sands were prepared in five different layers, deposited into the mould (appositely designed for this experimental campaign) and then vibrated to reach the desired density.

3.2 Testing programme

A total of 24 drained tests have been performed on both unreinforced and reinforced (wf =0.5%) specimens, imposing probing stress paths with different values of the orientation of the major principal stress direction α (see Fig.2c for its definition). Tests were carried out imposing rotation α of *0°*, *15°*, *30°*, *45°*, *60°* and *90°*. The nominal void ratio used was 0.94.The tests have been performed using the same value of internal and external confining cell pressure kept constant during the test. Two different confining pressures of 100kPa and 200kPa have been used.

4 RESULTS AND DISCUSSION

A typical comparison between reinforced and unreinforced failure envelopes at a fixed deviatoric strain (ε_q=10%) is presented in the normalised shear stress-deviatoric stress plane only for the confining pressure of 100 kPa (Figure 3).

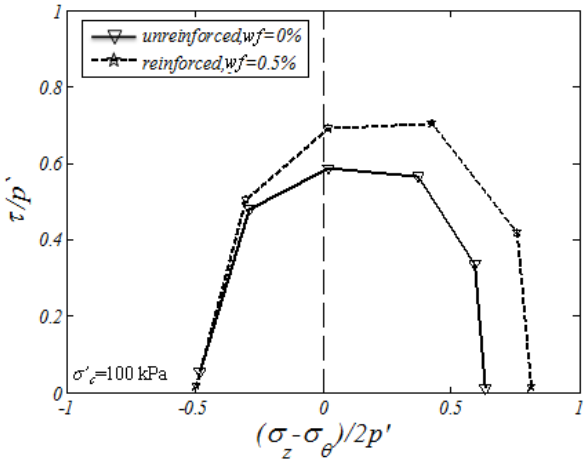

Figure 3 Rosette, for unreinforced (solid line) and reinforced samples (dotted line), plotted considering the stress state at ε_q=10% for samples under 100kPa.

The difference between the unreinforced failure envelope (solid line) and the reinforced one (dotted line) in Figure 3 represents the fibre strengthening effect. The reinforcement contribution is noticeable for lower rotation of the principal stress axis, such as α=0°, 15° and 30° (Figure 3) but become progressively closer towards the pure extension case (α=90°). The anisotropic strength of fibre reinforced specimen is related to the fibre orientation with to tensile strain direction. In triaxial compression (α=0°), the fibres, which are expected to be mostly horizontally oriented, lie in the same direction as tensile strain thus may mobilise consistent tensile stress. By increasing α, the tensile strain direction gradually rotates towards the vertical and thus the stretched amount of fibre is expected to decrease.
This outcome is even more evident in the following plot which collects the gain in friction angles ($\Delta\varphi'_{10}$) due to the addition of fibres:

(1)

where φ'_{10r} and φ'_{10u} are the friction angles for a reinforced and the correspondent unreinforced specimen at ε_q=10%.
The outcomes show a well-established benefit in using fibre as reinforcement, especially for the smaller value of α. In terms of friction angle it corresponds to an average increase from 17% to 25% for tests at α up to 30° (Figure 4). Strengthening effect drops between α=45° and 60°.

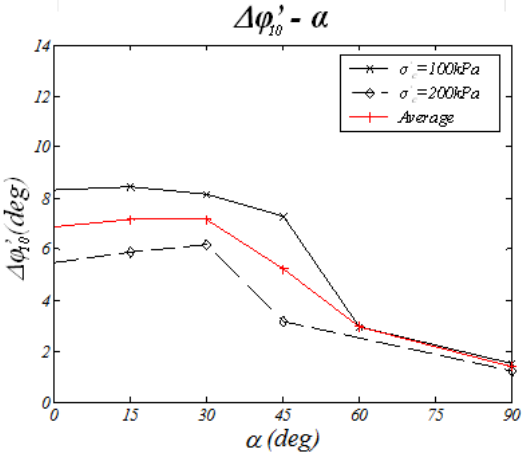

Figure 4 Variation of the friction angle (at ε_q=10%) between reinforced and unreinforced samples for different α angles.

5 CONCLUSIONS

In this research has been investigated the anisotropy of the fibre contribution effect under generalised loading condition.
The fibre contribution is highly dependent on the inclination of the major principal stress direction. Since the moist tamping method leads to a preferred sub-horizontal orientation of fibres, they result more effective when oriented along the direction of the tensile strains. A remarkable strengthening effect arises for loading direction α from 0° to 45°, while for further rotation (α=60° and 90°) the improvement gradually disappears. This point indeed concerns a potential field application where variation of the principal stress axis direction inevitably occurs along a failure surface (Figure 1).

6 ACKNOWLEDGEMENT

The author gratefully acknowledges the generous support from the EPSRC grant (reference number: EP/J010022/1) for funding the current research.

7 REFERENCES

Diambra, A., Russell, A.R., Ibraim, E. & Muir Wood, D., 2007 Determination of fibre orientation distribution in reinforced sand. *Géotechnique*, 57, No. 7, 623-628.

Diambra, A., 2010. Fibre reinforced sands: experiments and constitutive modelling, *PhD Thesis*. Department of Civil Engineering. University of Bristol.

Gray, D.H., Ohashi, H., 1983. Mechanics of fiber reinforcement in sands. *Geotechnical Engineering Journal* 109, 335-353.

Ibraim, E., Diambra, A., Muir Wood, D. & Russell, A.R., 2011 Assessment of laboratory sample preparation for fibre reinforced sands. *Geotextiles & Geomembranes*.

Mandolini, A., 2012. Triaxial behaviour of fibre-reinforced sands: Influence of the fiber length and grain size, *Master Thesis*, Civil Engineering. Universita' Politecnica delle Marche (Ancona).

Michałowski, R.L., Čermák, J., 2003. Triaxial compression of sand reinforced with fibers. *Journal of Geotechnical and Geoenvironmental Engineering.* 129, 125-136.

Sayão, A., Vaid, Y.P., 1991. A Critical Assessment of Stress Non-uniformities in Hollow Cylinder Test Specimens. *Soils and Foundations* 31, 61-72.

Study of particle crushing under compression

S. Luo
Department of Civil Engineering, the University of Bristol, Bristol, UK
Supervisors: Dr. E.Ibraim, Dr. A.Diambra

ABSTRACT: When the confining pressure is sufficiently large, grain breakage can occur and this can have a significant influence on the performance of a wide range of geotechnical systems such as shallow foundations, embankments and dams, railway substructures. However, the mechanics of particle crushing still remains one of the most difficult problems in geosciences. This paper analyses chalk particles with approximately 10mm size under uniaxial compression. The crushing behaviour, the distribution of the generated fragments and the data of particle shape description had been presented. It emerges that there is no clear link between these various parameters and further consideration of the internal structure of chalk is necessary.

KEYWORDS: single particle, crushing, compression.

1 INTRODUCTION

The link between the breakage of particles and the mechanical response of the soil is attracting much attention and the main challenge remains the development of a continuum constitutive model that would incorporate the changing of the particle size induced by the crushing process. However, before moving to an agglomerate of individual soil particles, our initial aim is to concentrate on the behaviour of individual particles first. Therefore, this study examines the mechanical response of single particles under uniaxial compression.

2 MATERIAL

While several individual particles of different materials will be considered, so far only chalk particles grouped by the different equivalent area diameters of 10mm, 7mm, 5mm and 2mm have been considered. However, this paper presents only the data obtained for 10mm equivalent diameter particles.

2.1 Particle shape characteristic

The literature is abundant on shape parameters like the form, sphericity, roundness, circularity, regularity, irregular shapes and roughness. Several parameters had therefore been considered to provide a link between the shape of particle and the mechanical behaviour of single particle under uniaxial compression. An optical microscope was used for measuring the pertinent parameters of a large number of particles, while the software ImageJ and Matlab had been used to generate the shape descriptors as defined ISO (2006):

(1)

; (2)

; (3)

); (4)

P; (5)

; (6)

where da is the equivalent area diameter, AR is the aspect ratio, IR is irregularity, C is the circularity, Cw2d is also a circularity index and Sw2d is the degree of sphericity both defined by Wadell (1933) (1932). In these relations, A is the projection area and P is the perimeter of the 2D particles. Feret diameter df is the distance between two parallel tangents to the particle outline while df_{max} and df_{min} are respectively the largest and the smallest values of df for a given outline; d_{imax} and d are respectively the diameters of the maximum inscribed circle and the minimum circumscribed circle: as can be observed in the Figure 1, the areas of the maximum inscribed circle and the minimum circumscribed circle are respectively 107.91mm and 75.10 mm^2, while df_{max} and df_{min} are respectively 11.22 mm and 10.85 mm, A is 90.39 mm^2 and P is 36.92mm. The results for 11 particles are presented in Table 1. All the data represents the average of at least four particle positions and corresponding photos taken of the by the digital microscope.

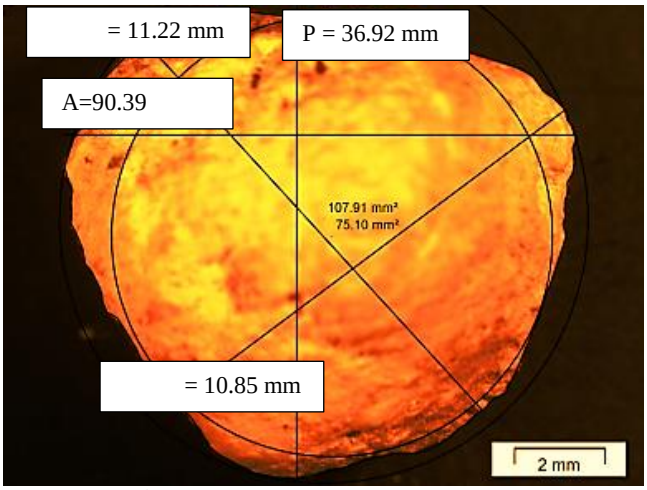

Figure 1. Photo from Microscope with parameters

Table 1. The particle shape defines parameters of 10mm group.

	Shape Description					
Particle Name	da(mm)	AR	IR	C	Cw2D	Sw2D
10_1	10.53	0.90	0.76	0.79	0.89	0.90
10_2	9.01	0.80	0.71	0.77	0.88	0.85
10_3	9.18	0.96	0.78	0.76	0.87	0.89
10_4	9.12	0.99	0.82	0.81	0.90	0.90

10_5	9.06	0.89	0.75	0.80	0.89	0.88
10_6	8.77	0.93	0.79	0.82	0.91	0.89
10_7	9.37	0.94	0.76	0.80	0.89	0.88
10_8	9.32	0.89	0.76	0.79	0.89	0.89
10_11	8.57	0.91	0.73	0.78	0.88	0.89
10_13	10.20	0.86	0.76	0.81	0.90	0.88
10_14	9.85	0.88	0.74	0.79	0.89	0.90

3 EXPERIMENTAL DATA AND RESULT

3.1 Experiment set up

This crushing machine used for the particle uniaxial compression tests is a displacement controlled electro-mechanical loading frame able to provide various constant displacement rates. The particles are placed between two rigid plates, of which one is fixed to the loading ram that incorporates an LVDT for axial displacement measurements and a 5kN loading cell. The speed of the displacement was set as 0.005mm/min. The photo of particle before and after test can be shown in figure 2 and figure 3. A recording camera for the study of the crushing mechanisms completes the experimental set-up.

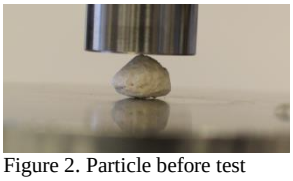

Figure 2. Particle before test

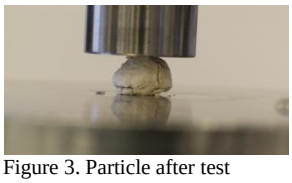

Figure 3. Particle after test

3.2 Results

The force-displacement diagrams recorded for each particle are plotted in Figures 4-6. Each figure shows the results that appear relatively similar. The critical crushing force ranges are 150-200N(group 1), 100N(group 2) and below 50N(group 3). Comparing the shape of the particles and the mechanical behaviour, even the particles have similar shape, the limit forces are still in a quite wide range. After crushing, the particles were recovered and the number and size of the generated fragments assessed. The distribution of the different sizes of the crushed fragments is showed in table 2. No clear correlation between the crushing behaviour and the distribution of the crushed fragments is observed. It is possible that the internal fabric of the particles to be responsible for these differences.

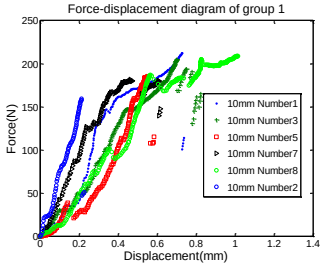

Figure 4. Force-displacement diagram of group 1

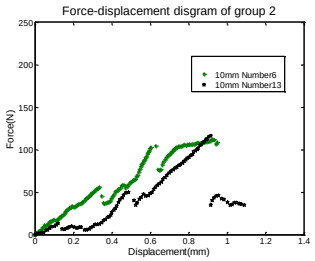

Figure 5. Force-displacement diagram of group 2

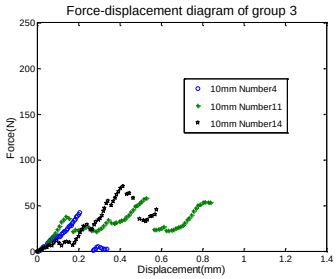

Figure 6. Force-displacement diagram of group 3

Table 2. The distribution of crushed fragments of 10mm.

Particle Name		*Total Number*	*Number*		
	Fragments Size		7-6 mm	5-4 mm	3-1 mm
Group1	10_1	7	1	0	6
	10_2	3	0	2	1
	10_3	6	0	2	4
	10_5	5	0	1	4
	10_7	7	1	1	5
	10_8	8	1	0	7
Group2	10_6	4	0	2	2
	10_13	8	1	1	6
Group3	10_4	6	1	0	5
	10_11	6	1	1	4
	10_14	5	1	0	4

4 CONCLUSION AND FUTURE WORK

From the data shown above, two points could be drawn: first, the analysis of the internal structure of the particles is important; second, there is no clear links between the crushing behaviour and the crushed fragments, and further investigation will be conducted. In the future, insight into the breakage mechanisms of various particles of different sizes and shapes made of different materials will be explored through some advanced complementary investigative techniques.

5 REFERENCES

ISO (2006). Representation of results of particle size analysis. Part 1-6. Part 6: Descriptive and quantitative representation of particle shape and morphology. *Draft International Standard ISO/DIS 9276*, Geneva

Wadell, H. (1932). Volume, shape, and roundness of rock particles. *Journal of Geology 40*, 443–451.

Wadell, H. (1933). Sphericity and roundness of rock particles. *Journal of Geology 41*, 310–330.